MODELING AND CONTROL OF CABLE-DRIVEN ROBOTS

Seyed Masood Dehghan Banadaki

NANYANG TECHNOLOGICAL UNIVERSITY

2007

MODELING AND CONTROL OF CABLE-DRIVEN ROBOTS

Seyed Masood Dehghan Banadaki

A THESIS SUBMITTED

FOR THE DEGREE OF MASTER OF ENGINEERING

SCHOOL OF MECHANICAL & AEROSPACE ENGINEERING

NANYANG TECHNOLOGICAL UNIVERSITY

2007

This thesis is dedicated to

my beloved wife, Dornoosh,

and

my parents

Acknowledgments

There are many people whom I wish to thank for the help and support they have given me throughout my Master's program. My foremost thank goes to my supervisor A/P Michael Lau Wai Shing. I thank him for his patience and encouragement that carried me on through all the difficult times, and for his insights and suggestions that helped to shape my research skills. His valuable feedback contributed greatly to my research work, definitely including this thesis. I also thank A/P Yeo Song Huat, my co-supervisor, for his valuable comments and sharing of knowledge in solving technical problems. I would like to take this opportunity to thank all the students and staffs in Mechatronics & Control Lab and Robotics Research Centre, whose presences and fun-loving spirits made the otherwise grueling experience tolerable. Special thanks goes to Erik Budiman, the FYP students, for his help in the design and fabrication of the prototype and for carrying out basic experiments and testings. I would also like to thank my friends Alireza Farjoud, Pham Cong Bang, and Mustafa Shabbir Kurbanhusen for their comments and suggestions on my research.

Last but not the least, I would like to thank my parents, my parents in law, my brother, and my sister for always being there when I needed them most, and for supporting me through all these years. I would especially like to thank my wife Dornoosh, who with her unwavering support, patience, and love has helped me to achieve this goal. This dissertation is dedicated to her.

Contents

Abstract

This thesis concerns the study of the modeling and control of cable-driven robots. A Cable-Driven Robot (CDR) is formed by replacing all the supporting legs of a parallel robot with cables. In comparison with the conventional serial and parallel robots, CDRs have the advantages of simple mechanical structure, large workspace, low moment inertia, and high speed motion. One distinctive characteristic of cable-driven robots is the unilateral property of the cables, i.e. they can only pull but not push.

In this thesis, the forward and inverse kinematics, velocity and acceleration analysis, tension analysis, dynamic modeling and control of the cable-driven robot are investigated. The forward kinematics of a CDR is difficult because of its closed-loop structures, while the inverse kinematics is relatively simple as it can be decoupled into individual cables. The Newton-Raphson method is adopted to solve the forward displacement numerically. Static and dynamic analysis for a cable-driven robots are also studied. A complete dynamic model of a CDR, including the end-effector dynamic model and actuator dynamic model has been derived. By combining these equations, the overall dynamic model of the system is obtained. Moreover, two approaches for the control of cable-driven robots has been pointed out, namely independent joint control approach and computed torque approach. The first method uses local independent PID controllers at each joint to control the position of the end-effector, while the second one is based on the control law

development using computed torque method. Finally, a planar cable-driven robot prototype has been build to investigate the control performance of CDRs. The conclusions of the present study and future research are also outlined in the thesis.

List of Figures

List of Tables

List of symbols

$\mathbf{a}$	Translational acceleration vector of the platform
a, b	Dimension of the base of planar CDR
B_i	Connecting point on the base
$\mathbf{b_i}$	Coordinate vector of the suspending point
$\mathbf{C}$	Equivalent vicious damping coefficient of the cable winding unit
c, d	Dimension of the end-effector of planar CDR
$\mathbf{e}$	Tracking error of actuator
$\mathbf{F_R}$	External force vector acting on the end-effector
$\mathbf{g}$	Gravitational acceleration
$\mathbf{h}$	Arbitrary small displacement normal to cable direction
$\mathbf{I}$	Identity matrix
$\mathbf{I_e}$	Inertia tensor of the end-effector with respect to body axis
$\mathbf{J_{NR}}$	Newton-Raphson matrix
$\mathbf{J}_\chi$	Jacobian matrix expressed in reference frame
K	Stiffness Matrix
K_{active}	Active Stiffness Matrix
K_D	Derivative gain of controller
K_I	Integral gain of controller
K_i	Elastic stiffness of a cable
K_P	Proportional gains of controller
$K_{passive}$	Passive Active Stiffness Matrix

k_a	Amplifier gain
k_{ENC}	Encoder constant
k_t	Actuator torque constant
$\mathbf{L}$	Vector of cables length
l_i	Cable length
$\mathbf{M_{eq}}$	Equivalent inertia matrix
M_p	Maximum overshoot
$\mathbf{M_R}$	External moment vector acting on the end-effector
m	Number of cables
m_e	Mass of the end-effector
$\mathbf{N}$	Null vector
$\mathbf{N}(\mathbf{X}, \dot{\mathbf{X}})$	Nonlinear term
n	Number of task-based dimension (degrees of freedom)
P_i	Connecting point on the moving platform
$\mathbf{p}$	Positional vector of point P
$\mathbf{q_i}$	Coordinate vector of the connecting point (in base frame)
$\mathbf{q_i^P}$	Coordinate vector of the connecting point (in end-effector frame)
$\mathbf{R}$	Rotation matrix
$\mathbf{r}$	Equivalent radius of the cable winding unit
r_c	Radius of circular trajectory
r_D	Radius of the cable winding drum
r_{p1},r_{p2}	Radius of the timing pulleys
$\mathbf{S}$	Structure matrix
S	Laplace variable
$\mathbf{S}^+$	Pseudo inverse of the structure matrix
s_s	Kinematic parameter at starting posture
s_e	Kinematic parameter at ending posture
$\mathbf{T}$	Vector of cables tension

T^0	Modified Tension Matrix
$\mathbf{T_P^O}$	Transformation matrix from end-effector frame to base frame
t	time
t_f	time duration of the motion
t_i	Cable tension
t_{min}	Pre-tension (Minimum tension)
t_s	Settling time
$\mathbf{u_i}$	Unit vector along the cable from P_i to B_i
V_a	Armature voltage
$\mathbf{v}$	Vector of translational velocities
$\mathbf{W}$	Dynamic wrench acting on the end-effector
$\mathbf{W_R}$	Expression vector representing external wrench
$\mathbf{W_v}$	Virtual Cartesian wrench
$\mathbf{X}$	Posture vector of the end-effector
$\mathbf{X_R}$	Commanded (reference) Cartesian pose
x, y, z	Coordinates of point P
$\mathbf{Z}$	Arbitrary column vector
α	Euler angle about z-axis
β	Euler angle about y-axis
γ	Euler angle about x-axis
ε	Arbitrary small real number
φ	Orientation angle of the end-effector in planar case
λ	Arbitrary scaler
θ	Actuator angle
τ	Actuator torque
τ_f	Friction torque of actuator
$\mathbf{\Omega}$	Matrix of cables' stiffness
$\boldsymbol{\omega}$	Vector of rotational velocities about body axis of the end-effector

ω_n	Natural frequency of system

Chapter 1

Introduction

1.1 Motivation

Robots are electromechanical devices, which are programmable to accomplish a variety of tasks. Robots are classified into four major types: serial robots, parallel robots, hybrid robots and mobile robots. These classifications are based on the layout and type of the joints and links that compose a robot and the ability of a robot to move independently.

A serial robotic system can be formally defined as a robot that has only a single kinematic chain between the base and the end effector, composed of links connected by joints, where each link is connected to two other links, except for the base and the end-effector links (Figure 1.1(a)).

Parallel robots, in contrast to serial robots, have multiple kinematic chains that form one or more closed loops between the base and the end-effector as shown in Figure 1.1(b). A single chain from the base to the end effector is termed a leg, an arm or a branch, interchangeably.

Hybrid robots are those which involve both parallel and serial stages between the base and the end effector, for example, a conventional serial arm with a parallel wrist mechanism (Figure 1.1(c)).

Mobile robots are able to move themselves, as a complete whole, rather than just an end-effector portion, through their environment. In the case of a free-flyer robot, which can move using rocket propulsion and reaction wheels, or a walking robot, the system may also be a serial, hybrid, or parallel robot, in addition to being mobile (Figure 1.1(d)).

(a) Serial Robot [1]

(b) Parallel Robot [21]

(c) Hybrid Robot [77]

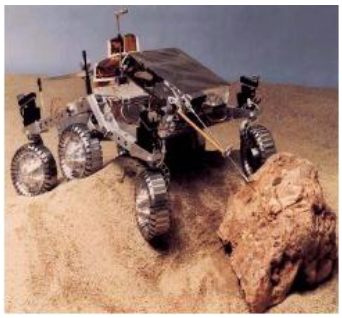

(d) Mobile Robot [34]

Figure 1.1: Conventional Robots.

Parallel robots provide several distinct advantages over conventional serial robots. Parallel machines are characterized by having multiple closed kinematic chains and actuate a subset of their joints. Due to this general arrangement, a parallel manipulator holds the potential for greater stiffness and higher speed and payload for a given weight. However, workspace is typically smaller than that of a similar serial machine, and dexterity may be compromised due to interference

of links, depending on the design. Therefore, both conventional serial and parallel manipulators are not effective for moving a heavy object in a large workspace. Cable-driven robots are more suited to this type of tasks.

Figure 1.2 shows a cable-driven robot or a wire-actuated manipulator which is formed by replacing all of the supporting legs of a parallel robot with cables. Cable-driven robots are closed-loop mechanisms in which the end-effector is connected to the base by several cables. They are relatively simple in form, with multiple cables attached to a mobile platform or end-effector. The end-effector is manipulated by motors that can extend or retract the cables. These motors may be in fixed locations or mounted on mobile bases. The end-effector may be equipped with various attachments, such as hooks, cameras, electromagnets and robotic grippers.

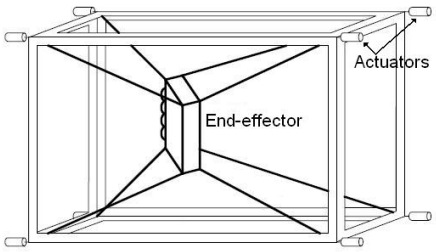

Figure 1.2: A Cable-Driven Robot [79]

Cable-driven robots have some desirable characteristics such as:

- Stationary heavy components and few moving parts resulting in low inertia, high acceleration.
- High payload-to-weight ratio
- Potentially large workspace, limited by cable lengths, and cable tension constraints
- Reconfigurability by simply relocating the motors and updating the control system accordingly

- Economical construction and maintenance due to few moving parts

Because of their advantages, cable-driven robots become an alternative of the rigid-link mechanisms in many applications such as material handling in large scales, manipulations of heavy payloads, rapidly deployable rescue robots, cleanup of disaster sites, access to remote areas, and interaction with hazardous environments. (Figure 1.3)

However, since cables are well known with their unilateral property (can pull but cannot push) the traditional methods for the kinematics analysis, workspace analysis, control, etc. of the rigid link robots cannot be directly applied for cable-driven robots.

Current research challenges for cable robots include the optimization of workspace properties, keeping the cables in tension dynamically, resisting external disturbances, design of suitable control algorithms, sensing of end-effector motion, sensing the tension of the cables and avoidance of cable interference.

1.2 Objectives and Scopes

Given the potential for cable-driven robots to be used in a variety of applications, it is important to have tools for analyzing and designing such manipulators. Therefore, the objective of this research is to develop kinematic and dynamic analysis and propose motion control strategies for cable-driven robots with redundant actuation, simulate the performance, and finally build a planar cable-driven robot for experimental verification of simulations.

The scope of this research will cover the following issues:

(a) Material Handling [8]

(b) Oil Well Fire Fighting [8]

(c) Rehabilitation System [26]

(d) SkyCam [61]

(e) Virtual Tennis System [29]

Figure 1.3: Cable-Driven Robots and Their Application.

- Kinematic analysis of cable-driven robots including forward and inverse displacement, velocity and acceleration analysis.
- Dynamic analysis of cable-driven robots.
- Motion control strategies for cable-driven robots with redundant actuation.
- Dynamic tension measurement and verification of the proposed control methods for cable-driven robots.

1.3 Thesis Organization

This thesis presents kinematics modeling, dynamics modeling, and control strategies for the planar cable-driven robots followed by some experimental results on a planar cable-driven robot prototype. A complete literature review of the relevant research area is presented in chapter two. Chapter three describes a model of cable-driven robots and also covers kinematic analysis. Tension analysis and stiffness modeling of cable-driven robots are presented in Chapter four, following by the dynamics modeling in Chapter five and development of a planar prototype in chapter six. Chapter seven covers control strategies of cable-driven robots. In addition, the implementation of the controllers and some experimental results are presented at the end of this chapter. An application of the planar prototype in rehabilitation is also presented in Chapter eight. Finally Chapter nine summarizes the research contributions and describes the future works.

Chapter 2

Literature Review

In this chapter, literature review of the research area is presented. For the comprehensive understanding of the research, related works is first presented in the areas of parallel mechanisms, cable-driven robots and their workspace analysis, followed by the areas most closely related to the control of cable-driven robots.

2.1 Parallel Mechanisms

A parallel robot is a closed-loop mechanism in which a moving platform is connected to the base by at least two serial kinematic chains called *legs* [40], as shown in Figure 2.1.

Getting its origin from the Stewart Platform designed by Stewart to simulate flight conditions by generating general motions in space [7], it has since found numerous applications in teleoperation hand controllers [13], high-speed machining equipments [39], high precision surgical tools [64], and modular reconfigurable robots [85].

Because the moving platform is connected to the base via numerous serial chains and having parallel actuation, the parallel mechanisms has greater rigidity, higher load-to-weight ratio, higher stiffness, and superior positioning capability compared to the serial mechanisms of similar dimension [71]. In addition, the parallel mechanism is able to provide a very complicated motion for the end-effector in a flexible way with many degrees-of-freedom (DOFs) by a combinational use of prismatic, revolute, universal and spherical joints.

However, these closed-loop kinematic chains also introduce limitations to the motion of the mobile platform and create complex singularities within the workspace. From the application point of view, limited workspace and complicated singularities are two drawbacks of parallel mechanisms. The potential benefits offered by parallel mechanisms have attracted many researchers in a great deal of effort in the workspace maximization and singularity determinations for the design and control of various types of parallel mechanisms [63].

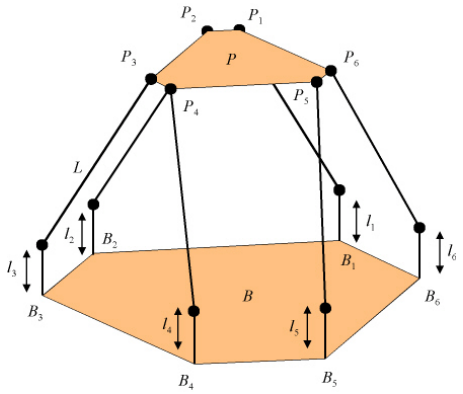

Figure 2.1: A Parallel Mechanism

2.1.1 Kinematic Analysis

Due to the closed-loop nature of parallel mechanisms, their forward kinematics is more challenging, since it is expressed in highly nonlinear equations with mul-

tiple solutions [78]. But on the other hand, the inverse kinematics is relatively straightforward, simply requiring direct substitution to obtain the unique set of answers for a given pose. Previous research efforts on forward kinematics [32] have focused on three main approaches: the polynomial-based, the extra-sensor, and the numerical-iterative approach. Due to the complex reduction process of the set of constraint equations into a uni-variant high-order polynomial equation in the polynomial-based approach, and high implementation costs and hardware complexities involved in the extra-sensor approach, the numerical-iterative approach has been widely used. One of the widely employed iterative methods is the Newton-Raphson method due to its quadratic convergence property. However, this approach also poses a potential problem of reliability and accuracy, as it is highly sensitive to the initial estimate values. This is generally minimized by using the previous point of the trajectory as a good initial guess [79].

2.1.2 Workspace

Workspace maximization is one of the goals of an optimal parallel mechanism design. In order to maximize the workspace of a parallel mechanism, quantitative and qualitative workspace evaluation has to be carried out in order to determine the geometrical limits of the task that can be performed. A common approach to workspace quantification is numerically discretizing the three dimensional space into grids, consisting of regular arrangement of points and solving the inverse kinematics at each point to see if it belongs to workspace or not [41]. It is important to take note that a manipulator designed for a maximum workspace may lead to undesirable kinematics characteristics such as poor dexterity or manipulability. Therefore, the quality of the workspace must also be considered while maximizing it [72]. A verity of workspace quality indices have been proposed such as manipulability, dexterity, and stiffness, which most of them depend on the Jacobian

matrix [41]. Therefore, if the Jacobian matrix of a parallel manipulator is well-conditioned (i.e. far away of singularities), the parallel mechanism will have a high quality workspace.

2.1.3 Singularity

Singularity determination is the other goal of an optimal parallel mechanism design. The notion of singularity refers to configurations in which the parallel robot has uncontrollable DOFs instantaneously. The occurrence of singularity configurations must be avoided during motion, as the actuators cannot control the motion even in the neighborhood of these singular configurations. As a consequence, the knowledge of singularities is vital for control purposes and singularity-free path planning. One of the first works to address the configuration singularity analysis of general closed-loop mechanisms was done by Gosselin and Angeles [22]. In this work, the singularity configurations were classified into three main groups, namely the forward, inverse and combined singularity, based on the properties of the Jacobian matrix of the parallel mechanism.

The classical method of determining singularity configurations is finding the roots of the determinant of the Jacobian matrix [41] i.e. $\det \|\mathbf{J}\| = 0$ or $\det \left\|\mathbf{J}^T\mathbf{J}\right\| = 0$. The first step involves calculation of the determinant while the second step involves finding its roots within the workspace, which is challenging, as the determinant is nonlinear in the pose parameters. Intuitive geometry methods such as Grassmann Line geometry [24] and unified geometric approaches [85], have been utilized to determine these singularities. Numerical approaches have also been proposed to obtain the information on the nearness of a singular configuration, based on the fact that the end-effector forces become extremely large near singularity configurations.

In conclusion, the understanding of the singularities and their relations with the kinematic parameters and the workspace is of ultimate importance in design, planning and control of parallel mechanisms.

2.2 Cable-Driven Robots

A *cable-driven robot* (CDR) or cable-driven mechanism (CDM) is a mechanism that utilizes light flexible cables instead of heavy rigid links to position the end-effector as shown in Figure 1.2. With multiple cables attached to the end-effector, it is manipulated by motors that can extend or retract the cables, allowing them to have a large motion range compared to conventional actuators.

The concept of CDRs was first introduced in the early 1980's where the Defense Advances Research Projects Agency (DARPA) sponsored the National Institute of Standard and Technology (NIST) a project on robot crane technology called the ROBOCRANE for use in shipping ports [11]. As shown in Figure 2.2 it is similar to an upside down six degrees-of-freedom Stewart platform, but with six cables instead of hydraulic-cylinder legs. In this system, gravity is an implicit actuator that ensures the cables are always in tension.

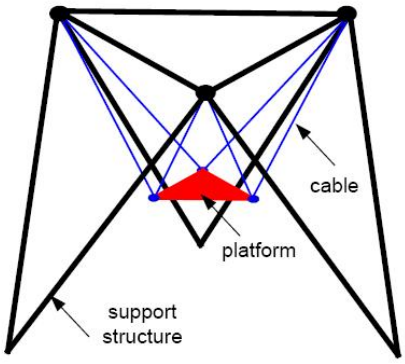

Figure 2.2: The ROBOCRANE developed by NIST [1]

The basic idea of ROBOCRANE was the utilization of Stewart Platform parallel link manipulators but with the unique features of utilizing cables as parallel links and winches as the actuators to control the length of the cables. As long as all the cables are in tension, the load is kinematically constrained and there exists a known mathematical relationship between the length of the cables and the position of the platform. ROBOCRANE was recognized to have the benefits of allowing an operator to locate and orient a load without sway and oscillation. In addition, it does not require any counterweight and experiences negligible twisting or bending moments due to its octahedral geometry. As a result it can lift at least five times of its own weight, which is significantly more than any robot or crane in use.

With the above benefits, and depending on what is suspended from its platform, the ROBOCRANE could perform a variety of tasks such as material handling, inspection, pipe fitting and manufacturing operations such as welding, sawing and grinding [10]. Several versions of the ROBOCRANE are shown in Figure 2.3, including a ROBOCRANE mounted to a mobile base (Figure 2.3.(a)), a ROBOCRANE used as a gantry crane (Figure 2.3.(b)) and a ROBOCRANE modified to handle pallets of munitions (Figure 2.3.(c)).

In 1994, Ming and Higuchi [42, 43] provided a basic understanding of CDRs. Their work presented the necessary and sufficient conditions for positioning by cables, the rigid link equivalent of cables in positive tension and a general classification of CDRs. Cables have the unique property of unilaterality that cannot bear compression (i.e. cannot push onto the end-effector). It can only exert tensions when it is fully stretched, hence requiring a pre-tension. In CDRs the position of the end-effector is controlled by the length of the cables attached to it. Therefore, the unilateral property of cables implies that when a cable is no longer in positive tension (or active), the position of the end-effector is no longer under control as well. The necessary and sufficient condition for controlling the position of the end-effector with positive cable tensions was also stated by Ming and Higuchi [43].

(a) Robocrane mounted to mobile bases [8]

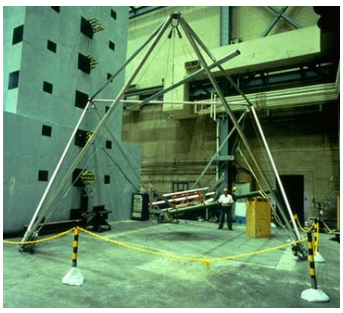

(b) Robocrane as a Gantry Crane [8]

(c) Robocrane modify to handle munitions [8]

Figure 2.3: The ROBOCRANE Application.

It was mathematically proven that a CDM with n DOFs, requires a minimum of (n+1) active cables to fully restrain the end-effector. Following this, they proposed a kinematically equivalent rigid-link mechanism for an active cable, consisting of a spherical joint at both ends of a prismatic joint (SPS) as shown in Figure 2.4. In addition, they have presented a classification of CDRs [43].

2.2.1 Classification of Cable-Driven Robots

Cable-driven robots can be divided into two categories, based on whether there are sufficient cables to provide complete constraint for the end-effector. Assuming number of cables m and number of degrees of freedom n, the cable-driven robots can be classified into *incompletely restrained* (m<n+1) and *fully restrained* (m≥n+1)

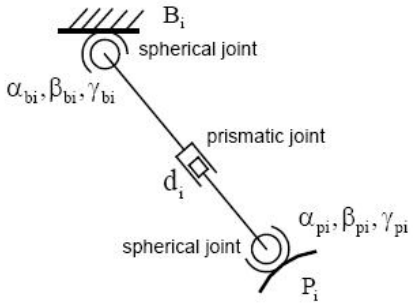

Figure 2.4: Equivalent Mechanism of a Cable [42]

as illustrated in Figure 2.5. The fully restrained robots can be further classified into completely restrained (m=n+1) and redundantly restrained (m>n+1).

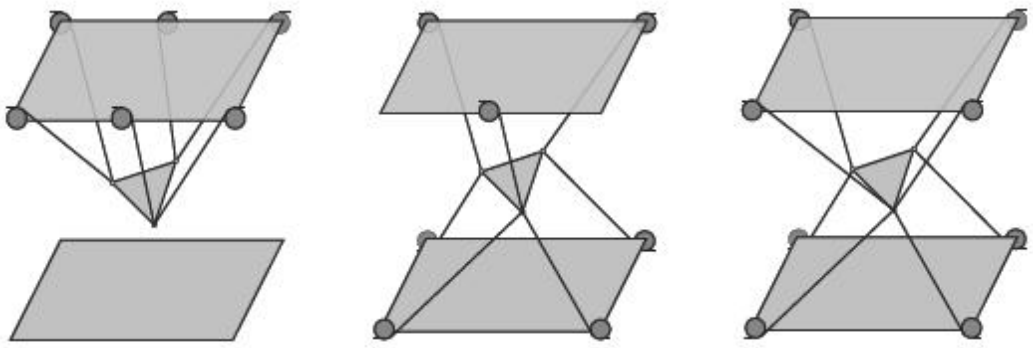

(a) Incompletely Restrained (m<n+1)

(b) Completely Restrained (m=n+1)

(c) Redundantly Restrained (m>n+1)

Figure 2.5: Classification of Cable-Driven Robots [54]

Incompletely restrained cable-driven robots: Figure 2.5(b) shows an incompletely restrained cable-driven robot. For such a robot, only certain degrees of freedom (DOF) of the moving platform can be realized by kinematic constraints. Motion on the other DOFs is governed by the dynamics of moving platform and cables. Hence, external forces like gravity should be applied to get additional (non-kinematic) constraints. These robots have more typically designed for applications where large workspace is required. Because of the incompleteness of constraints, the end-effector which is driven by this type of robots such as conventional crane

is easy to swing. To overcome this problem, dynamics control strategies need to be considered for precision control of the end-effector.

A point mass cable-driven robot (Figure 2.6) is a special group of incompletely restrained cable robots, in which all cables attach to a single point on the end-effector and can change lengths to control the position of the end-effector. Typically the end-effector is modeled as a lumped mass located at the point of intersection of the cables. Although in many cases the center of mass of the end-effector is not truly located at the point of intersection of the cables, the distance of this offset is assumed small in comparison to the scale of the manipulator. Point-mass cable robots are well suited to perform operations similar to those of construction cranes (positioning an end-effector but not controlling its orientation). However, a cable-driven robot has significantly less swaying of the payload than a crane in performing the same operation due to its parallel structure. This class of robots is also useful for camera positioning operations and is a promising candidate for rapidly-deployable manipulators for disaster relief [9].

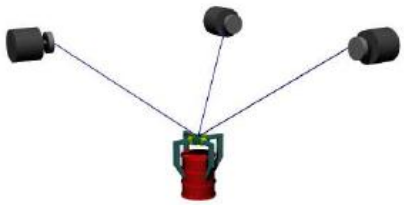

Figure 2.6: A Point-mass Cable-Driven Robot [9]

Fully restrained cable-driven robots: For fully restrained cable-driven robots, all the DOFs can be determined by using kinematics of the mechanism. For such a robot, there exists actuation redundancy. Although redundant actuation is an effective approach for enlarging workspace and avoiding singularity, sophisticated tension distribution need to be investigated. These robots are further divided into

completely restrained as shown in Figure 2.5(b) and redundantly restrained as shown in Figure 2.5(c). Completely restrained cable robot is a special case of fully restrained robots in which the minimum number of cables (m = n+1) is used. Fully restrained cable-driven robots have often been designed for applications that require high speed, high acceleration or high stiffness. High stiffness can be achieved by pre-tensioning the cables. However, these manipulators have their own problems such as the possibility of cables interfering with the end-effector, surroundings and each other and necessity of large number of motors.

2.2.2 Applications

Some of the typical applications of cable-driven robots include hyper-redundant flexible manipulators [62], virtual tennis system [29] shown in Figure 2.7.(a), haptic devices [19], and leg rehabilitation systems [26] shown in Figure 2.7.(b).

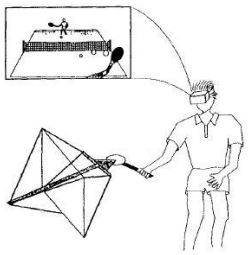

(a) Concept of Virtual Tennis System [29]

(b) Rehabilitation System [26]

Figure 2.7: Typical Application of Cable-Driven Robots.

Cable-driven robots have also been proposed for use in transferring cargo to and from ships. One such system is the Automated All-Weather Cargo Transfer System (AACTS) [16] made by August Design which is shown in Figure 2.8. The system utilizes a large SCARA robotic arm combined (shown in Figure 2.8.(a)) with a rigid hoist to position a six-cable, six degree-of-freedom spreader bar cable-driven robot (shown in Figure 2.8.(b)) that will pick up freight containers from cargo ships in

high sea states. Another manipulator designed for transferring cargo is the Cable Array Robot [20]. The Cable Array Robot was developed at the Pennsylvania State University and is a 4-cable point-mass cable-driven robot. Figure 2.9.(a) shows a prototype of the Cable Array Robot and Figure 2.9.(b) shows a diagram of the Cable Array Robot being used to load containers onto a ship. Another point-mass manipulator is the SkyCam [1], made by August Design. SkyCam is a cable-driven robot that positions a video camera for use in stadiums and indoor arenas (shown in Figure 2.10). The use of under-constrained cable-driven robots has also been proposed for search and rescue in the event of urban earthquakes [67], and pose-measurement systems [69]. Cable-driven robots have even been proposed as bathroom cleaning robots [68].

(a) AACTS Unloading Cargo [16]

(b) Rehabilitation System [16]

Figure 2.8: The Automated All-weather Cargo Transfer System (AACTS) and Intelligent Spreader Bar (ISB)

(a) Prototype of the Cable Array Robot [20]

(b) Diagram of the Cable Array Robot used for loading containers onto a ship [20]

Figure 2.9: The Cable Array Robot

Fully restrained CDRs have often been designed for applications that require

Figure 2.10: The SkyCam [61]

high speed or acceleration or high stiffness. High speed CDRs include the WARP manipulator [37] which uses 8 cables and the FALCON [28], a 7-cable manipulator (shown in Figure 2.11) that was able to achieve accelerations up to 43g. The Charlotte robot (shown in Figure 2.12) is an 8-cable manipulator designed for use inside space structures, where the motors that control the cables are located inside the end-effector [70].

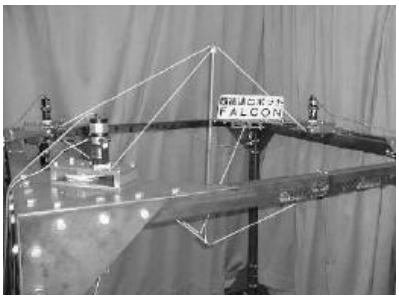

(a) A prototype of the FALCON

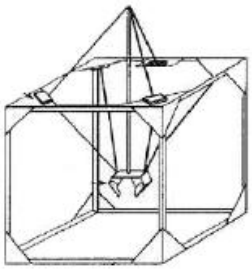

(b) A diagram of the FALCON

Figure 2.11: The FALCON [28]

2.2.3 Kinematic Analysis

Kinematic analysis is to determine the kinematic relations between the task space and the cable space (or the joint space). All cables are supposed to be in tension so that they are in straight lines. Therefore, kinematic analysis of cable-driven robots is related to that of rigid-link parallel mechanisms. Similar to the parallel manipu-

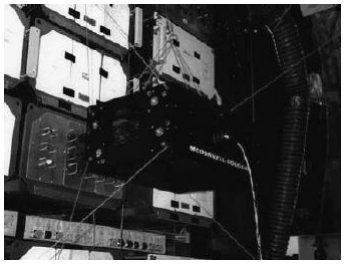

Figure 2.12: The Charlotte Developed By McDonnel Douglas [70]

lators with rigid links, the forward kinematics is difficult because of its closed-loop structures, while the inverse kinematics is relatively simple as it can be decoupled into each of the cables. Hence, one challenging issue in kinematics analysis is the forward displacement analysis, i.e., to determine the end-effector pose with given cable's lengths. Because of the coupled motion characteristics of a cable-driven robot, multiple forward displacement solutions exist. As a result, previous efforts are focused on the numerical algorithms based on Newton-Raphson methods [80]. However, such a method has two drawbacks. First, it can only give one solution each time. Second, the solution largely depends on the initial guess solution. Ming and Higuchi [42] have made use of results of rigid-link parallel mechanisms by obtaining the pose of the n-DOF platform from m cable lengths. This is followed by utilizing inverse kinematics to obtain the lengths of the remaining lengths of (m-n) cables. Generally, it is also found not convenient for a general cable-driven robot. This makes the numerical-iterative approach being widely utilized because numerical-iterative methods generally result in a faster generation of the forward displacement solution and can be expanded for any cable-driven robot.

2.2.4 Tension Analysis

Since cables can only pull but cannot push the end-effector, the cable tension becomes one of the most important issues in analyzing the kinetostatic performance

of the fully restrained cable-driven robots. Cable tension must be constrained positively so that it can control the end-effector. Currently, the null space approach has been widely used in constraining the tension. For completely restraint robots, the homogeneous solution degenerates to a column vector which its components can be obtained in symbolic forms. However, for redundantly restraint robots, this approach has been found to be difficult because the redundancy of cables results in difficulty of obtaining homogeneous solutions [50, 57]. Another approach is known as a geometrical method in which tension vectors form convex polyhedrons and the external wrench is checked as to whether it is inside the convex set or not [88]. However, this approach becomes more challenging for mechanisms with higher dimensional task-spaces, i.e. the number of DOFs of the end-effector is greater than three, and for applications that require a complicated set of force and moment. Moreover, as the minimum tension is taken into account, this approach is much more complicated.

2.2.5 Workspace Analysis

Several different workspaces have been addressed previously. A number of researchers have investigated the set of all poses that the end-effector can attain statically (with no external forces or moments acting besides gravity called Static Equilibrium Workspace) [1], [2]. In most cases formulation of the Static Equilibrium Workspace has been done numerically via *brute force* methods, where the entire task space is discretized and exhaustively searched to find the statically reachable poses. One exception is in Fattah [17], where the boundaries of the Static Equilibrium Workspace were defined analytically for an under constrained and fully-constrained planar cable-driven robot. However, this was done for a special geometry end-effector and does not generalize to other geometries. Another workspace that has been researched is the 'dynamic workspace', defined in [5] as

the set of all poses where the end-effector can be given a specific acceleration. This workspace was determined for a planar cable-driven robot by analytically forming the workspace boundaries. The *Wrench-Feasible Workspace* is defined as the set of poses where the manipulator can counteract a specified set of wrenches. For many applications the Wrench-Feasible Workspace constitutes the *usable workspace* of the manipulator. While the Wrench-Feasible Workspace has been defined in general terms [18], it has generally been formed numerically using an exhaustive search approach [37], [74], [73]. The boundaries of the *Wrench-Feasible Workspace* were determined analytically for planar 4-cable fully-constrained cable robots in [23], assuming infinite upper tension limits. Some additional workspaces that are very similar to the *Wrench-Feasible Workspace* have also been defined. In [23] the *force-closure workspace* was introduced, which is a special case of the *Wrench-Feasible Workspace* where only forces are considered. The *workspace with tension conditions* [75], [76] is defined similarly to the *Wrench-Feasible Workspace* with the additional constraint that all cable tensions must remain above a minimum tension value and below a maximum tension value. The *workspace with stiffness conditions* [76] is defined similar to the *Wrench-Feasible Workspace*, with the additional constraint that the stiffness of the end-effector should be above a threshold value. Some researchers have also incorporated workspace limits based on cable interference, but these workspace limits were determined either experimentally or numerically [80]. There are several similar concepts that have been developed by other researchers. The *capable force region* is defined in [53] as the set of forces that the manipulator can exert without consideration for the associated moments. In [58], [59] a 3-cable planar cable robot with point-mass end-effector was examined and a *set of manipulating forces* was formed. This is the set of all forces that the 3 cables could exert on the end-effector. A similar set of wrenches was also defined in [5] and termed a *pseudo-pyramid*. This pseudo-pyramid includes the set of all wrenches (force/moment combinations) that the cables could apply to the

end-effector at a pose if the cables have no upper tension limits. Besides workspace quantization, it is also important to determine the quality of the workspace, since a mechanism designed for a maximum workspace may lead to undesirable kinematic characteristics such as poor dexterity or manipulability. Various performance indices such as the velocity/force ellipsoid, the condition number, and the manipulability measure have been devised for assessing kinematic performance of robotic manipulators.

2.2.6 Design Optimization

Due to the importance of workspace, various cable-driven robots design problems are formed to optimize the workspace. Similar to parallel mechanisms, the goals of an optimal design include workspace maximization and singularity minimization, but with additional goals of optimal tension distributions. In order to compensate the limited workspace and low stiffness, redundancy (increasing the number of cables) has been generally introduced [65], although it makes the design and control aspects more complex. Redundant actuation enlarges the workspace and increases the stiffness of the mechanism through the use of internal forces among the cables [12]. Cable-driven hybrid robots have also been proposed to increase the stiffness of cable robots [62].

2.2.7 Dynamic Analysis

It is known that dynamic modeling is essential to improve the control system when a mechanism has to provide high velocity and acceleration motion. Dynamics modeling is concerned with relating the Cartesian motion of the end-effector to the required joint torques. Due to the cable actuation, the dynamic modeling of cable-driven robots is different from that of parallel rigid-link mechanisms. Similar to

tension analysis, torque equation is an under-determined system. Torque solution has to be solved systematically in a limited torque range (from $\tau_{\min}$ to $\tau_{\max}$). The value $\tau_{\min}$ is required to keep the cables taut, whereas the value $\tau_{\max}$) is limited by the maximum torque of actuators or by the maximum allowable tension within the cables. Besides, for dynamic analysis, the cables are assumed to be mass-less and perfectly stiff so that their inertias and spring stiffness can be ignored.

2.2.8 Control

As stated before, cables have one unique property; that is they carry loads in tension but not in compression. Due to this feature, well known approaches in robotics for trajectory planning and control are not directly applicable to cable robots. Moreover, one of the major issues in the control of CDRs is maintaining positive cable tensions. Researchers used different strategies for controlling the cable robots. Some of the proposed control strategies are reviewed here for incompletely restrained, completely restrained, and redundantly restrained CDRs.

2.2.8.1 Control of incompletely restrained CDRs

Yanai and Yamamoto [84] presented a feedback control method for general incompletely restrained wire-suspended mechanisms. Because of the incompleteness of the constraint for the suspended object, the object is easy to swing. To overcome this problem, the authors considered inverse dynamics of the object for precise control. In this method the end-effector is controlled along a trajectory with no swing by adopting a dynamic control method for the mechanism using the inverse dynamic calculation. The response of the system was not highly affected by changing the parameters, because the nonlinearity of the mechanism is compensated by the

inverse dynamic calculations. As a result, this control method (called *anti-swing*) restrained swing of the object along the whole trajectory of the object motion.

Maier and Woernle [38] proposed a novel cable suspension manipulator CABLEV (Figure 2.13) and used flatness-based control architecture to control it. A cascade feedback structure including tracking and anti-swing controller and trolley/winches motion controller was used to asymptotically stabilize the tracking behavior of the system.

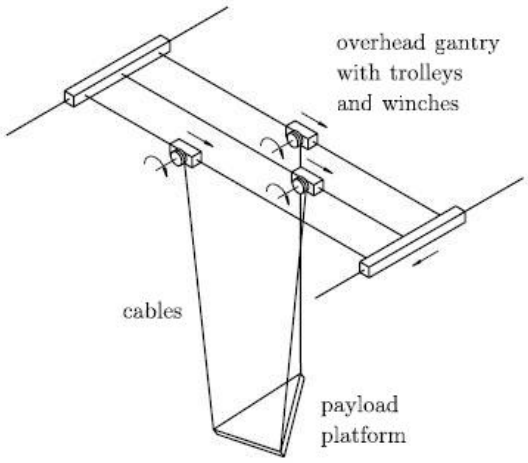

Figure 2.13: The Cable Suspension Manipulator CABLEV [38]

Alp and Agrawal [3] obtained the dynamic model of a six-degrees-of-freedom cable suspended robot shown in Figure 2.14. They designed two controllers for the cable suspended robot using *Lyapunov controller* method and *feedback linearization* method. Through computer simulations the effectiveness of the controllers were investigated and compared. Since proportional and derivative terms were used, both controllers achieved the desired steady-state values with errors. Finally the controllers were implemented on the real hardware to validate the theory with experimental results. They also mentioned that the cable friction and using the encoder on the motors with forward kinematics to obtain the feedback are some

potential sources of the error in the experiment.

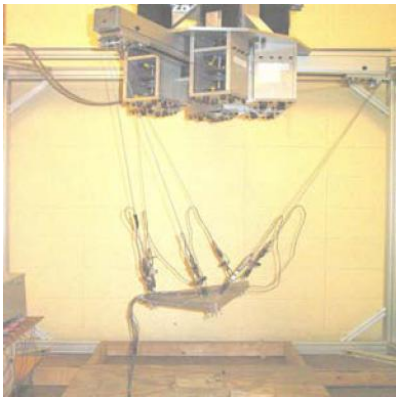

Figure 2.14: 6-DOF Cable Suspended Robot [3]

So-Ryeok Oh [50] designed a controller for non-redundant cable robots under input constraints using the method of a *reference governor* (RG). The control design is based on feedback linearization augmented with RG. RG solves the constraint problem at a hierarchical level so that the feedback linearization controller of the inner loop can stabilize the plant and provide good tracking in the absence of constraints. An algorithm was also introduced to predict the system's future behavior by obtaining the analytical solution of the system states using the dynamics of inner feedback loop. Finally the effectiveness of the program was illustrated through a Matlab Simulink program.

A sliding-mode controller has also been applied to cable robots in [49]. This sliding mode controller deals with the characterization of the feasible workspace for set point control of a cable-suspended robot under input constraints and disturbances. The implemented sliding mode controller acts as a stabilizing controller for a given uncertain system. The proposed method estimates the admissible workspace for set-point control. The computational procedures to obtain the admissible workspace consist of calculating the range of system states during motion in terms of set-points by solving the reaching condition ($\dot{S} > q$) and sliding mode ($S = 0$) and replacing all the states in the control law with their upper and

lower values in such a way that the positive input constraints were met. Effects of the disturbances on the set-point's feasible region were also investigated.

2.2.8.2 Control of completely restrained and redundantly restrained CDRs

Kawamura [28] described the development of an ultra high speed cable-driven robot called FALCON, based on the cable-driven parallel manipulators. This robot can achieve peak accelerations of up to 43g and maximum velocities of 13 (m/sec). Due to the use of wires in actuation, the problem of vibration arises which is solved by employing internal force control among the wires and implementing point to point control using linear PD feedback. The use of wires with nonlinear spring characteristics improved the system transient response, but it also complicates the study of the stability.

Kino [30] investigated the principle of *orthogonalization* for completely restrained parallel-wire driven systems. This principle clarified the relation between wire tension and driving force-moment on the object. Since wire length can be easily obtained by calculation of Euclidean norm between endpoints of the wire, under an assumption that an endpoint of wire in each actuator is fixed, the feedback control in the wire length coordinates is a widely used method for the parallel-wire systems. Therefore, a Lyapunov function using the principle of orthogonalization has been introduced to prove the motion convergence of wire length feedback scheme for general parallel-wire robots with more than n+1 wires.

Morizono and Kurahashi [44] proposed a force display system using parallel wire mechanism for virtual sports training with high speed motion (Figure 2.15). They investigated the dynamic characteristics of the parallel wire mechanism through a simple model. In addition, some control laws were proposed based on the dynamic characteristics of the parallel wire mechanism.

Figure 2.15: Realized Virtual Tennis System [44]

They modeled a 1-DOF system (Figure 2.16) and considered the equivalent stiffness of the motor unit and cables by measuring the deflection of the cable under certain amount of tensions with a laser ranger. Using the dynamic equations of motion, they implement a tension feedback law with a high gain feedback to compensate the nonlinear effects of the elasticity of the system. However, there was a limitation of the feedback gain because of the stability problem. They also implemented a *tension and reaction force* (**T R F**) feedback law to reduce the dynamic effects of the grip handle. The effectiveness of the control law has been demonstrated through basic experiments.

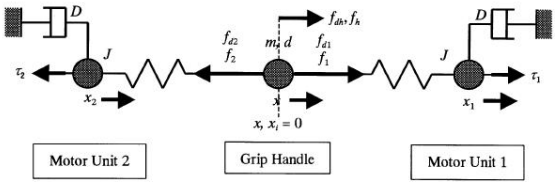

Figure 2.16: Model of One-DOF Force Display System [44]

Williams and Gallina [79] presented a hybrid parallel/serial manipulator architecture where translational freedom is provided by a cable direct driven robot (CDDR) and the rotational freedoms is provided by a serial wrist mechanism. They presented three cables and four cables CDDR with two and one degree of actuation

redundancy, respectively. They presented kinematics and static modeling of CDDR and a method to maintain positive cable tension. They also presented a dynamics modeling of hybrid parallel/serial manipulator using a Cartesian dynamic model for the end-effector and actuator, and finally combine them to obtain the dynamic model of the whole system. In addition, a control architecture of the CDDR and a method to calculate optimal actuator torques was presented.

Williams and Vadia [82] presented a hardware implementation of a planar, translational cable direct-driven robot (CDDR). They presented kinematics and static modeling of the CDDR along with the method to maintain positive cable tension and implemented them on CDDR hardware for experimental verification. Only translational CDDR was considered and it was tried to attempt zero orientation by control. They used four independent length PD controllers. Cable lengths were calculated online using the encoder feedback for each cable pulley. It was found that the whole theoretical static workspace could not be achieved in hardware as it was difficult to move the end-effector in the region close to the edges of the static workspace as it was approaching the singularity points.

So-Reyok Oh and Agrawal [51] proposed a control approach for a cable suspended robot with redundant cables to follow prescribed trajectories. They sketched the feasible workspace for a planar cable robot with one, two, and three extra cables (one, two, and three degrees of redundancy respectively) at a point during motion. The feasible space was a line for one extra cable and increases in dimension by one, i.e., became an area with two extra cables and a volume as a third cable was added. They have formulated the controller design problem to keep positive tensions in the cables using Linear Programming (LP) and Quadratic Programming (QP). By simulations, they have investigated the proposed methods. The algorithm was also tested experimentally on a 3-DOF planar cable robot (Figure 2.17) to show the feasibility of the control strategy. These methods were classified as point-wise since they do not ensure continuity of the cable tensions as the trajectory evolves

in time.

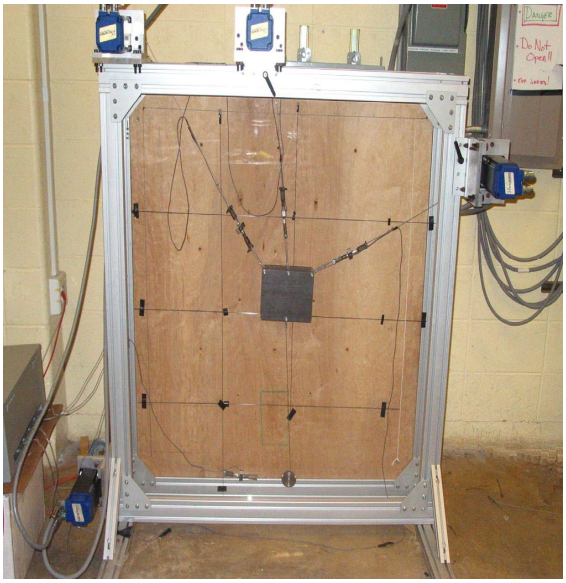

Figure 2.17: Planar Cable Robot [51]

Kalyan [27] presented a dynamic model for a dual-stage planar cable robot (shown in Figure 2.18), incorporating the disturbance from the sea condition. In addition, a robust controller for end-effector control was developed. The problem of positive cable tensions was tackled using redundancy. This redundancy was then used to assure positive tensions in cables and keep the uncontrolled states within the specified bounds. A sliding-mode controller (SMC), which belongs to a class of variable structure systems (VSS), is considered for the control of the dual-stage cable robot in the presence of uncertainties, since SMC not only provides a robust and accurate response, but also makes the system response insensitive to changes in the system parameters and load disturbances. It is assumed that all the cables keep positive tensions during the motion and the actuators are ideal and cable stiffness is longitudinally large to instantaneously carry the wrench torque to the end-effector. The designed controller based on sliding mode theory can asymptotically stabilize the system to desired position ($\mathbf{X}_d$) as long as cables are in tension during the motion. Also simulation results using Matlab Simulink showed

the proposed control strategy, which uses the system redundancy to satisfy the positive tension and minimize the uncontrolled states.

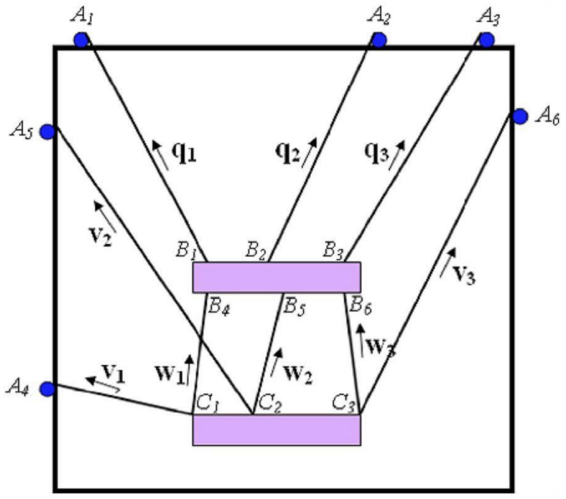

Figure 2.18: Planar Cable Robot [51]

2.3 Summary

In this chapter, literatures of parallel mechanisms and cable-driven robots have been surveyed. Different issues such as kinematic, tension, workspace, dynamic, and control of cable-driven robots have been reviewed completely. Cable-driven robots have raised significant attention because of their advantages such as large workspace and low weight. The unilateral property of cables is the main issue in cable-driven robots, i.e. keeping the cables in tension is the goal of the design process. By adding more cables (redundancy) we get more opportunity to keep all the cables in tension, but on the other hand the analysis of the system and control strategy become more complicated. Although a lot of work have been carried out on the kinematic analysis and workspace determination of the cable-driven robots, the control issues have not been well investigated. Different control approaches have been used for incompletely restraint robots and usually gravity force helps to

guaranty the tension in the cables. However, completely restraint robots suffer from the lack of efficient control methods that have both positional accuracy and tension control, simultaneously. Therefore, it is necessary to investigate the fundamental of control aspects of cable-driven robots.

Chapter 3

Kinematic Modeling

In this chapter, kinematic modeling of a general cable-driven robot is described in details, followed by derivation of the equations for a planar cable-driven robot. This chapter includes the displacement, velocity, and acceleration analysis. The kinematic modeling presented in this chapter is based on the work done by C.B. Pham [54].

3.1 Model Description

In this thesis, a Cable-Driven Robot consists of a single end-effector rigid body supported in parallel by m cables controlled by m actuators. Figure 3.1 shows a general cable-driven robot, in which the end-effector is connected to the base through m active cables, i.e. B_iP_i. P_i is the connecting point on the end-effector and B_i is the suspending point on the base. An inertial fixed reference frame $\{O\}$ is attached to the base and a local body frame $\{P\}$ is attached to the end-effector. In convention, all quantities are written in frame $\{O\}$ unless there is a trailing superscript p which denotes the quantity in frame $\{P\}$.The length of each cable is denoted as l_i.

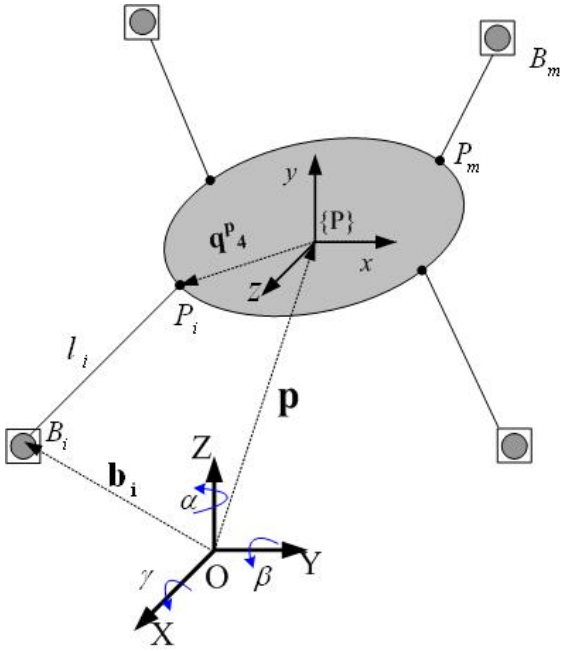

Figure 3.1: Kinematic Diagram of A Cable-Driven Robot

The end-effector position vector in Cartesian space is represented by $\mathbf{p} = \overrightarrow{OP} = \{x \ y \ z\}^T$, which is the position of point P with respect to the reference frame $\{O\}$. The end-effector can have six degrees of freedom in the general case, so with the condition of $m \geq (n+1)$, we will have some degrees of redundancy regarding to the number of cables. This scenario represents actuation redundancy but not kinematic redundancy. That is, there are extra actuators which provide infinite choices for applying 6-DOF Cartesian wrench vectors, but the moving rigid body has only six Cartesian degrees-of-freedom $\{x, y, z, \alpha, \beta, \gamma\}^T$.

3.2 Kinematics Modeling

Kinematics modeling is concerned with relating the active joint variables and rates to the Cartesian pose and rate variables of the end-effector. The intermediate, passive cable lengths and directions and rates are also involved. Hence, the purpose of kinematic analysis is to determine the kinematic relations between the cables as

input and the end-effector as output. Assuming that cables are always in tension, CDR kinematics is similar to parallel-actuated robot kinematics (e.g. [71], [22]). Similar to the parallel manipulators with rigid links, the forward kinematics of a CDR is difficult because of its closed-loop structure, while the inverse kinematics is relatively simple as it can be decoupled into each of the cables. Hence, one challenging issue in kinematic analysis is the forward displacement analysis, i.e. to determine the end-effector pose with given cable's lengths.

3.2.1 Displacement analysis

The purpose of displacement analysis is to derive the kinematic relationship between the driving-cable displacements and the end-effector pose. As shown schematically in Figure 3.1, the frame $\{P\}$ is given with respect to the frame $\{O\}$ by the kinematic transformation matrix $\mathbf{T}_{\mathbf{P}}^{\mathbf{O}}$ as follows:

$$\mathbf{T}_{\mathbf{P}}^{\mathbf{O}} = \begin{bmatrix} \mathbf{R} & \mathbf{p} \\ \mathbf{0} & \mathbf{1} \end{bmatrix} \tag{3.1}$$

where,

$\mathbf{p}=\{x, y, z\}^T$: is the position of point P with respect to the frame $\{O\}$.

$$\mathbf{R} = \begin{bmatrix} c\alpha.c\beta & (-s\alpha.c\gamma + c\alpha.s\beta.s\gamma) & (s\alpha.s\gamma + c\alpha.s\beta.c\gamma) \\ s\alpha.c\beta & (c\alpha.c\gamma + s\alpha.s\beta.s\gamma) & (-c\alpha.s\gamma + s\alpha.s\beta.c\gamma) \\ -s\beta & c\beta.s\gamma & c\beta.c\gamma \end{bmatrix}$$

$\mathbf{R}$ is the orthonormal rotation matrix representing the orientation of frame $\{P\}$ with respect to frame $\{O\}$, in which α, β and γ are the Z - Y - X angular rotations that takes place about an axis in the fixed reference frame$\{O\}$ [14].

The local coordinates of point P_i (the end of the cables) with respect to the frame $\{P\}$ is represented by $\mathbf{q_i^p} = \{q_{i,x}^p \;\; q_{i,y}^p \;\; q_{i,z}^p\}^T$, whereas the fixed coordinates of B_i with respect to the frame $\{O\}$ are represented by $\mathbf{b}_i = \{b_{i,x} \;\; b_{i,y} \;\; b_{i,z}\}^T$. For each of the cables, the following vector loop-closure equation can be written:

$$\overrightarrow{OB_i} + \overrightarrow{B_iP_i} = \overrightarrow{OP} + \overrightarrow{PP_i} \qquad (i = 1, 2, ..., m) \tag{3.2}$$

Hence, the cable lengths are related to the pose of the end-effector via the length (Euclidean norm) of the vector $\mathbf{l_i}$.

$$l_i = ||\overrightarrow{B_iP_i}|| = ||\overrightarrow{OP} + \overrightarrow{PP_i} - \overrightarrow{OB_i}|| = ||\mathbf{p} + \mathbf{R}\,\mathbf{q_i^p} - \mathbf{b_i}|| \tag{3.3}$$

3.2.1.1 Forward Displacement Analysis

The forward displacement analysis is to determine the pose of the end-effector when the lengths of the m cables l_i are known. Equation (3.3) can be squared and written m times, one for each cable, to give m equations in the six unknowns $\mathbf{X}$=(x, y, z, α, β, γ).

$$F_i(\mathbf{X}) = (\mathbf{p} + \mathbf{R}\,\mathbf{q_i^p} - \mathbf{b_i})^T(\mathbf{p} + \mathbf{R}\,\mathbf{q_i^p} - \mathbf{b_i}) - l_i^2 = 0 \qquad (i = 1, ..., m) \tag{3.4}$$

Given the cable lengths li, the forward pose solution calculates the end-effector pose. This problem is not straightforward because it requires the solution of coupled highly non-linear equations and generally results in multiple solutions. Analytical solutions have been presented for similar problems in the past (e.g. [47], [87]).

However, these techniques involve highly complicated symbolic terms and the final result requires finding the roots of a high-order polynomial, which must be performed numerically (for order greater than four). A practical approach is to solve the forward displacement problem numerically using the Newton-Raphson method.

Newton-Raphson Method: For numerical methods, an initial estimated $\mathbf{X_0}$ is chosen arbitrarily. In general, this will not be the root of Equation (3.4). However, there exists a certain $\Delta\mathbf{X}$ which, when added to $\mathbf{X}$, will give the roots of equation. This can be expressed as follows:

$$F_i(\mathbf{X} + \mathbf{\Delta X}) = F_i(\mathrm{x} + \delta\mathrm{x}, \mathrm{y} + \delta\mathrm{y}, ..., \gamma + \delta\gamma) = 0 \quad (\mathrm{i} = 1, 2, ..., \mathrm{m}) \tag{3.5}$$

In order to find this $\Delta\mathbf{X}$, a linear approximation to this function is obtained by taking the first six terms of its *Taylor Series* expansion about the point (x, y, z, α, β, γ).

$$\begin{aligned} F_i(\mathbf{X} + \mathbf{\Delta X}) = F_i(\mathbf{X}) + \left(\frac{\partial F_i(\mathbf{X})}{\partial x}\right)\delta x + \left(\frac{\partial F_i(\mathbf{X})}{\partial y}\right)\delta y + \left(\frac{\partial F_i(\mathbf{X})}{\partial z}\right)\delta z + \\ \left(\frac{\partial F_i(\mathbf{X})}{\partial \alpha}\right)\delta\alpha + \left(\frac{\partial F_i(\mathbf{X})}{\partial \beta}\right)\delta\beta + \left(\frac{\partial F_i(\mathbf{X})}{\partial \gamma}\right)\delta\gamma = 0 \end{aligned} \tag{3.6}$$

Equation (3.6) is a linear system. Hence, the Newton-Raphson Jacobian matrix $\mathbf{J_{NR}}$ can be formulated in the following form:

$$\mathbf{J_{NR}} = \begin{bmatrix} \frac{\partial F_1(\mathbf{X})}{\partial x} & \frac{\partial F_1(\mathbf{X})}{\partial y} & \cdots & \frac{\partial F_1(\mathbf{X})}{\partial \gamma} \\ \frac{\partial F_2(\mathbf{X})}{\partial x} & \frac{\partial F_2(\mathbf{X})}{\partial y} & \cdots & \frac{\partial F_2(\mathbf{X})}{\partial \gamma} \\ \vdots & \vdots & & \vdots \\ \frac{\partial F_m(\mathbf{X})}{\partial x} & \frac{\partial F_m(\mathbf{X})}{\partial y} & \cdots & \frac{\partial F_m(\mathbf{X})}{\partial \gamma} \end{bmatrix} \tag{3.7}$$

Starting from an initial guess $\mathbf{X_0}$, the process for step (k + 1) is:

- Solve $\mathbf{J_{NR}}\mathbf{\Delta X}_k = -F(\mathbf{X}_k)$ for $\mathbf{\Delta X}_k$:

$$\mathbf{\Delta X}_k = -\mathbf{J}^{+}_{\mathbf{NR}} F(\mathbf{X}_k) \tag{3.8}$$

- Then let $\mathbf{X}_{k+1} = \mathbf{X}_k + \mathbf{\Delta X}_k$.
- Iterate until: $||\delta \mathbf{X}_k|| < \varepsilon$

Where $\mathbf{J}^{+}_{\mathbf{NR}} = (\mathbf{J}^{\mathbf{T}}_{\mathbf{NR}}\mathbf{J}_{\mathbf{NR}})^{-1}\mathbf{J}^{\mathbf{T}}_{\mathbf{NR}}$ is the pseudo-inverse of over constrained Jacobian matrix $\mathbf{J_{NR}}$, $\delta(\mathbf{X}) = \{\delta x,\ \delta y,\ \delta z,\ \delta\alpha,\ \delta\beta,\ \delta\gamma\}^T$, and ε is a user-defined tolerance (ε can be different for translational and rotational terms).

Generally, the convergence rate of the method depends on the initial guess $\mathbf{X_0}$. In continuous motion of the end-effector, using the previous solution as the initial guess generally yields convergence to the proper solution.

3.2.1.2 Inverse Displacement Analysis

The inverse displacement analysis is to determine the lengths of cables l_i with the given end-effector pose. Comparing with the forward displacement analysis, the inverse displacement analysis is simple and straightforward. A unique solution can be determined for each of the cables if the pose of the end-effector is given. In Equation (3.3), the length of each cable can be directly calculated from the given pose (x, y, z, α, β, γ) of the end-effector as follows:

$$l_i^2 = \mathbf{p^T\,p} + \mathbf{q_i^{pT}\,q_i^p} + \mathbf{b_i^T\,b_i} + \mathbf{2p^T\,R\,q_i^p} - \mathbf{2p^T\,b_i} - \mathbf{2b_i^T\,R\,q_i^p} \quad (i = 1, ..., m) \tag{3.9}$$

3.2.2 Velocity Analysis

The purpose of velocity analysis is to determine the relationship between the velocity of end-effector and the rate of change of the cable lengths. The instantaneous kinematic relationship between the translational velocity of the driving-cables and the velocity of the end-effector is generally expressed by:

$$\dot{\mathbf{L}} = \mathbf{J}_{\chi}\, \dot{\boldsymbol{\chi}} \tag{3.10}$$

where

$\dot{\mathbf{L}} = \{\dot{l}_1, \dot{l}_2, ..., \dot{l}_m\}^T$: is the vector of rate of change in cable lengths,

$\mathbf{J}_{\chi}$: is the Jacobian matrix expressed in reference frame $\{O\}$,

$\dot{\boldsymbol{\chi}} = \{\mathbf{v}, \boldsymbol{\omega}\}^T = \{\dot{x}, \dot{y}, \dot{z}\ ,\ \omega_x, \omega_y, \omega_z\}^T$, $\mathbf{v}$ is the vector of translational velocities and $\boldsymbol{\omega}$ is the vector of rotational velocities about the body axis of the end-effector.

With the representation of orientation which is based on Z-Y-X angles, the mapping from the angular velocity $\{\omega_x, \omega_y, \omega_z\}^T$ to the instantaneous values of the angle set $\{\dot{\gamma}, \dot{\beta}, \dot{\alpha}\}^T$ is expressed as follows [14]:

$$\boldsymbol{\omega} = \begin{Bmatrix} \omega_x \\ \omega_y \\ \omega_z \end{Bmatrix} = \begin{bmatrix} c\alpha.c\beta & -s\alpha & 0 \\ s\alpha.c\beta & c\alpha & 0 \\ -s\beta & 0 & 1 \end{bmatrix} \begin{Bmatrix} \dot{\gamma} \\ \dot{\beta} \\ \dot{\alpha} \end{Bmatrix} \tag{3.11}$$

By differentiating equation (3.3) with respect to time, we have:

$$\begin{aligned}\dot{l}_i &= \tfrac{d}{dt}||\mathbf{l_i}|| = \tfrac{1}{||\mathbf{l_i}||}\tfrac{d}{dt}\left[\tfrac{1}{2}||\mathbf{l_i}||^2\right] = \tfrac{1}{2||\mathbf{l_i}||}\tfrac{d}{dt}\left[||\mathbf{p}+\mathbf{R}\,\mathbf{q_i^p}-\mathbf{b_i}||^2\right] \\ &= \tfrac{1}{2||\mathbf{l}_i||}\tfrac{d}{dt}\left[||\mathbf{p}||^2+||\mathbf{R}\,\mathbf{q}_i^p||^2+||\mathbf{b}_i||^2+2\mathbf{p}^T\mathbf{R}\,\mathbf{q}_i^p-2\mathbf{p}^T\mathbf{b}_i-2\mathbf{b}_i^T\mathbf{R}\,\mathbf{q}_i^p\right] \\ &= \tfrac{1}{||\mathbf{l}_i||}\left[(\mathbf{p}+\mathbf{R}\,\mathbf{q}_i^p-\mathbf{b}_i).\mathbf{v}+(\mathbf{p}-\mathbf{b}_i)^{\mathbf{T}}\dot{\mathbf{R}}\mathbf{q}_i^p\right] \\ &= \tfrac{1}{||\mathbf{l}_i||}\left[\mathbf{l}_i.\mathbf{v}+(\mathbf{p}-\mathbf{b}_i).\dot{\mathbf{R}}\,\mathbf{q}_i^p\right]\end{aligned} \tag{3.12}$$

Working on the rotational term, since $\dot{\mathbf{R}}\,\mathbf{q}_i^p = \boldsymbol{\omega}\times\boldsymbol{R}\,\mathbf{q}_i^p$, we have:

$$\begin{aligned}&(\mathbf{p}-\mathbf{b}_i).\dot{\mathbf{R}}\,\mathbf{q}_i^p = (\mathbf{p}-\mathbf{b}_i).[\boldsymbol{\omega}\times\mathbf{R}\,\mathbf{q}_i^p] = \boldsymbol{\omega}.[\mathbf{R}\,\mathbf{q}_i^p\times(\mathbf{p}-\mathbf{b}_i)] \\ &= \boldsymbol{\omega}.[\mathbf{R}\,\mathbf{q}_i^p\times(\mathbf{p}-\mathbf{b}_i+\mathbf{R}\,\mathbf{q}_i^p)] = \boldsymbol{\omega}.[\mathbf{R}\,\mathbf{q}_i^p\times\mathbf{l}_i] \\ &= \omega.(-\mathbf{l}_i\times\mathbf{R}\mathbf{q}_i^p)\end{aligned} \tag{3.13}$$

Where we have used $a\cdot(b\times c) = b\cdot(c\times a)$ and $(a\times b) = a\times(b+a)$. Now the relationship between one cable rate and the Cartesian rates is:

$$\dot{l}_i = \frac{1}{||\mathbf{l}_i||}\left[\mathbf{l_i}.\mathbf{v}+\boldsymbol{\omega}.(-\mathbf{l}_i\times\mathbf{R}\,\mathbf{q}_i^p)\right] = \begin{bmatrix}\hat{\mathbf{l}}_i^T & -(\hat{\mathbf{l}}_i\times\mathbf{R}\,\mathbf{q}_i^p)^T\end{bmatrix}\begin{Bmatrix}\mathbf{v}\\ \boldsymbol{\omega}\end{Bmatrix} \tag{3.14}$$

Where, $\hat{\mathbf{l}}_i = \frac{\mathbf{l}_i}{||\mathbf{l}_i||}$ is a unit vector in the i^{th} cable direction with respect to $\{O\}$. Therefore, the Jacobian matrix is:

$$\mathbf{J}_\chi = \begin{bmatrix}\hat{\mathbf{l}}_1^T & -(\hat{\mathbf{l}}_1\times\mathbf{R}\mathbf{q}_1^p)^T\\ \hat{\mathbf{l}}_2^T & -(\hat{\mathbf{l}}_2\times\mathbf{R}\mathbf{q}_2^p)^T\\ \vdots & \vdots\\ \hat{\mathbf{l}}_m^T & -(\hat{\mathbf{l}}_m\times\mathbf{R}\mathbf{q}_m^p)^T\end{bmatrix} = \begin{bmatrix}\hat{\mathbf{l}}_1^T & -(\hat{\mathbf{l}}_1\times\mathbf{q}_1)^T\\ \hat{\mathbf{l}}_2^T & -(\hat{\mathbf{l}}_2\times\mathbf{q}_2)^T\\ \vdots & \vdots\\ \hat{\mathbf{l}}_m^T & -(\hat{\mathbf{l}}_m\times\mathbf{q}_m)^T\end{bmatrix} \tag{3.15}$$

3.2.3 Singularity

In a serial-chain robotic arm, kinematic singularities physically correspond to configurations where the robot loses one or more degrees-of-freedom. For parallel-manipulators, kinematic singularities physically correspond to configurations where the device gains additional, unwanted, or uncontrollable degrees-of-freedom. Therefore, a singularity configuration is obviously undesirable and should be excluded from the workspace. Equation (3.15) is a useful equation for investigating the singularity configuration in cable-driven robots. Through rank analysis of Jacobian matrix $\mathbf{J}_\chi$, the forward kinematics singularity configurations can be identified. Kinematic singularities occur at configurations where the Jacobian matrix $\mathbf{J}_\chi$ has less than full rank. It means if $rank(\mathbf{J}_\chi) < n$ (where n is the dimension of Cartesian space), then kinematic singularity occurs. In the neighborhood of kinematic singularities, the determinant $|\mathbf{J}_\chi \mathbf{J}_\chi^T|$ approaches zero and cables must apply infinity tensions to overcome these configurations.

3.2.4 Acceleration Analysis

Acceleration analysis deals with the relationship between the translational acceleration of the cables and the acceleration of the end-effector. By applying acceleration analysis we can calculate the kinematic changes of the cables length as the end-effector is tracking a specified trajectory. The linear accelerations of the cables can be obtained by differentiating equation (3.10) with respect to time directly.

$$\ddot{\mathbf{L}} = \mathbf{J}_\chi \ddot{\boldsymbol{\chi}} + \frac{d}{dt}(\mathbf{J}_\chi)\ \dot{\boldsymbol{\chi}} \tag{3.16}$$

where

$\ddot{\mathbf{L}} = \{\ddot{l}_1, \ddot{l}_2, ..., \ddot{l}_m\}^T$: is the vector of cable accelerations.

$\ddot{\boldsymbol{\chi}} = \{\ \mathbf{a}\ \ \dot{\boldsymbol{\omega}}\ \}^T = \{\ddot{x}, \ddot{y}, \ddot{z}, \dot{\omega}_x, \dot{\omega}_y, \dot{\omega}_z\}^T$: $\mathbf{a}$ is the vector of translational accelerations and $\dot{\boldsymbol{\omega}}$ is the vector of rotational accelerations about body axis of the end-effector. Therefore, the general acceleration equation will be in the following form:

$$\ddot{\mathbf{L}} = \mathbf{J}_\chi \begin{Bmatrix} \ddot{x} \\ \vdots \\ \dot{\omega}_z \end{Bmatrix} + (\tfrac{\partial \mathbf{J}_\chi}{\partial x}\dot{x} + \tfrac{\partial \mathbf{J}_\chi}{\partial y}\dot{y} + \cdots + \tfrac{\partial \mathbf{J}_\chi}{\partial \gamma}\dot{\gamma}) \begin{Bmatrix} \dot{x} \\ \vdots \\ \omega_z \end{Bmatrix} \tag{3.17}$$

3.2.5 Kinematic Relations for a Planar Cable-Driven Robot

A planar cable-driven robot is shown in Figure 3.2, in which the end-effector is connected to the base through four cables, i.e. B_1P_1, B_2P_2, B_3P_3, and B_4P_4. The pose of the end-effector is given by (x, y, φ), where φ is the orientation angle of frame $\{P\}$ about the Z-axis. Rewriting the vector-loop closure equation we have:

$$\begin{aligned} \mathbf{l}_i &= \mathbf{p} + \mathbf{R}\,\mathbf{q}_i^p - \mathbf{b}_i \\ l_i &= ||\mathbf{l}_i|| = ||\mathbf{p} + \mathbf{R}\,\mathbf{q}_i^p - \mathbf{b}_i|| \end{aligned} \tag{3.18}$$

Where, $\mathbf{p} = (x, y)^T$ is the position vector of point P expressed in the reference frame $\{O\}$, and $\mathbf{R} = \begin{bmatrix} \cos\varphi & -\sin\varphi \\ \sin\varphi & \cos\varphi \end{bmatrix}$ represents the orientation of end-effector with respect to reference frame $\{O\}$ in planar configuration.

Inverse Kinematic for a Planar Cable-Driven Robot: By expanding equation (3.18), the cable lengths l_i can be calculated from equation (3.19).

$$\begin{aligned} l_i^2 = {} & x^2 + y^2 + {q_{i,x}^p}^2 + {q_{i,y}^p}^2 + b_{i,x}^2 + b_{i,y}^2 \\ & + 2x(q_{i,x}^p \cos\varphi - q_{i,y}^p \sin\varphi - b_{i,x}) + 2y(q_{i,x}^p \sin\varphi - q_{i,y}^p \cos\varphi - b_{i,y}) \\ & - 2(q_{i,x}^p b_{i,x} + q_{i,y}^p b_{i,y})\cos\varphi + 2(q_{i,y}^p b_{i,x} - q_{i,x}^p b_{i,y})\sin\varphi \end{aligned} \tag{3.19}$$

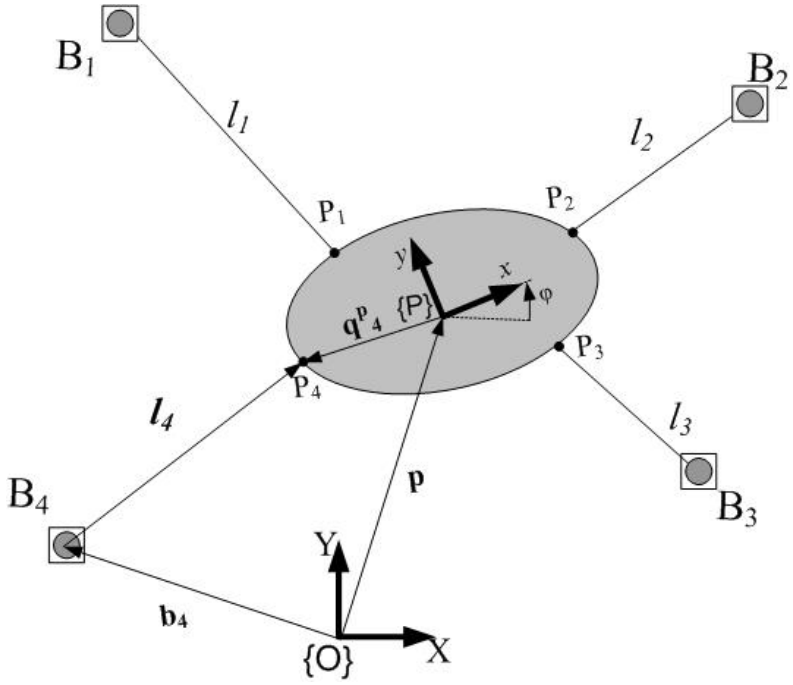

Figure 3.2: Kinematic Diagram of a Planar Cable-Driven Robot

Computational Example of Inverse and Forward Kinematics: In order to verify the effectiveness of the numerical methods, computational examples are provided for symmetric planar CDR, which its kinematic parameters are shown in Figure 3.3, with 2a = 2b = 1.0 m and 2c = 0.1 m, 2d=0.08 m.

The verification process was consist of obtaining the cables' length from the end-effector poses (inverse kinematics) and then, use these cable lengths as the input of Newton-Raphson algorithm to determine the end-effector pose (forward kinematics). The value of the tolerance ε is set to 0.0001 for x, y, and φ in all cases. Initial values are selected all zero in position as well as in orientation. Three examples have been provided in Table 3.1. The results show that with given cable lengths, all the poses are returned successfully in less than ten iterations. In terms of errors, the positional errors are zero whereas the orientational error is less than 0.05 (degrees).

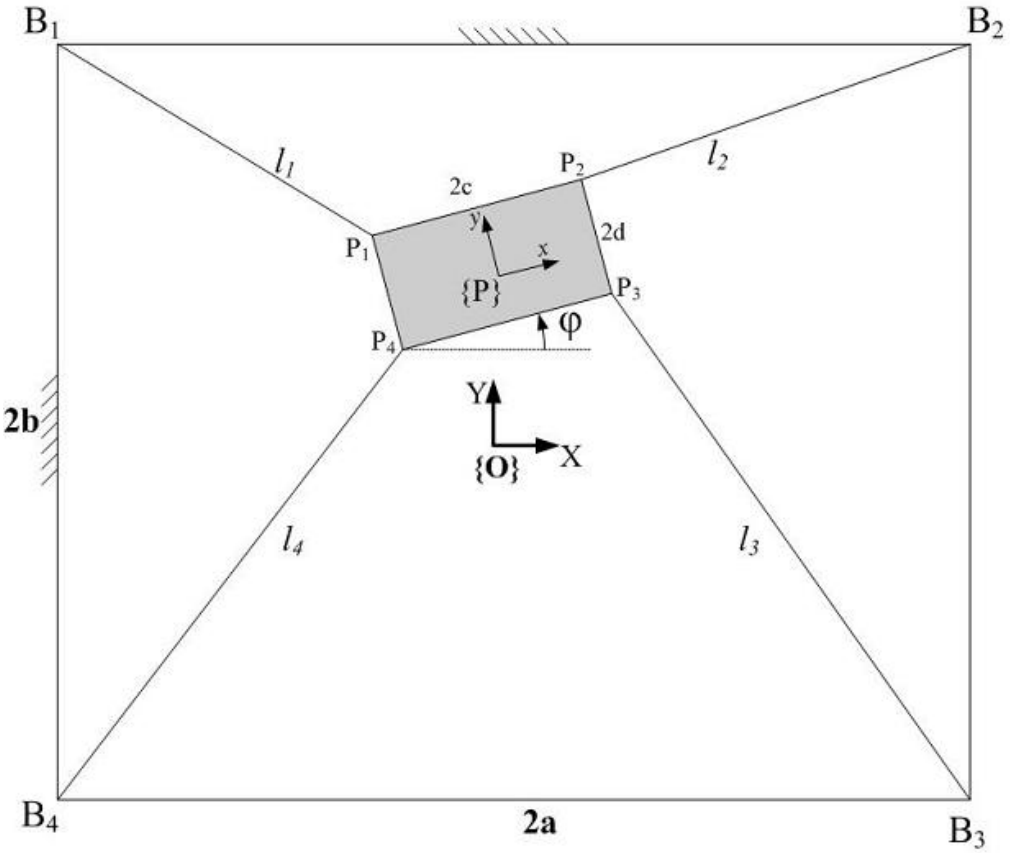

Point	B_1	B_2	B_3	B_4	P_1^P	P_2^P	P_3^P	P_4^P
Coordinate	(-a,b)	(a,b)	(a,-b)	(-a,-b)	(-c,d)	(c,d)	(c,-d)	(-c,-d)

Figure 3.3: Kinematic Diagram of Symmetric Planar CDR

Case		Inverse Kinematics	Forward Kinematics	Error %	No. of Iterations
1	**Input** $x = 0.4$ $y = 0.4$ $\varphi = 5^o$	$l_1 = 0.8492$ l_2 =0.0774 l_3 =0.8658 l_4 =1.2088	**Output** x =0.4 y =0.4 $\varphi = 4.972^o$	 0 0 0.6	8
2	**Input** x = -0.20 $y = 0.10$ $\varphi = 2^o$	$l_1 = 0.4390$ $l_2 = 0.7435$ $l_3 = 0.8581$ $l_4 = 0.6123$	**Output** x = -0.2 $y = 0.1$ $\varphi = 1.994^o$	 0 0 0.3	7
3	**Input** x = -0.1 y = -0.3 $\varphi = -1^o$	$l_1 = 0.8362$ $l_2 = 0.9384$ $l_3 = 0.5732$ $l_4 = 0.3846$	**Output** x = -0.1 y = -0.3 $\varphi = -1.003^o$	 0 0 0.3	6

Table 3.1: Computational examples: Inverse and Forward Kinematics

Velocity Analysis for a Planar Cable-Driven Robot: For a planar cable-driven robot the velocity analysis yields to:

$$\begin{aligned}&\mathbf{l}_i = \mathbf{p} + \mathbf{q}_i - \mathbf{b}_i\\&\begin{Bmatrix} l_{i,x} \\ l_{i,y} \end{Bmatrix} = \begin{Bmatrix} x \\ y \end{Bmatrix} + \begin{bmatrix} \cos\varphi & -\sin\varphi \\ \sin\varphi & \cos\varphi \end{bmatrix} \begin{Bmatrix} q^p_{i,x} \\ q^p_{i,y} \end{Bmatrix} - \begin{Bmatrix} b_{i,x} \\ b_{i,y} \end{Bmatrix}\end{aligned} \tag{3.20}$$

Differentiating Equation (3.20) with respect to time:

$$\begin{aligned}\dot{l}_{i,x} &= \dot{x} - (q^p_{i,x}\sin\varphi + q^p_{i,y}\cos\varphi)\dot{\varphi}\\ \dot{l}_{i,y} &= \dot{y} + (q^p_{i,x}\cos\varphi - q^p_{i,y}\sin\varphi)\dot{\varphi}\end{aligned} \tag{3.21}$$

Knowing that $l_i^2 = l_{i,x}^2 + l_{i,y}^2$, differentiating both side of this equation with respect to time, and substituting equation (3.21) in it we have:

$$\dot{l}_i = J_{i,x}\,\dot{x} + J_{i,y}\,\dot{y} + J_{i,\varphi}\,\dot{\varphi} \tag{3.22}$$

We can re-arrange the equation in a matrix form to have:

$$\begin{Bmatrix} \dot{l}_1 \\ \dot{l}_2 \\ \dot{l}_3 \\ \dot{l}_4 \end{Bmatrix} = \begin{bmatrix} J_{1,x} & J_{1,y} & J_{1,\varphi} \\ J_{2,x} & J_{2,y} & J_{2,\varphi} \\ J_{3,x} & J_{3,y} & J_{3,\varphi} \\ J_{4,x} & J_{4,y} & J_{4,\varphi} \end{bmatrix} \begin{Bmatrix} \dot{x} \\ \dot{y} \\ \dot{\varphi} \end{Bmatrix} = \mathbf{J}_\chi \begin{Bmatrix} \dot{x} \\ \dot{y} \\ \dot{\varphi} \end{Bmatrix} \tag{3.23}$$

where the velocity coefficients $J_{i,x}, J_{i,y}, J_{i,\varphi}$ are:

$$J_{i,x} = \frac{l_{i,x}}{l_i} \tag{3.24}$$

$$J_{i,y} = \frac{l_{i,y}}{l_i} \tag{3.25}$$

$$\begin{aligned} J_{i,\varphi} = & \frac{-l_{i,x}}{l_i}(q_{i,x}^p \sin\varphi + q_{i,y}^p \cos\varphi) \\ & + \frac{l_{i,y}}{l_i}(q_{i,x}^p \cos\varphi - q_{i,y}^p \sin\varphi) \end{aligned} \tag{3.26}$$

Acceleration Analysis for a Planar Cable-Driven Robot: From equations (3.18), (3.19) and (3.23)-(3.26) we have:

$$\mathbf{L} = \begin{Bmatrix} l_1 \\ \vdots \\ l_4 \end{Bmatrix} = \begin{Bmatrix} \sqrt{(x+q_{1,x}-b_{1,x})^2+(y+q_{1,y}-b_{1,y})^2} \\ \vdots \\ \sqrt{(x+q_{4,x}-b_{4,x})^2+(y+q_{4,y}-b_{4,y})^2} \end{Bmatrix} \tag{3.27}$$

$$\dot{\mathbf{L}} = \begin{Bmatrix} \dot{l}_1 \\ \vdots \\ \dot{l}_4 \end{Bmatrix} = \mathbf{J}_\chi \begin{Bmatrix} \dot{x} \\ \dot{y} \\ \dot{\varphi} \end{Bmatrix}$$

$$\ddot{\mathbf{L}} = \begin{Bmatrix} \ddot{l}_1 \\ \vdots \\ \ddot{l}_4 \end{Bmatrix} = \mathbf{J}_\chi \begin{Bmatrix} \ddot{x} \\ \ddot{y} \\ \ddot{\varphi} \end{Bmatrix} + \left(\frac{\partial \mathbf{J}_\chi}{\partial x}\dot{x} + \frac{\partial \mathbf{J}_\chi}{\partial y}\dot{y} + \frac{\partial \mathbf{J}_\chi}{\partial \varphi}\dot{\varphi}\right) \begin{Bmatrix} \dot{x} \\ \dot{y} \\ \dot{\varphi} \end{Bmatrix} \tag{3.29}$$

$$\frac{\partial \mathbf{J}_\chi}{\partial x} = \begin{bmatrix} \frac{\partial J_{1,x}}{\partial x} & \frac{\partial J_{1,y}}{\partial x} & \frac{\partial J_{1,\varphi}}{\partial x} \\ \vdots & \vdots & \vdots \\ \frac{\partial J_{4,x}}{\partial x} & \frac{\partial J_{4,y}}{\partial x} & \frac{\partial J_{4,\varphi}}{\partial x} \end{bmatrix} \tag{3.30}$$

$$\frac{\partial \mathbf{J}_\chi}{\partial y} = \begin{bmatrix} \frac{\partial J_{1,x}}{\partial y} & \frac{\partial J_{1,y}}{\partial y} & \frac{\partial J_{1,\varphi}}{\partial y} \\ \vdots & \vdots & \vdots \\ \frac{\partial J_{4,x}}{\partial y} & \frac{\partial J_{4,y}}{\partial y} & \frac{\partial J_{4,\varphi}}{\partial y} \end{bmatrix} \tag{3.31}$$

$$\frac{\partial \mathbf{J}_\chi}{\partial \varphi} = \begin{bmatrix} \frac{\partial J_{1,x}}{\partial \varphi} & \frac{\partial J_{1,y}}{\partial \varphi} & \frac{\partial J_{1,\varphi}}{\partial \varphi} \\ \vdots & \vdots & \vdots \\ \frac{\partial J_{4,x}}{\partial \varphi} & \frac{\partial J_{4,y}}{\partial \varphi} & \frac{\partial J_{4,\varphi}}{\partial \varphi} \end{bmatrix} \tag{3.32}$$

where,

$$\begin{aligned} \frac{\partial J_{i,x}}{\partial x} &= +\frac{l_{iy}^2}{l_i^3} \\ \frac{\partial J_{i,x}}{\partial y} &= -\frac{l_{ix} l_{iy}}{l_i^3} \\ \frac{\partial J_{i,x}}{\partial \varphi} &= -\frac{l_{iy}(q_{ix} l_{ix} + q_{iy} l_{iy})}{l_i^3} \end{aligned}$$

$$\begin{aligned} \frac{\partial J_{i,y}}{\partial x} &= -\frac{l_{ix} l_{iy}}{l_i^3} \\ \frac{\partial J_{i,y}}{\partial y} &= +\frac{l_{ix}^2}{l_i^3} \\ \frac{\partial J_{i,y}}{\partial \varphi} &= +\frac{l_{ix}(q_{ix} l_{ix} + q_{iy} l_{iy})}{l_i^3} \end{aligned}$$

$$\begin{aligned} \frac{\partial J_{i,\varphi}}{\partial x} &= -\frac{l_{iy}(q_{ix} l_{ix} + q_{iy} l_{iy})}{l_i^3} \\ \frac{\partial J_{i,\varphi}}{\partial y} &= +\frac{l_{ix}(q_{ix} l_{ix} + q_{iy} l_{iy})}{l_i^3} \\ \frac{\partial J_{i,\varphi}}{\partial \varphi} &= -\frac{(q_{ix} l_{iy} - q_{iy} l_{ix})^2}{l_i^3} + \frac{q_i^2}{l_i} - \left(\frac{q_{ix} l_{ix}}{l_i} + \frac{q_{iy} l_{iy}}{l_i}\right) \end{aligned}$$

3.3 Summary

In this chapter, the kinematic analysis of a general cable-driven robot is presented. The forward displacement solution of a general cable-driven robot is approached by the numerical Newton-Raphson method. The inverse displacement solution of a general cable-driven robot is also presented, followed by the derivation of the expressions for the velocity analysis. This relation shows that forward singularity exists in CDRs. It is also noted that velocities of the cables are the linear combination of the linear and angular velocities of the platform through the Jacobian matrix. Finally, expressions of acceleration analysis are derived in details; typically for a planar CDR. They will be employed for calculating joint kinematics as the end-effector is planned along a certain trajectory which is discussed in next chapters. Acceleration analysis of other configurations with different number of cables can be easily developed from equations derived in this chapter.

Chapter 4

Tension Analysis and Stiffness Modeling

In this chapter, tension analysis and stiffness modeling of cable-driven robots are described. In the static condition, cables' tension is the important issue for analyzing the kinetostatic of the cable-driven robots. Based on the tension solution of the cables, the static workspace of planar CDRs is obtained. Moreover, a complete stiffness model of CDRs is described in details.

4.1 Tension Analysis

This section presents the tension analysis for cable-driven robots in static condition. For static equilibrium the sum of external forces and moments exerted on the end-effector by the cables must be equal to the resultant external wrench exerted on the environment. Figure 4.1 shows the end-effector free-body diagram of a cable-driven robot.

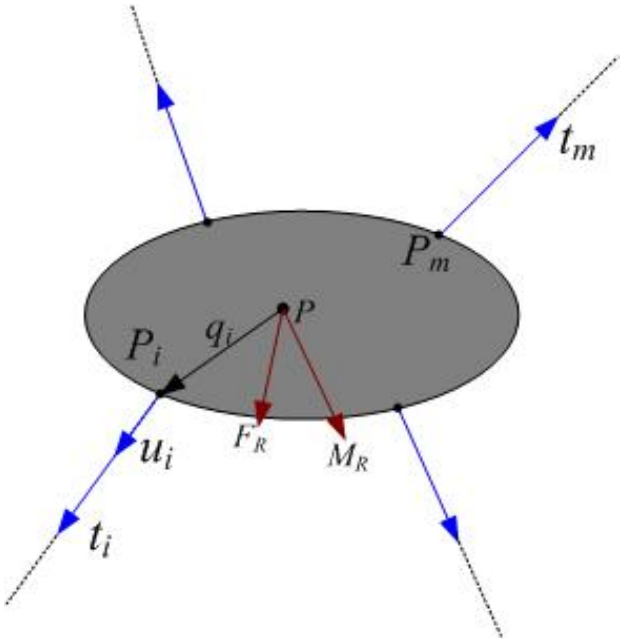

Figure 4.1: Free Body Diagram of The End-Effector

The static equilibrium condition is:

$$\sum_{i=1}^{m} \mathbf{t}_i + \mathbf{F}_R = \mathbf{0} \tag{4.1}$$

$$\sum_{i=1}^{m} \mathbf{q}_i \times \mathbf{t}_i + \mathbf{M}_R = \sum_{i=1}^{m} (\mathbf{R}\,\mathbf{q}_i^p) \times \mathbf{t}_i + \mathbf{M}_R = \mathbf{0} \tag{4.2}$$

In equations (4.1) and (4.2), $\mathbf{t}_i$ is the cable tension applied at the i^{th} cable (in the negative direction of cable length unit vector $\hat{\mathbf{l}}_i$). For simplification we let:

$$\mathbf{u}_i = -\hat{\mathbf{l}}_i = -\frac{\mathbf{l}_i}{||\mathbf{l}_i||} \Rightarrow \mathbf{t}_i = t_i \mathbf{u}_i = -t_i \frac{\mathbf{l}_i}{||\mathbf{l}_i||} \tag{4.3}$$

$\mathbf{R}$ is the orthonormal rotation matrix relating the orientation of P to O; $\mathbf{F}_R$ and $\mathbf{M}_R$ are the resultant vector force and moment (taken together, wrench) exerted on the end-effector. Substituting equation (4.3) into (4.1) and (4.2) yields:

$$\mathbf{S}\,\mathbf{T} = \mathbf{W}_R \tag{4.4}$$

where,

$$\mathbf{S} = \begin{bmatrix} \mathbf{u}_1 & \mathbf{u}_2 & \dots & \mathbf{u}_m \\ \mathbf{q}_1 \times \mathbf{u}_1 & \mathbf{q}_2 \times \mathbf{u}_2 & \dots & \mathbf{q}_m \times \mathbf{u}_m \end{bmatrix} \in \Re^{n\times m}\text{: Structure matrix}$$

$\mathbf{T} = \{\ t_1 \quad t_2 \quad \dots \quad t_m\ \}^T \in \Re^m$: is the vector of cables tension

$$\mathbf{W}_R = -\begin{Bmatrix} \mathbf{F}_R \\ \mathbf{M}_R \end{Bmatrix} \in \Re^n\text{: is the external wrench}$$

Note that $\mathbf{S} = \mathbf{J}_\chi^T$ ($\mathbf{J}_\chi$ is the Jacobian matrix expressed in equation (3.15))

The directional unit vector $\mathbf{u_i}$ (i = 1, 2, ... , m) in the structure matrix $\mathbf{S}$ depends on the posture of the end-effector, which is obtained by the vector loop-closure equation for the cable i as:

$$\mathbf{u_i} = \frac{\overrightarrow{OB_i} - \overrightarrow{OP} - \overrightarrow{PP}_i}{||\overrightarrow{OB_i} - \overrightarrow{OP} - \overrightarrow{PP}_i||} = \frac{\mathbf{b_i} - \mathbf{p} - \mathbf{R}\mathbf{q_i^p}}{||\mathbf{b_i} - \mathbf{p} - \mathbf{R}\mathbf{q_i^p}||} \tag{4.5}$$

For cable-driven robots with actuation redundancy, the system is under constrained (i.e. in equation (4.4), the number of unknown variables (m) is more than the number of equations (n), therefore there are infinite solutions to the cable tension vector $\mathbf{T}$ to exert the required Cartesian wrench $\mathbf{W_R}$.

In the case of m > n, Nakamura [46] has shown that the tension solution can be written by using pseudo-inverse matrix to invert equation (4.4) and obtain the well-known particular and homogeneous solution for the cable tensions as follows:

$$\mathbf{T} = \mathbf{S}^+\,\mathbf{W}_R + (\mathbf{I} - \mathbf{S}^+\,\mathbf{S})\mathbf{Z} \tag{4.6}$$

where,

$\mathbf{S}^{+}= \mathbf{S}^{T}(\mathbf{S}\,\mathbf{S}^{T})^{-1} \in \Re^{m\times n}$: is pseudo-inverse of the structure matrix $\mathbf{S}$

$\mathbf{I} \in \Re^{m\times m}$: is the identity matrix

$\mathbf{Z} = \{\ z_1 \quad z_2 \quad \cdots \quad z_m\}^T$: is an arbitrary column vector

In equation (4.6), the first term $\mathbf{S}^{+}\,\mathbf{W}_R$ is the particular tension solution to achieve the desired wrench $\mathbf{W_R}$. The second term $(\mathbf{I}-\mathbf{S}^{+}\,\mathbf{S})\mathbf{Z}$, which is called the homogeneous solution, is the effect of redundancy that projects $\mathbf{Z}$ into the null space of $\mathbf{S}$. Since the tension solution depends on the degree of redundancy, three cases exist.

Necessary Condition When m=n (*Incompletely Restrained*), we have $\mathbf{S}^{+}= \mathbf{S}^{-1}$ and $(\mathbf{I}-\mathbf{S}^{+}\,\mathbf{S})= \mathbf{0}$, therefore, $\mathbf{T} = \mathbf{S}^{-1}\,\mathbf{W}_R$. In this case, the solution is unique, but there is no guarantee that all of the cables have positive tensions. Hence, the necessary condition for keeping tension of each cable positive is m>n [46].

Sufficient Condition For m>n, two cases can be considered to determine the sufficient condition for keeping cables in positive tension; namely with minimum number of cables m=n+1 (*Completely Restrained*) and with redundant cables m>n+1 (*Redundantly Restrained*).

Minimum Cables (m=n+1): In this case, there is one degree of actuation redundancy which can be used to maintain the positive tension in each cable. The positive cable tension method [58] can be adapted to determine the static workspace. Accordingly, the equivalence of equation (4.6) for this case is:

$$\mathbf{T} = \mathbf{S}^{+}\,\mathbf{W}_R + \lambda\mathbf{N} \tag{4.7}$$

where the homogeneous solution is now expressed as the kernel vector of structure matrix ($\mathbf{N} = \{n_1, n_2, ..., n_m\}^T$) multiplied by an arbitrarily scalar λ.

Using this method to ensure positive tensions t_i on all cables, *for all possible exerted forces and moments*, it is necessary and sufficient that all kernel vector components n_i have the same sign. That is, for a given point to lie within the static workspace, all n_i>0 or all n_i<0. If one of these two conditions is satisfied, regardless of the particular solution, a scalar λ can be found in equation (4.7). This guarantees that all cable tensions $\mathbf{T}$ are positive by adding (or subtracting) enough homogeneous solution. Note that a strict inequality is required; if one or more n_i=0, the configuration in question does not lie within the static workspace. This method is simple but powerful since there is no need to consider a specific wrenches (i.e. it works for all possible wrenches). Note that this method is applicable to any planar and spatial cable-driven robot with one degree of actuation redundancy.

In this approach (the null space approach), the kernel vector can be found by using the Cramer's rule. Therefore, the i^{th} null component is the determinant of the matrix formed by deleting the i^{th} column of the structure matrix $\mathbf{S}$. The sign is opposite from one component to next component. From the expression of $\mathbf{S}$ in equation (4.4), null components can be expressed as:

$$n_i = (-1)^i \begin{vmatrix} \mathbf{u}_1 & \cdots & \mathbf{u}_{i-1} & \mathbf{u}_{i+1} & \cdots & \mathbf{u}_m \\ \mathbf{q}_1 \times \mathbf{u}_1 & \cdots & \mathbf{q}_{i-1} \times \mathbf{u}_{i-1} & \mathbf{q}_{i+1} \times \mathbf{u}_{i+1} & \cdots & \mathbf{q}_m \times \mathbf{u}_m \end{vmatrix} \tag{4.8}$$

After the determination of the kernel vector it is just needed to check if all of

the null components have the same sign (i.e. $\sum_{i=1}^{m} |n_i| = \left| \sum_{i=1}^{m} n_i \right|$ and $n_i \neq 0$). After verifying this condition, the proper scalar λ can be found in order to keep all the cables in tension.

Redundant Cables (m>n+1): When m>n+1, rank($\mathbf{I} - \mathbf{S}^{+}\mathbf{S}$) $= m - n$, the tension solution can be written as equation (4.9) in which m-n independent vectors $\mathbf{N_i}$ $(i = 1, 2, ..., m - n)$ exists [15], such that:

$$\mathbf{T} = \mathbf{S}^{+}\,\mathbf{W}_R + \lambda_1 \mathbf{N}_1 + \lambda_2 \mathbf{N}_2 + \cdots + \lambda_{m-n} \mathbf{N}_{m-n} \tag{4.9}$$

Comparing the above equation with equation (4.7), it is concluded that there are more redundancy, introduced here by (m - n) arbitrary coefficients. Therefore, there are more options to keep the cables in positive tension. However, the determination of null vectors ($\mathbf{N}_i$) and arbitrary coefficients (λ_i) is not straight forward. Some other methods such as *geometrical approach* through the construction of convex polyhedrons [17, 42, 74] and dimension reduction techniques [55] can be used to determine the cables' tensions effectively.

4.1.1 Tension Solution for Symmetric Planar CDRs

The tension solution for the symmetric planar configuration may be written in the following form:

$$T = \begin{Bmatrix} t_1 \\ t_2 \\ t_3 \\ t_4 \end{Bmatrix} = \begin{Bmatrix} t_{P1} \\ t_{P2} \\ t_{P3} \\ t_{P4} \end{Bmatrix} + \lambda \begin{Bmatrix} n_1 \\ n_2 \\ n_3 \\ n_4 \end{Bmatrix} \tag{4.10}$$

In the static condition of a planar cable robot with one degree of actuation redundancy, the cable tensions, are calculated by equation (4.10), choosing (λ) so that one component of $\mathbf{T}$ is zero (or a small positive tension value) and the remaining terms are positive.

In order to verify the effectiveness of this method, the resultant tension for the symmetric configuration of Figure 3.3 is calculated. A minimum tension value $t_{\min}$ is considered to avoid slackness of the cables. For each cable $\lambda_i = \frac{(t_{\min} - t_p)}{n_i}$ is calculated and λ is obtained as the maximum of λ_i's. As an example, following results are obtained for Figure 4.2 with 2a = 2b = 1.0^m and 2c = 0.1 m, 2d=0.08 m . The external wrench is zero and $t_{\min}$=1 N.

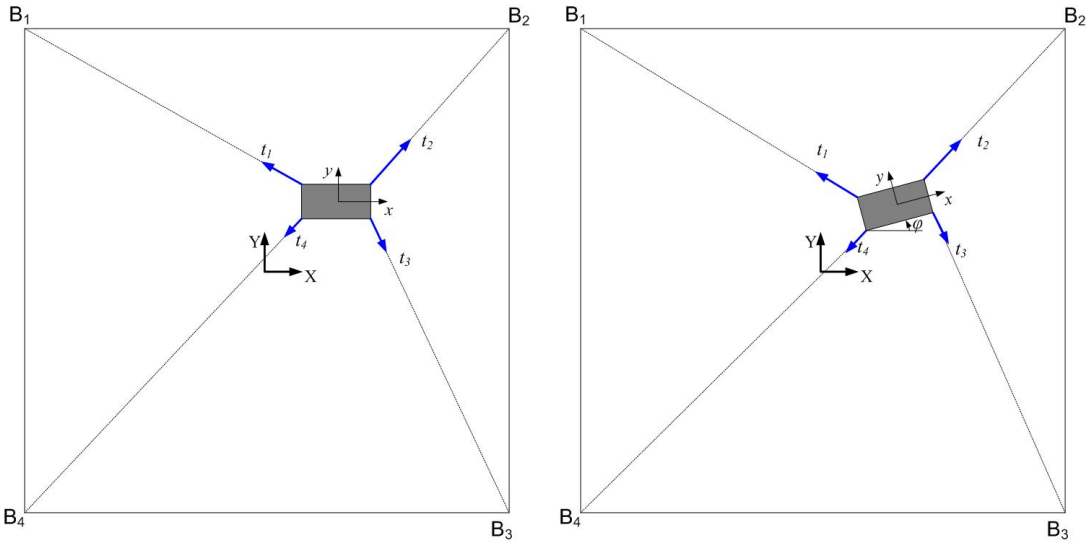

(a) $x = 0.1^m, y = 0.1^m, \varphi = 0^o$

$$T = \begin{Bmatrix} t_1 \\ t_2 \\ t_3 \\ t_4 \end{Bmatrix} = \begin{Bmatrix} 1.4853 \\ 1.9486 \\ 1.6096 \\ 1.0000 \end{Bmatrix}$$

(b) $x = 0.1^m, y = 0.1^m, \varphi = 2^o$

$$T = \begin{Bmatrix} t_1 \\ t_2 \\ t_3 \\ t_4 \end{Bmatrix} = \begin{Bmatrix} 1.1080 \\ 1.7075 \\ 1.2034 \\ 1.0000 \end{Bmatrix}$$

Figure 4.2: Example of Tension Calculation for the Planar CDR

Note that when there is no external wrench applied to the end-effector, the cable with the shorter length will hold a greater tension. Moreover, in this method, the tension in one of the cables is always equal to $t_{\min}$.

The static condition which was described above is a limited subset of the gen-

eral dynamic cases, with high velocities and accelerations. Therefore, dynamics modeling is essential, which will be discussed in the next chapter.

4.1.2 Static Workspace of Symmetric Planar CDR

Static workspace is the set of all poses that the end-effector can attain statically (with no external forces or moments) [1]. In other words, static workspace consists of end-effector poses that satisfy positive tension solution. Therefore, the boundary of the workspace can be generated by letting $\mathbf{W}_R = 0$ in equation (4.7), and obtain the workspace purely based on the null vector ($\mathbf{N}$) analysis. For planar CDR, with one degree of redundancy, the workspace consists of set of postures that satisfy the following constraint:

$$\begin{cases} \sum_{i=1}^{m} |n_i| = \left| \sum_{i=1}^{m} n_i \right| \\ n_i \neq 0 \end{cases} \tag{4.11}$$

Equation 4.11 states that, a posture belongs to the workspace, if all of the null vector components have the same sign. Note that $n_i = 0$ is the representation of workspace boundaries.

As an example, static workspace of planar CDR (figure 3.3), is obtained numerically, by discretizing the entire task space and finding the statically reachable poses for different end-effector orientations (φ). Figure 4.3 shows the static workspace of the planar CDR with $\varphi = 0$, $\varphi = 2^o$, $\varphi = 6^o$, and $\varphi = 7^o$.

The interesting features of the results are that the maximum values of φ occur diagonally across the base and the position with the maximum range of orientations is at the base center. Moreover, it is observed that increasing the orientation, decreases the workspace area; Therefore, planar CDRs have some limitations in the orientation angle (φ).

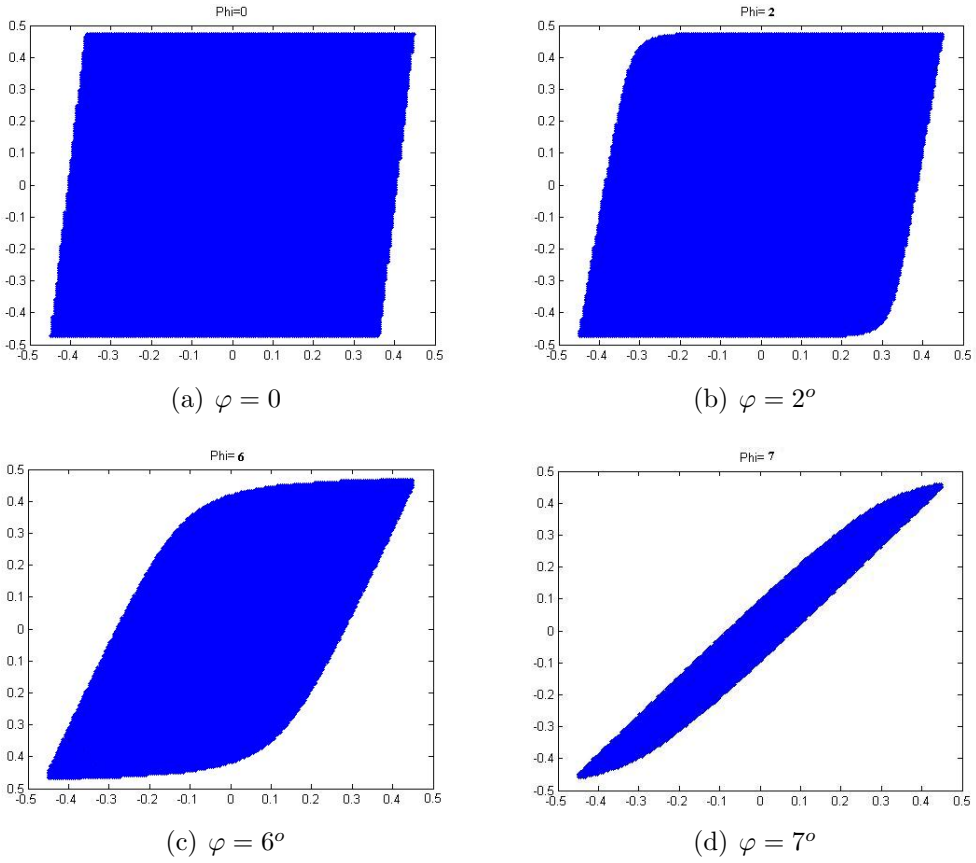

(a) $\varphi = 0$ (b) $\varphi = 2^o$

(c) $\varphi = 6^o$ (d) $\varphi = 7^o$

Figure 4.3: Static Workspace of Planar CDR

4.2 Stiffness Modeling

When a CDR performs a given task, the end-effector exerts wrench (force and moment) on its environment. This contact wrench will cause the end-effector to elastically deviate from its desired motion. The amount of deflection $\delta\mathbf{X}$ is a function of the applied wrench $\mathbf{W}_R$, and the stiffness $\mathbf{K}$ of the robot [40]. The mathematical relation is:

$$\delta\mathbf{W}_R = \mathbf{K}\ \delta\mathbf{X} \tag{4.12}$$

Therefore, the stiffness matrix of the manipulator can be found by taking derivatives of $\mathbf{W_R}$ with respect to $\mathbf{X}$:

$$\mathbf{K} = \frac{d\mathbf{W}_R}{d\mathbf{X}} \tag{4.13}$$

Substituting the static equilibrium equation (4.4) in equation (4.13) yields:

$$\mathbf{K} = \frac{d\mathbf{W}_R}{d\mathbf{X}} = \frac{d(\mathbf{ST})}{d\mathbf{X}} = \mathbf{S}\frac{d\mathbf{T}}{d\mathbf{X}} + \frac{d\mathbf{S}}{d\mathbf{X}}\mathbf{T^0} \tag{4.14}$$

$(\frac{d\mathbf{T}}{d\mathbf{X}})$ can be written as $(\frac{\partial\mathbf{T}}{\partial\mathbf{l}})(\frac{\partial\mathbf{l}}{\partial\mathbf{X}})$ and knowing that $\mathbf{S}^T = \frac{\partial\mathbf{l}}{\partial\mathbf{X}}$, the stiffness matrix becomes

$$\begin{aligned} \mathbf{K} &= \mathbf{K_{passive}} + \mathbf{K_{active}} \\ \mathbf{K}_{passive} &= \mathbf{S\Omega S}^T \\ \mathbf{K}_{active} &= \tfrac{d(\mathbf{S})}{d\mathbf{X}}\mathbf{T^0} \end{aligned} \tag{4.15}$$

where,

$\mathbf{\Omega} = \frac{\partial\mathbf{T}}{\partial\mathbf{l}} = diag(k_1, ..., k_m)$, k_i is the *elastic stiffness* of a cable, which is a function of the cable length, $\frac{d(\mathbf{S})}{d\mathbf{X}}$ is an $(n \times (n \times m))$ matrix and $\mathbf{T^0}$ is the modified tension matrix:

$$\mathbf{T^0} = \begin{bmatrix} \mathbf{T} & \mathbf{0} & \cdots & \mathbf{0} \\ \mathbf{0} & \mathbf{T} & & \mathbf{0} \\ \vdots & & \ddots & \vdots \\ \mathbf{0} & \mathbf{0} & \cdots & \mathbf{T} \end{bmatrix} \in \Re^{((n\times m)\times n)} \tag{4.16}$$

The stiffness of a cable-driven robot is the summation of the two terms (equation (4.15)). The first term, called *passive stiffness* ($\mathbf{K_{passive}}$), represents the force change of an elastic cable with pretension [76], while the second term (*active stiffness* ($\mathbf{K_{active}}$)) is caused by the constant tension forces, that have been applied to

the end-effector. Note that the cable forces considered in $\mathbf{K_{active}}$ are absolutely constant both in magnitude and direction, since any change in these forces is already taken into account in the $\mathbf{K_{passive}}$. However, their moments change upon any rotation of the end-effector and, hence, should be considered in the overall stiffness of the robot. It should be also noted that, if a CDR does not suffer from singularities, then the structure matrix $\mathbf{S}$ is full rank, and the stiffness matrix $\mathbf{K}$ is a symmetric matrix [46].

4.2.1 Stabilizability of a CDR

DEFINITION: *A cable-driven robot is stabilizable if its total stiffness matrix can be made positive definite under any arbitrary load by choosing a proper set of internal forces. Internal forces are cable tensions that satisfy static equilibrium of the end-effector without any external wrench* [6].

Stabilizability of a CDR guarantees the stability of the end-effector in any circumstances as long as the internal forces are large enough. In other words, this property indicates that the end-effector becomes stiffer by increasing the tension in the cables. As a result, the stabilizability of a CDR becomes an essential issue in the design of a robot when a certain payload capacity is required. It can be also concluded that the stabilizability is a necessary condition if cables tension are to be used to improve the stiffness of a CDR. In addition, for a CDR to be stabilizable, at a given pose, it is sufficient and necessary that the end-effector be kinematically non-singular and the stiffness matrix be positive definite [6]. It should be noted that, being kinematically non-singular is equivalent to be located inside the static workspace. In order to elaborate the concept of stabilizability, the stiffness matrix of a single cable robot and a planar CDR is computed in the following section.

4.2.2 Stiffness of a Single Cable

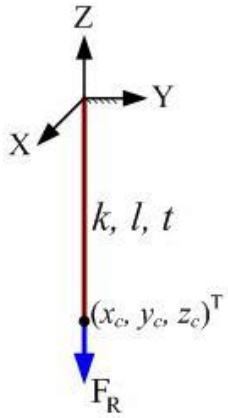

Figure 4.4: A single cable with internal force t_0

Figure 4.4 shows a cable with elastic stiffness coefficient of k, length of l, and tension of t that is statically balanced by force F_R. Using $X = \{x_c, y_c, z_c\}^T$ as the position vector of the cable end, the structure matrix can be easily obtain as $S = (1/l)[x_c, y_c, z_c]^T$ and thus, the stiffness matrix would be (using equation (4.15)):

$$\mathbf{K} = \frac{k}{l^2}\begin{bmatrix} x_c^2 & x_c y_c & z_c x_c \\ x_c y_c & y_c^2 & y_c z_c \\ z_c x_c & y_c z_c & z_c^2 \end{bmatrix} + \frac{t}{l^3}\begin{bmatrix} l^2 - x_c^2 & -x_c y_c & -z_c x_c \\ -x_c y_c & l^2 - y_c^2 & -y_c z_c \\ -z_c x_c & -y_c z_c & l^2 - z_c^2 \end{bmatrix} \tag{4.17}$$

$$= \frac{k}{l^2}\mathbf{X}\,\mathbf{X}^T + \frac{t}{l^3}(l^2\mathbf{I} - \mathbf{X}\,\mathbf{X}^T)$$

where $\mathbf{I}$ is the identity matrix.

It can be shown that this system has a stiffness of k along the cable direction and (t/l) along any direction perpendicular to the cable. For a small displacement

along the cable such as $\varepsilon\mathbf{X}$, where ε is an arbitrary small real number, $\delta\mathbf{F_R}$ which is the change in $\mathbf{F_R}$ can be obtained from :

$$\begin{aligned}\delta\mathbf{F}_R = \mathbf{K}(\varepsilon\mathbf{X}) &= \varepsilon\tfrac{k}{l^2}\mathbf{X}\,\mathbf{X}^T\mathbf{X} + \varepsilon\tfrac{t}{l^3}(l^2\mathbf{I} - \mathbf{X}\,\mathbf{X}^T)\mathbf{X} \\ &= \varepsilon\tfrac{k}{l^2}\mathbf{X}l^2 + \varepsilon\tfrac{t}{l^3}(l^2\mathbf{X} - \mathbf{X}\,l^2) \\ &= k(\varepsilon\mathbf{X})\end{aligned} \tag{4.18}$$

Note that for a single cable $\mathbf{X}^T\mathbf{X} = l^2$. Equation (4.18) indicates that k is the elastic stiffness along the cable direction. Similarly, for a displacement $\mathbf{h}$ normal to the cable direction, i.e. $\mathbf{X^T h} = \mathbf{0}$, we have

$$\begin{aligned}\delta\mathbf{F}_R = \mathbf{K}(\mathbf{h}) &= \tfrac{k}{l^2}\mathbf{X}\,\mathbf{X}^T\mathbf{h} + \tfrac{t_0}{l^3}(l^2\mathbf{I} - \mathbf{X}\,\mathbf{X}^T)\mathbf{h} \\ &= 0 + \tfrac{t_0}{l^3}(l^2\mathbf{h}) \\ &= \tfrac{t_0}{l}(\mathbf{h})\end{aligned} \tag{4.19}$$

Equation (4.19) shows that (t/l) is the stiffness in the normal direction to the cable. In other words, equation (4.19) states that the normal stiffness of a cable increases, by raising the cable tension or shortening its length.

The stiffness matrix for a single cable (equation (4.17)) is a positive definite matrix and its eigenvalues are $(k,\ (t/l),\ (t/l))$, which are all positive. Therefore, the single cable is stabilizable, i.e., we can increase the stiffness of the system by increasing the tension of the cable, provided that the static equilibrium is maintained.

4.2.3 Stiffness of a planar CDR

Assuming all of the cables has the same elastic stiffness ($k_1, ..., k_4$=k), the passive and active stiffness matrices of a planar CDR (Figure 3.3) becomes:

$$\mathbf{K}_{passive} = \mathbf{S\Omega S}^T = \begin{bmatrix} k_{11} & k_{12} & k_{13} \\ k_{21} & k_{22} & k_{23} \\ k_{31} & k_{32} & k_{33} \end{bmatrix} \tag{4.20}$$

where, $l_i = {l_{ix}}^2 + {l_{iy}}^2$: is the i^{th} cable length

$$k_{11} = k \sum_{i=1}^{4} \frac{{l_{ix}}^2}{{l_i}^3}$$

$$k_{12} = k_{21} = k \sum_{i=1}^{4} \frac{(l_{ix})(l_{iy})}{{l_i}^3}$$

$$k_{13} = k_{31} = k \sum_{i=1}^{4} \left[\frac{-l_{ix}\left(q_{ix}^P(s\varphi(l_{ix}) - c\varphi(l_{iy})) + q_{iy}^P(s\varphi(l_{iy}) + c\varphi(l_{ix}))\right)}{l_i^3} \right]$$

$$k_{22} = k \sum_{i=1}^{4} \frac{(l_{iy})^2}{{l_i}^3}$$

$$k_{23} = k_{32} = k \sum_{i=1}^{4} \left[\frac{-l_{iy}\left(q_{ix}^P(s\varphi(l_{ix}) - c\varphi(l_{iy})) + q_{iy}^P(s\varphi(l_{iy}) + c\varphi(l_{ix}))\right)}{l_i^3} \right]$$

$$k_{33} = k \sum_{i=1}^{4} \left[\frac{\left(q_{ix}^P(s\varphi(l_{ix}) - c\varphi(l_{iy})) + q_{iy}^P(s\varphi(l_{iy}) + c\varphi(l_{ix}))\right)^2}{l_i^3} \right]$$

$$\mathbf{K}_{active} = \frac{d(\mathbf{S})}{d\mathbf{X}}\mathbf{T^0} = \begin{bmatrix} \frac{\partial \mathbf{S}}{\partial x} & \frac{\partial \mathbf{S}}{\partial y} & \frac{\partial \mathbf{S}}{\partial \varphi} \end{bmatrix} \mathbf{T^0} \tag{4.21}$$

where,

$\mathbf{S} = \begin{bmatrix} S_{1x} & S_{2x} & S_{3x} & S_{4x} \\ S_{1y} & S_{2y} & S_{3y} & S_{4y} \\ S_{1\varphi} & S_{2\varphi} & S_{3\varphi} & S_{4\varphi} \end{bmatrix}$: is the structure matrix

$$\frac{\partial \mathbf{S}}{\partial x} = \begin{bmatrix} \frac{\partial S_{1x}}{\partial x} & \cdots & \frac{\partial S_{4x}}{\partial x} \\ \frac{\partial S_{1y}}{\partial x} & \cdots & \frac{\partial S_{4y}}{\partial x} \\ \frac{\partial S_{1\varphi}}{\partial x} & \cdots & \frac{\partial S_{4\varphi}}{\partial x} \end{bmatrix}, \frac{\partial \mathbf{S}}{\partial y} = \begin{bmatrix} \frac{\partial S_{1x}}{\partial y} & \cdots & \frac{\partial S_{4x}}{\partial y} \\ \frac{\partial S_{1y}}{\partial y} & \cdots & \frac{\partial S_{4y}}{\partial y} \\ \frac{dS_{1\varphi}}{dy} & \cdots & \frac{dS_{4\varphi}}{dy} \end{bmatrix}, \frac{\partial \mathbf{S}}{\partial \varphi} = \begin{bmatrix} \frac{\partial S_{1x}}{\partial \varphi} & \cdots & \frac{\partial S_{4x}}{\partial \varphi} \\ \frac{\partial S_{1y}}{\partial \varphi} & \cdots & \frac{\partial S_{4y}}{\partial \varphi} \\ \frac{\partial S_{1\varphi}}{\partial \varphi} & \cdots & \frac{\partial S_{4\varphi}}{\partial \varphi} \end{bmatrix}$$

$$\frac{\partial S_{ix}}{\partial x} = \frac{-l_{iy}^2}{l_i^3}$$

$$\frac{\partial S_{iy}}{\partial x} = \frac{\partial S_{iy}}{\partial y} = \frac{l_{iy} l_{ix}}{l_i^3}$$

$$\frac{\partial S_{i\varphi}}{\partial x} = \frac{\partial S_{ix}}{\partial \varphi} = \frac{(q_{ix}s\varphi + q_{iy}c\varphi - q_{ix}c\varphi + q_{iy}s\varphi) l_{iy} l_{ix}}{-l_i^3}$$

$$\frac{\partial S_{iy}}{\partial y} = \frac{-l_{ix}^2}{l_i^3}$$

$$\frac{\partial S_{i\varphi}}{\partial y} = \frac{\partial S_{iy}}{\partial \varphi} = \frac{(q_{ix}c\varphi + q_{iy}s\varphi - q_{iy}c\varphi - q_{ix}s\varphi)(l_{iy} + l_i)(l_{iy} - l_i)}{l_i^3}$$

$$\begin{aligned} \frac{\partial S_{i\varphi}}{\partial \varphi} = \frac{1}{l_i^3} [& (q_{ix}s\varphi + q_{iy}c\varphi) l_{iy} l_i^2 - (q_{ix}c\varphi - q_{iy}s\varphi)^2 l_i^2 + \\ & (q_{ix}c\varphi - q_{iy}s\varphi) l_{iy} (l_{ix} (-q_{ix}s\varphi - q_{iy}c\varphi) + l_{iy} (q_{ix}c\varphi - q_{iy}s\varphi)) + \\ & (q_{ix}c\varphi - q_{iy}s\varphi) l_{iy} l_i^2 + (q_{ix}s\varphi + q_{iy}c\varphi) (q_{ix}c\varphi - q_{iy}s\varphi) l_i^2 - \\ & (q_{ix}s\varphi + q_{iy}c\varphi) l_{iy} l_{ix} (-q_{ix}s\varphi - q_{iy}c\varphi) + l_{iy} (q_{ix}c\varphi - q_{iy}s\varphi)] \end{aligned}$$

The total stiffness matrix for a given posture of the end-effector, can be obtained by adding the passive and active stiffness matrices. If the eigenvalues of the stiffness matrix are all positive, then the end-effector is stabilizable at that pose. Using the concept of stabilizability, a new workspace can be obtained, which is the set of all poses that have positive definite stiffness matrices. This workspace is called *stiffness workspace*, which is a subset of the static workspace, since the tension solution is needed for computation of the active stiffness matric. For the points that belongs to this workspace, it is possible to increase the stiffness by increasing the cables' tension.

In order to further elaborate the concept of stabilizability, the stiffness matrices of two poses has been computed and the results are shown in Table 4.1. The stiffness matrix of the first case is positive definite, i.e.it has positive eigenvalues.

Hence, this pose is stabilizable and belongs to the stiffness workspace. While, for the second case, the stiffness matrix is not positive definite, as it has one negative eigenvalue. Therefore, the second pose is not within the stiffness workspace.

Pose	x=0.1, y=0.1, $\varphi = 0$	x=0.1, y=0.1, $\varphi = 2^o$
$\mathbf{K}_{passive}$	$\begin{bmatrix} 1817.37 & 84.00 & 1.93 \\ 84.00 & 2182.63 & 23.09 \\ 1.93 & 23.09 & 5.50 \end{bmatrix}$	$\begin{bmatrix} 1819.68 & 85.04 & 1.98 \\ 85.04 & 2180.33 & 21.12 \\ 1.98 & 21.12 & 4.58 \end{bmatrix}$
$\mathbf{K}_{active}$	$\begin{bmatrix} -387.6 & 61.99 & 3.45 \\ 61.99 & -316.5 & 0.33 \\ 3.45 & 0.33 & -4.2 \end{bmatrix}$	$\begin{bmatrix} -396.7 & 73.17 & 3.21 \\ 73.17 & -326.2 & 0.27 \\ 3.21 & 0.27 & -4.59 \end{bmatrix}$
$\mathbf{K} = \mathbf{K}_{pas} + \mathbf{K}_{act}$	$\begin{bmatrix} 1429.77 & 146.00 & 5.38 \\ 146.00 & 1866.13 & 23.42 \\ 5.38 & 23.42 & 1.30 \end{bmatrix}$	$\begin{bmatrix} 1422.98 & 158.21 & 5.19 \\ 158.21 & 1854.13 & 21.39 \\ 5.19 & 21.39 & -0.01 \end{bmatrix}$
Eigenvalues	[1910.8, 1385.4, 1.0]	[1906.2, 1371.2, -0.3]
Comments	Stabilizable	Un-stabilizable

Table 4.1: Computational examples of stiffness matrix

The total stiffness matrix of a planar CDR can also be expressed as:

$$\mathbf{K} = \begin{bmatrix} k_{xx} & k_{xy} & k_{x\varphi} \\ k_{yx} & k_{yy} & k_{y\varphi} \\ k_{\varphi x} & k_{\varphi y} & k_{\varphi\varphi} \end{bmatrix} \tag{4.22}$$

where k_{xx}, k_{yy} are the translational stiffness, $k_{\varphi\varphi}$ is the torsional stiffness, and k_{xy}, $k_{x\varphi}$, $k_{y\varphi}$ are the cross stiffness terms. The computational examples illustrate that, the diagonal elements (k_{xx}, k_{yy}) are much more greater than the other elements, which means that CDRs' suffer from low torsional stiffness and should not be used in applications that require high torsional stiffness.

Figure 4.5, shows the stiffness workspace of planar CDR in black and the static workspace in blue. As it was explained, the stiffness workspace is a sub-set of static workspace, and its area decreases by increasing the orientation of the end-effector (φ).

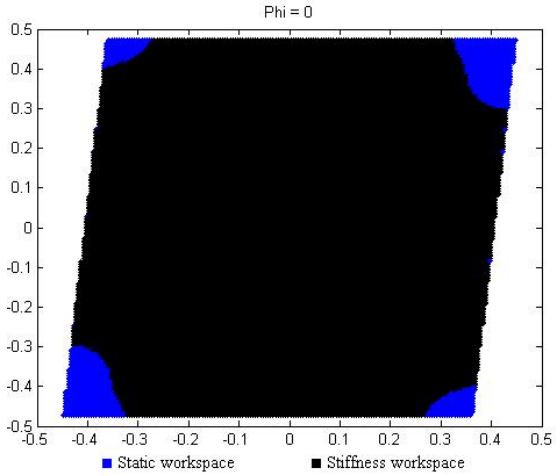

(a) $\varphi = 0$

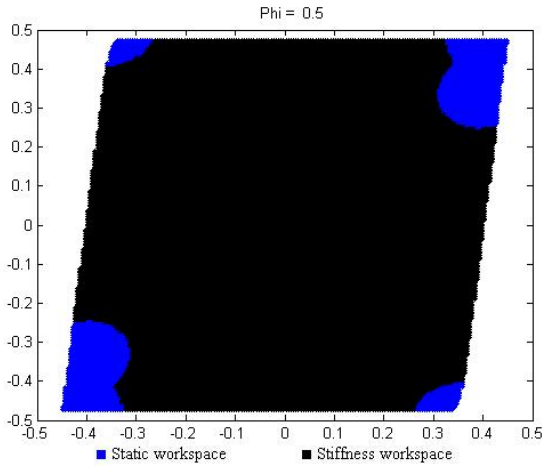

(b) $\varphi = 0.5^o$

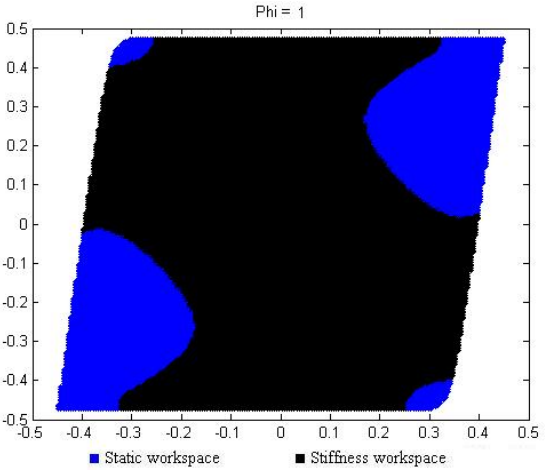

(c) $\varphi = 1^o$

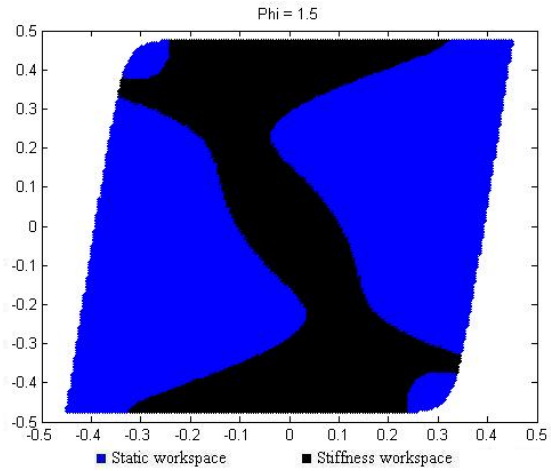

(d) $\varphi = 1.5^o$

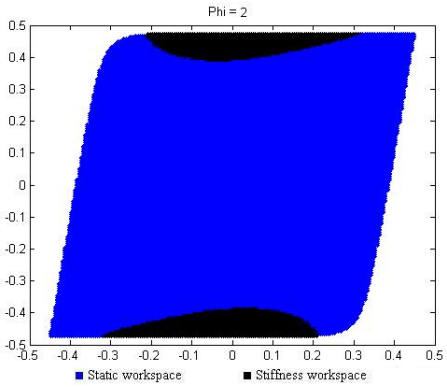

(e) $\varphi = 2^o$

Figure 4.5: Comparison of Stiffness and Static Workspace of Planar CDR

4.3 Summary

In this chapter, first the tension solution of CDRs was discussed and based on the existence of positive tension solution, the static workspace of the planar CDR was obtained. It was also concluded that the orientation range of the end-effector within the workspace is very limited. Second, the complete stiffness model of planar CDRs was formulated, including the passive and active stiffness model. Finally, the concept of the stabilizability was introduced and the stiffness workspace was generated. It was observed that the stiffness workspace is a sub-set of the static workspace. Moreover, the torsional stiffness of the CDR is much lower than the translational stiffness, which means that CDRs are not appropriate for the applications that require high torsional stiffness.

The tension, stiffness, and workspace analysis in this chapter was based only on the static condition of the end-effector. However, with high accelerations, the tensions of the cables will be affected considerably by the inertial forces. Therefore, dynamic modeling is needed to be studied, which is presented in the next chapter.

Chapter 5

Dynamic Modeling

This chapter presents dynamic modeling of cable-driven robots. Dynamic modeling is required for improved control (compared to using kinematics and static modeling only), when CDRs are needed to provide high velocities and accelerations in motion. Dynamic modeling is concerned with relating the motion of the end-effector to the required active joint torques. The motion of the end-effector can be decomposed into the translational motion of an arbitrary point fixed to the end-effector, and the rotational motion of the end-effector about that point. The dynamics equations of the end-effector can also be represented by two equations: one describes the translational motion of the centroid (Newton's equation), while the other describes the rotational motion about the centroid (Euler's equation). Due to the cable actuation, CDRs dynamic modeling is not very similar to parallel-actuated robots [22,71]. Another complicating factor is that the joint space is over constrained with respect to the Cartesian space due to redundant actuation.

For the dynamics model derived in this thesis it is assumed that all of the cables are mass-less and perfectly stiff so that their inertias or spring stiffness are not considered. Linear viscous friction is also modeled to account for the frictional losses. Despite these simplifications, the resulting model is coupled and highly

nonlinear. The end-effector, actuator, and overall system dynamic models are presented here.

5.1 End-effector Dynamic Model

The dynamic equations of a general cable-driven robot using Newton's second law is given here; an alternative derivation using the Lagrangian approach that takes into account the cable tension model is also presented in Appendix B.

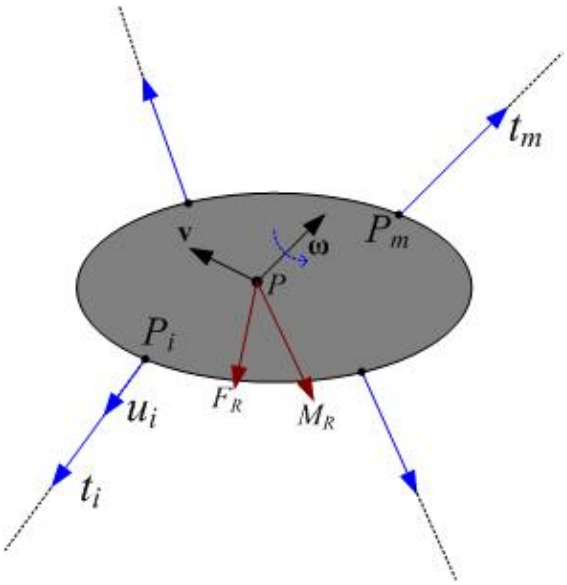

Figure 5.1: Free Body Diagram of End-effector

$$\sum \mathbf{t}_i + m_e\mathbf{g} + \mathbf{F}_R = m_e\dot{\mathbf{v}} \tag{5.1}$$

$$\sum \mathbf{q}_i \times \mathbf{t}_i + \mathbf{M}_R = \mathbf{I_e}\,\dot{\boldsymbol{\omega}} + \boldsymbol{\omega} \times (\mathbf{I_e}\,\boldsymbol{\omega}) \tag{5.2}$$

where,

m_e: is the mass of the end-effector.

$\mathbf{I_e}$: is the inertia tensor of end-effector with respect to body axis

$\mathbf{g}$: is the gravitational acceleration vector.

$\mathbf{v}, \boldsymbol{\omega}$: are velocity and angular velocity of the centroid of the end-effector.

By combining Equations (5.1) and (5.2) in to the matrix form, the end-effector dynamic equation of motion will be:

$$\mathbf{S}\,\mathbf{T} = \mathbf{W} \tag{5.3}$$

where,

$\mathbf{S} = \begin{bmatrix} \mathbf{u}_1 & \mathbf{u}_2 & \cdots & \mathbf{u}_m \\ \mathbf{q}_1 \times \mathbf{u}_1 & \mathbf{q}_2 \times \mathbf{u}_2 & \cdots & \mathbf{q}_m \times \mathbf{u}_m \end{bmatrix} \in \Re^{n \times m}$: Structure matrix

$\mathbf{T} = \{t_1, t_2, ..., t_m\}^T \in \Re^m$: Tension vector

$\mathbf{W} = \begin{Bmatrix} m_e \dot{\mathbf{v}} - m_e \mathbf{g} - \mathbf{F}_R \\ \mathbf{I_e}\,\dot{\boldsymbol{\omega}} + \boldsymbol{\omega} \times \mathbf{I_e}\,\boldsymbol{\omega} - \mathbf{M}_R \end{Bmatrix} \in \Re^n$: Dynamic wrench acting on the end-effector

Equation (5.3) is similar to the static equation of CDRs (4.4), with the difference that the external wrench ($\mathbf{W}_R$) is replaced by dynamic wrench ($\mathbf{W}$). Therefore, the null space method that was explained in chapter 4, can be used here for obtaining the dynamic cables' tension, provided that dynamic terms are included in the dynamic wrench.

5.2 Actuator Dynamic Model

In this section, the dynamic behavior of the lumped motor shaft and cable winding drum is considered; the free body diagram for the motor shaft and cable winding

drum subsystem is shown in Figure 5.2. The combined dynamics equation of the cable winding unit including the motor, the reduction gear, and the cable winding drum is expressed by the relationship:

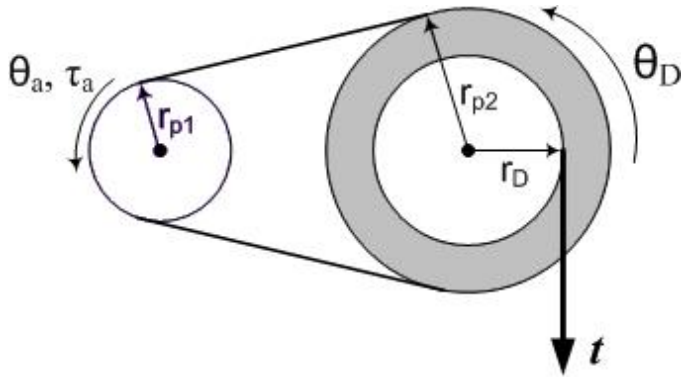

Figure 5.2: Free Body Diagram of Motor and Cable Winding Drum

$$\tau_{a_i} - \tau_{f_i} - r_i t = J_i \ddot{\theta}_i + C_i \dot{\theta}_i \tag{5.4}$$

$$\begin{aligned} J_i &= J_a + (\tfrac{r_{p1}}{r_{p2}})^2 J_D \\ C_i &= C_a + (\tfrac{r_{p1}}{r_{p2}})^2 C_D \\ r_i &= (\tfrac{r_{p1}}{r_{p2}}) r_D \end{aligned} \tag{5.5}$$

Where,

(J_i, C_i): are the combined rotational inertia and damping coefficient of the cable winding unit, referred to motor side
(J_a, C_a): are the rotational inertia and viscous damping coefficient of the actuator
(J_D, C_D): are the rotational inertia and viscous damping coefficient of the winding drum
r_i : is the equivalent radius of cable winding unit
r_D: is the radius of winding drum
(r_{p_2}/r_{p_1}): is the gear ratio, where r_{p_1}, r_{p_2} are radius of timing pulleys
τ_{f_i}: is the friction torque of actuator

Assuming that the torque applied by each actuator is large enough to keep the cables in tension, equation (5.4) is rewritten in general matrix form to express the cable tensions as a function of actuator torques:

$$\mathbf{T} = \mathbf{r}^{-1}\left(\boldsymbol{\tau} - \boldsymbol{\tau}_f - \mathbf{J}\,\ddot{\boldsymbol{\theta}} - \boldsymbol{C}\,\dot{\boldsymbol{\theta}}\right) \tag{5.6}$$

where, $\mathbf{J} = diag(J_1, ..., J_m)$
$\mathbf{C} = diag(C_1, ..., C_m)$
$\mathbf{r} = diag(r_1, ..., r_m)$
$\mathbf{T} = [t_1, ..., t_m]^T$
$\boldsymbol{\tau} = [\tau_1, ..., \tau_m]^T$
$\boldsymbol{\tau}_f = [\tau_{f_1}, ..., \tau_{f_m}]^T$: is the vector of friction torque of the actuators
$\boldsymbol{\theta} = [\theta_1, ..., \theta_m]^T$: is the vector of actuators' angular position.

5.3 System Dynamic Model

The overall system dynamics model is derived by combining the end-effector and actuator dynamics equations of motion. To derive an inverse kinematic mapping relating the motor angles $\theta_i\,(i = 1, ..., m)$ to the end-effector posture $\mathbf{X}$, we define all θ_i to be zero when the end-effector centroid is located at the origin of base frame $\{O\}$, with zero rotation. From this configuration, a positive angle θ_i on each motor will cause a negative change Δl_i in the length of the i^{th} cable.

$$r_1\theta_i = -\Delta l_i \tag{5.7}$$

The change of the length in the i^{th} cable is $\Delta l_i = l_i - l_{i0}$, where l_i is the cable length obtained from the inverse pose solution and l_{i0} is the initial length of the i^{th} cable.

$$l_i = ||\mathbf{p} + \mathbf{R}\,\mathbf{q}_i^p - \mathbf{b}_i|| \tag{5.8}$$

$$l_{i0} = ||\mathbf{q}_i - \mathbf{b}_i|| \tag{5.9}$$

$$\boldsymbol{\theta} = \begin{Bmatrix} \theta_1(\mathbf{X}) \\ \vdots \\ \theta_m(\mathbf{X}) \end{Bmatrix} = \mathbf{r^{-1}} \begin{Bmatrix} ||\mathbf{q}_1 - \mathbf{b}_1|| - ||\mathbf{p} + \mathbf{R}\,\mathbf{q}_1^p - \mathbf{b}_1|| \\ \vdots \\ ||\mathbf{q}_m - \mathbf{b}_m|| - ||\mathbf{p} + \mathbf{R}\,\mathbf{q}_m^p - \mathbf{b}_m|| \end{Bmatrix} \tag{5.10}$$

Successive time derivatives of equation (5.10) yields:

$$\dot{\boldsymbol{\theta}} = \frac{\partial \boldsymbol{\theta}}{\partial \mathbf{X}} \dot{\mathbf{X}} \tag{5.11}$$

$$\ddot{\boldsymbol{\theta}} = \frac{d}{dt}\left(\frac{\partial \boldsymbol{\theta}}{\partial \mathbf{X}}\right)\dot{\mathbf{X}} + \left(\frac{\partial \boldsymbol{\theta}}{\partial \mathbf{X}}\right)\ddot{\mathbf{X}} \tag{5.12}$$

Where $\left(\frac{\partial \boldsymbol{\theta}}{\partial \mathbf{X}}\right)$ may easily be derived from (5.10); it is a function of the Cartesian pose kinematics terms. Substituting (5.11) and (5.12) into (5.6) yields:

$$\mathbf{T} = \mathbf{r^{-1}}\left(\boldsymbol{\tau} - \boldsymbol{\tau}_\mathbf{f} - \mathbf{J}\left(\mathbf{d}\mathbf{t}\left(\frac{\partial \boldsymbol{\theta}}{\partial \mathbf{X}}\right)\dot{\mathbf{X}} + \left(\frac{\partial \boldsymbol{\theta}}{\partial \mathbf{X}}\right)\ddot{\mathbf{X}}\right) - \mathbf{C}\left(\frac{\partial \boldsymbol{\theta}}{\partial \mathbf{X}}\dot{\mathbf{X}}\right)\right) \tag{5.13}$$

Finally by combining equations (5.3) and (5.13) the overall dynamic equations of motion can be obtained, expressed in a standard Cartesian form for robotic systems [35]:

$$\mathbf{M}_{eq}.\ddot{\mathbf{X}} + \mathbf{N}(\mathbf{X}, \dot{\mathbf{X}}) = \mathbf{S}\boldsymbol{\tau} \tag{5.14}$$

Where, the equivalent inertia matrix $\mathbf{M}_{eq}$ and nonlinear terms $\mathbf{N}(\mathbf{X}, \dot{\mathbf{X}})$ are:

$$\mathbf{M}_{eq} = \mathbf{SJ}\left(\frac{\partial \boldsymbol{\theta}}{\partial \mathbf{X}}\right) + \mathbf{r}\begin{bmatrix} m_e\mathbf{I}_{3\times 3} & 0 \\ 0 & \mathbf{I_e} \end{bmatrix} \tag{5.15}$$

$$\mathbf{N}(\mathbf{X}, \dot{\mathbf{X}}) = \mathbf{S}\left(\mathbf{J}\frac{d}{dt}\left(\frac{\partial \boldsymbol{\theta}}{\partial \mathbf{X}}\right) + \mathbf{C}(\frac{\partial \boldsymbol{\theta}}{\partial \mathbf{X}})\right)\dot{\mathbf{X}} + \mathbf{S}\,\boldsymbol{\tau}_f + \mathbf{r}\begin{Bmatrix} -m_e\mathbf{g} - \mathbf{F}_R \\ \boldsymbol{\omega} \times \boldsymbol{I_e}\boldsymbol{\omega} - \mathbf{M}_R \end{Bmatrix} \tag{5.16}$$

5.4 Dynamic Equations for a Planar CDR

As an example, the general dynamic equations have been derived and simulated for a planar CDR case, in this section.

End-effector dynamic of planar CDR:

Simplifying equations (5.10)-(5.16) for a planar CDR yields:

$$l_i = \sqrt{(x + q_{ix}c\varphi - q_{iy}s\varphi - b_{ix})^2 + (y + q_{ix}s\varphi + q_{iy}c\varphi - b_{iy})^2}$$

$$l_{ix} = (x + q_{ix}c\varphi - q_{iy}s\varphi - b_{ix})$$

$$l_{iy} = (y + q_{ix}s\varphi + q_{iy}c\varphi - b_{iy})$$

$$l_{i0} = \sqrt{(q_{ix} - b_{ix})^2 + (q_{iy} - b_{iy})^2}$$

$$\mathbf{X} = \begin{Bmatrix} x & y & \varphi \end{Bmatrix}^T$$

$$\theta = \begin{Bmatrix} \theta_1 \\ \theta_2 \\ \theta_3 \\ \theta_4 \end{Bmatrix} = \frac{1}{r} \begin{Bmatrix} l_{1_0} - l_1 \\ l_{2_0} - l_2 \\ l_{3_0} - l_3 \\ l_{4_0} - l_4 \end{Bmatrix}$$

$$\dot{\theta} = \begin{Bmatrix} \dot{\theta}_1 \\ \dot{\theta}_2 \\ \dot{\theta}_3 \\ \dot{\theta}_4 \end{Bmatrix} = \begin{bmatrix} \frac{\partial \theta_1}{\partial x} & \frac{\partial \theta_1}{\partial y} & \frac{\partial \theta_1}{\partial \varphi} \\ \vdots & \vdots & \vdots \\ \frac{\partial \theta_4}{\partial x} & \frac{\partial \theta_4}{\partial y} & \frac{\partial \theta_4}{\partial \varphi} \end{bmatrix} \begin{Bmatrix} \dot{x} \\ \dot{y} \\ \dot{\varphi} \end{Bmatrix}$$

$$\frac{\partial \theta_i}{\partial x} = \frac{-1}{r_i . l_i} (l_{ix})$$

$$\frac{\partial \theta_i}{\partial y} = \frac{-1}{r_i . l_i} (l_{iy})$$

$$\frac{\partial \theta_i}{\partial \varphi} = \frac{-1}{r_i . l_i} \left[(-q_{ix} s\varphi - q_{iy} c\varphi)(l_{ix}) + (q_{ix} c\varphi - q_{iy} s\varphi)(l_{iy}) \right]$$

$$\ddot{\theta} = \begin{Bmatrix} \ddot{\theta}_1 \\ \ddot{\theta}_2 \\ \ddot{\theta}_3 \\ \ddot{\theta}_4 \end{Bmatrix} = [\mathbf{S}_x(\dot{x}) + \mathbf{S}_y(\dot{y}) + \mathbf{S}_\varphi(\dot{\varphi})] \begin{Bmatrix} \dot{x} \\ \dot{y} \\ \dot{\varphi} \end{Bmatrix} + \begin{bmatrix} \frac{\partial \theta_1}{\partial x} & \frac{\partial \theta_1}{\partial y} & \frac{\partial \theta_1}{\partial \varphi} \\ \vdots & \vdots & \vdots \\ \frac{\partial \theta_4}{\partial x} & \frac{\partial \theta_4}{\partial y} & \frac{\partial \theta_4}{\partial \varphi} \end{bmatrix} \begin{Bmatrix} \ddot{x} \\ \ddot{y} \\ \ddot{\varphi} \end{Bmatrix}$$

$$\mathbf{S}_x = \begin{bmatrix} \frac{\partial}{\partial x}\left(\frac{\partial \theta_1}{\partial x}\right) & \frac{\partial}{\partial x}\left(\frac{\partial \theta_1}{\partial y}\right) & \frac{\partial}{\partial x}\left(\frac{\partial \theta_1}{\partial \varphi}\right) \\ \vdots & \vdots & \vdots \\ \frac{\partial}{\partial x}\left(\frac{\partial \theta_4}{\partial x}\right) & \frac{\partial}{\partial x}\left(\frac{\partial \theta_4}{\partial y}\right) & \frac{\partial}{\partial x}\left(\frac{\partial \theta_4}{\partial \varphi}\right) \end{bmatrix}$$

$$\frac{\partial}{\partial x}\left(\frac{\partial \theta_i}{\partial x}\right) = \frac{1}{r_i . l_i} \left[\frac{1}{l_i^2} (l_{ix})^2 - 1 \right]$$

$$\frac{\partial}{\partial x}\left(\frac{\partial \theta_i}{\partial y}\right) = \frac{1}{r_i . l_i} \left[\frac{1}{l_i^2} (l_{ix})(l_{iy}) \right]$$

$$\frac{\partial}{\partial x}\left(\frac{\partial \theta_i}{\partial \varphi}\right) = \frac{1}{r_i . l_i} \{ \frac{l_{ix}}{l_i^2} [(-q_{ix} s\varphi - q_{iy} c\varphi)(l_{ix}) + (q_{ix} c\varphi - q_{iy} s\varphi)(l_{iy})] + (q_{ix} s\varphi + q_{iy} c\varphi) \}$$

$$\mathbf{S}_y = \begin{bmatrix} \frac{\partial}{\partial y}\left(\frac{\partial \theta_1}{\partial x}\right) & \frac{\partial}{\partial y}\left(\frac{\partial \theta_1}{\partial y}\right) & \frac{\partial}{\partial y}\left(\frac{\partial \theta_1}{\partial \varphi}\right) \\ \vdots & \vdots & \vdots \\ \frac{\partial}{\partial y}\left(\frac{\partial \theta_4}{\partial x}\right) & \frac{\partial}{\partial y}\left(\frac{\partial \theta_4}{\partial y}\right) & \frac{\partial}{\partial y}\left(\frac{\partial \theta_4}{\partial \varphi}\right) \end{bmatrix}$$

$$\frac{\partial}{\partial y}\left(\frac{\partial \theta_i}{\partial x}\right) = \frac{1}{r_i.l_i}\left[\frac{1}{l_i^2}\left(l_{ix}\right)\left(l_{iy}\right)\right]$$

$$\frac{\partial}{\partial y}\left(\frac{\partial \theta_i}{\partial y}\right) = \frac{1}{r_i.l_i}\left[\frac{1}{l_i^2}\left(l_{iy}\right)^2 - 1\right]$$

$$\frac{\partial}{\partial y}\left(\frac{\partial \theta_i}{\partial \varphi}\right) = \frac{1}{r_i.l_i}\{\frac{l_{iy}}{l_i^2}[(-q_{ix}s\varphi - q_{iy}c\varphi)(l_{ix}) + (q_{ix}c\varphi - q_{iy}s\varphi)(l_{iy})] - (q_{ix}c\varphi - q_{iy}s\varphi)\}$$

$$\mathbf{S}_\varphi = \begin{bmatrix} \frac{\partial}{\partial \varphi}\left(\frac{\partial \theta_1}{\partial x}\right) & \frac{\partial}{\partial \varphi}\left(\frac{\partial \theta_1}{\partial y}\right) & \frac{\partial}{\partial \varphi}\left(\frac{\partial \theta_1}{\partial \varphi}\right) \\ \vdots & \vdots & \vdots \\ \frac{\partial}{\partial \varphi}\left(\frac{\partial \theta_4}{\partial x}\right) & \frac{\partial}{\partial \varphi}\left(\frac{\partial \theta_4}{\partial y}\right) & \frac{\partial}{\partial \varphi}\left(\frac{\partial \theta_4}{\partial \varphi}\right) \end{bmatrix}$$

$$\frac{\partial}{\partial \varphi}\left(\frac{\partial \theta_i}{\partial x}\right) = \frac{1}{r_i.l_i}\{\frac{1}{l_i^2}[(-q_{ix}s\varphi - q_{iy}c\varphi)(l_{ix})^2 + (q_{ix}c\varphi - q_{iy}s\varphi)(l_{iy})^2] + (q_{ix}s\varphi + q_{iy}c\varphi)\}$$

$$\frac{\partial}{\partial \varphi}\left(\frac{\partial \theta_i}{\partial y}\right) = \frac{1}{r_i.l_i}\{\frac{l_{iy}}{l_i^2}[(-q_{ix}s\varphi - q_{iy}c\varphi)(l_{ix}) + (q_{ix}c\varphi - q_{iy}s\varphi)(l_{iy})] - (q_{ix}c\varphi - q_{iy}s\varphi)\}$$

$$\frac{\partial}{\partial \varphi}\left(\frac{\partial \theta_i}{\partial \varphi}\right) = \frac{1}{r_i.l_i}\{\frac{l_{ix}}{l_i^2}[(-q_{ix}s\varphi - r_{iy}c\varphi)(l_{ix}) + (q_{ix}c\varphi - q_{iy}s\varphi)(l_{iy})](-q_{ix}s\varphi - q_{iy}c\varphi)$$
$$+(q_{ix}c\varphi - q_{iy}s\varphi)(l_{iy})\}$$

Actuator dynamics:

Simplifying actuator dynamic equation (5.6) for a planar CDR yields:

$$\begin{bmatrix} J_1 & & 0 \\ & \ddots & \\ 0 & & J_4 \end{bmatrix} \begin{Bmatrix} \ddot{\theta}_1 \\ \ddot{\theta}_2 \\ \ddot{\theta}_3 \\ \ddot{\theta}_4 \end{Bmatrix} + \begin{bmatrix} C_1 & & 0 \\ & \ddots & \\ 0 & & C_4 \end{bmatrix} \begin{Bmatrix} \dot{\theta}_1 \\ \dot{\theta}_2 \\ \dot{\theta}_3 \\ \dot{\theta}_4 \end{Bmatrix} =$$
$$\begin{Bmatrix} \tau_1 \\ \tau_2 \\ \tau_3 \\ \tau_4 \end{Bmatrix} - \begin{Bmatrix} \tau_{f1} \\ \tau_{f2} \\ \tau_{f3} \\ \tau_{f4} \end{Bmatrix} - \begin{bmatrix} r_1 & & 0 \\ & \ddots & \\ 0 & & r_4 \end{bmatrix} \begin{Bmatrix} t_1 \\ t_2 \\ t_3 \\ t_4 \end{Bmatrix}$$

5.5 Trajectory planning:

In order to simulate the dynamics of a cable-driven robot, it is desirable to move the end-effector smoothly along a trajectory. For a given starting posture and a given ending posture of the end-effector, a fifth order polynomial can be used as the time history of postures to avoid vibrations caused by rough and jerky motion, i.e. to satisfy the required velocity as well as acceleration at the starting posture and the ending posture [58]. If the kinematic parameters at the starting posture are $s_s, \dot{s}_s, \ddot{s}_s$ and the kinematic parameters at the ending posture are $s_e, \dot{s}_e, \ddot{s}_e$, intermediate postures with respect to time t can be calculated as follows:

$$\begin{aligned} s(t) = & \left[12(s_e - s_s) - 6(\dot{s}_e + \dot{s}_s)t_f + (\ddot{s}_e - \ddot{s}_s)t_f^2\right] \frac{t^5}{2t_f^5} \\ & + \left[-30(s_e - s_s) + 2(7\dot{s}_e + 8\dot{s}_s)t_f - (2\ddot{s}_e - 3\ddot{s}_s)t_f^2\right] \frac{t^4}{2t_f^4} \\ & + \left[20(s_e - s_s) - 4(2\dot{s}_e + 3\dot{s}_s)t_f + (\ddot{s}_e - 3\ddot{s}_s)t_f^2\right] \frac{t^3}{2t_f^3} \\ & + \frac{\ddot{s}_s}{2}t^2 + \dot{s}_s t + s_s \end{aligned} \tag{5.17}$$

while t_f is the time duration of the motion.

As soon as the displacement function is determined, the instantaneous velocity and acceleration can be easily obtained by the first order differentiation and the second order differentiation of displacement with respect to time, respectively. These values are substituted into the dynamic equation in which the actuators' torque and cables' tension are obtained. Basically, any trajectory can be approximately interpolated into lines and circles. The following illustrate a linear and a circular trajectory planning for a planar cable-driven robot.

Linear trajectory: For linear trajectories as shown in Figure 5.3(a), if the velocity and the acceleration are required to be zero at the starting posture and

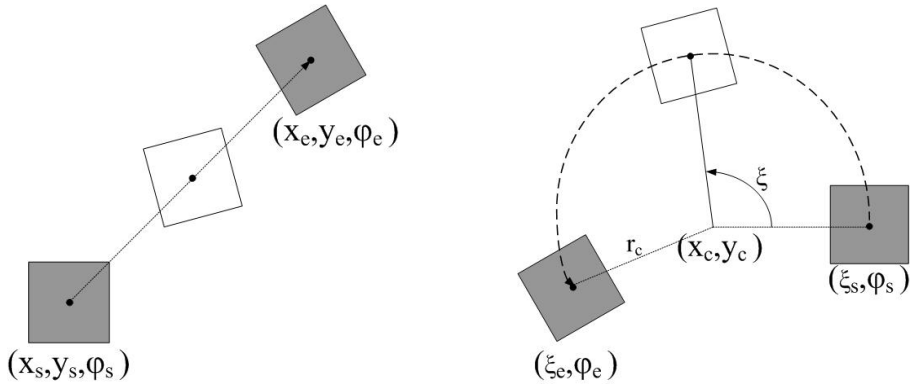

(a) linear Trajectory (b) Circular Trajectory

Figure 5.3: Trajectory Planning.

the ending posture, the intermediate postures in equation (5.17) are simplified as below:

$$\begin{Bmatrix} x(t) \\ y(t) \\ \varphi(t) \end{Bmatrix} = \begin{Bmatrix} x_s \\ y_s \\ \varphi_s \end{Bmatrix} + \left[6(\tfrac{t}{t_f})^5 - 15(\tfrac{t}{t_f})^4 + 10(\tfrac{t}{t_f})^3\right] \begin{Bmatrix} x_e - x_s \\ y_e - y_s \\ \varphi_e - \varphi_s \end{Bmatrix} \tag{5.18}$$

Circular trajectory: Similarly to circular trajectories (shown in Figure 5.3(b)), the intermediate postures are calculated from the following equations.

$$\begin{aligned} x(t) &= x_c + r_c \cos\left(\xi_s + \left[6(\tfrac{t}{t_f})^5 - 15(\tfrac{t}{t_f})^4 + 10(\tfrac{t}{t_f})^3\right](\xi_e - \xi_s)\right) \\ y(t) &= y_c + r_c \sin\left(\xi_s + \left[6(\tfrac{t}{t_f})^5 - 15(\tfrac{t}{t_f})^4 + 10(\tfrac{t}{t_f})^3\right](\xi_e - \xi_s)\right) \\ \varphi(t) &= \varphi_s + \left[6(\tfrac{t}{t_f})^5 - 15(\tfrac{t}{t_f})^4 + 10(\tfrac{t}{t_f})^3\right](\varphi_e - \varphi_s) \end{aligned} \tag{5.19}$$

5.6 Dynamic Simulation

In this section, dynamics of planar CDR (Figure 3.3) have been simulated, while the end-effector traces a half-circular path. In the following simulation, the dimension of the base is (2a=2b=1.0 m). The end-effector is a rectangle with dimensions (2c=0.1 m, 2d=0.08 m), mass $m_e = 1$ kg, and moment of inertia about Z-axis $I_z = 1.667 \times 10^{-3}$ kg m^2. Cable driving units are selected to be the same, with rotational moment of inertia of $J = 2.2 \times 10^{-4}$ kg m^2 and winding drum radius $r_D = 0.025$ m.

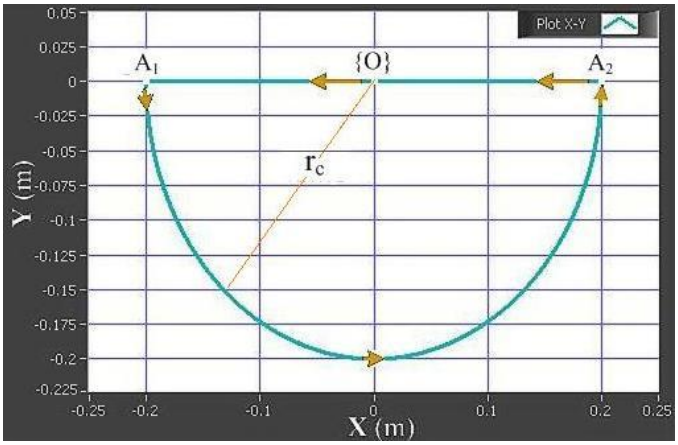

Figure 5.4: Dynamic Simulation: X-Y motion of the end-effector

The end-effector motion starts from origin $\{O\}$, goes along X-axis to $A_1 = (-0.2, 0)$, follows by a semi-circular path (with radius $r_c = 0.2$ m) to A_2=(0.2,0), and finally moves back to origin (Figure 5.4). Note that $r_c = 0.2$ m have been chosen to locate the whole path within the static workspace of the planar CDR (Figure 4.3. The trajectory planning method of section 5.5 is used for linear and circular segments of motion.

Simulation results are shown in Figures 5.5 and 5.6. Figure 5.5 shows the actuators' dynamics through out the motion, including their angular position, velocity, and acceleration. Moreover, cables' tension and actuators' torque are simulated with different pre-tension values, $t_{min} = 0\,(N)$, $t_{min} = 1\,(N)$, and $t_{min} = 3\,(N)$ in

Figure 5.6.

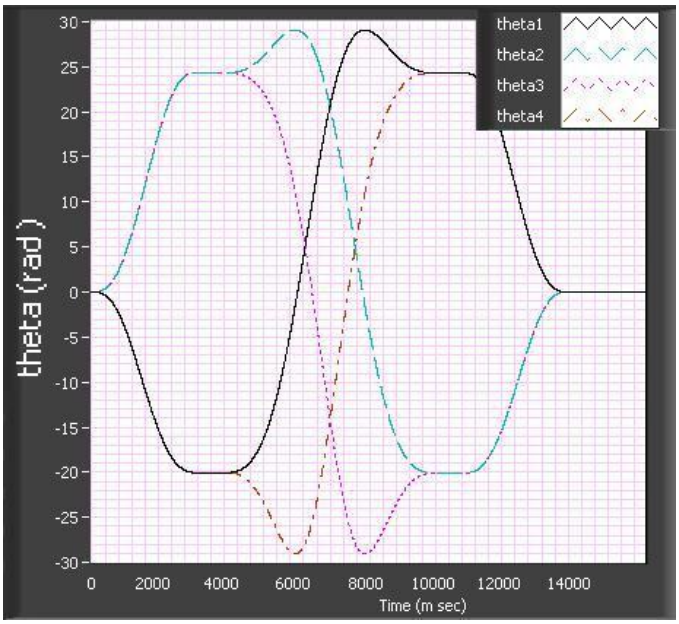

(a) Angular position ($\boldsymbol{\theta}$) of actuators

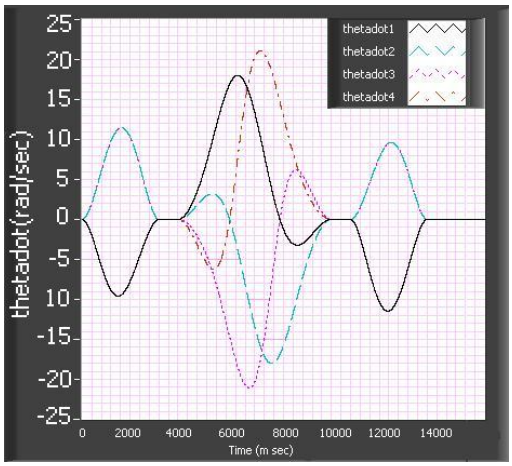

(b) Angular velocity ($\dot{\boldsymbol{\theta}}$)

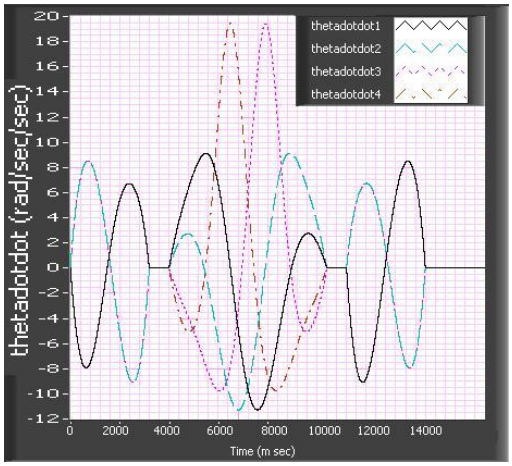

(c) Angular acceleration ($\ddot{\boldsymbol{\theta}}$)

Figure 5.5: Actuators Dynamic Simulation

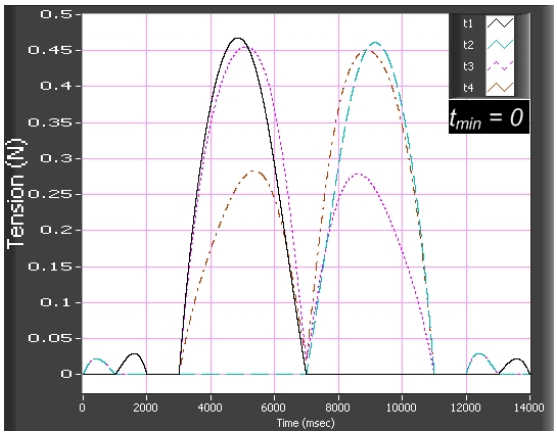

(a) Tension of cables with $t_{min} = 0$

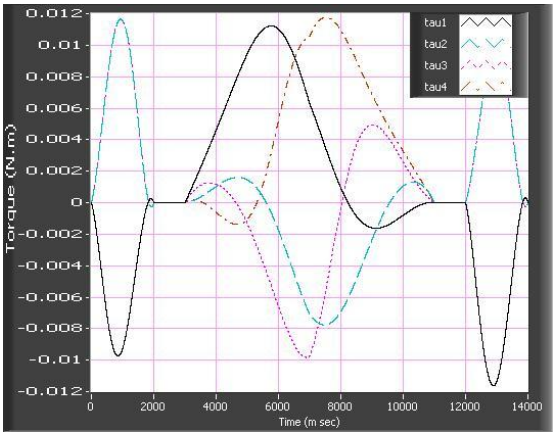

(b) Torque of actuators with $t_{min} = 0$

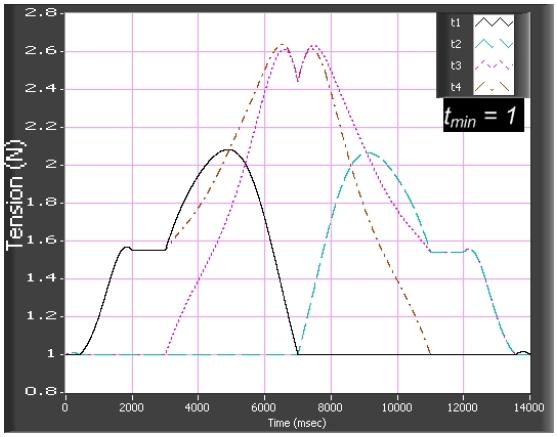

(c) Tension of cables with $t_{min} = 1\,N$

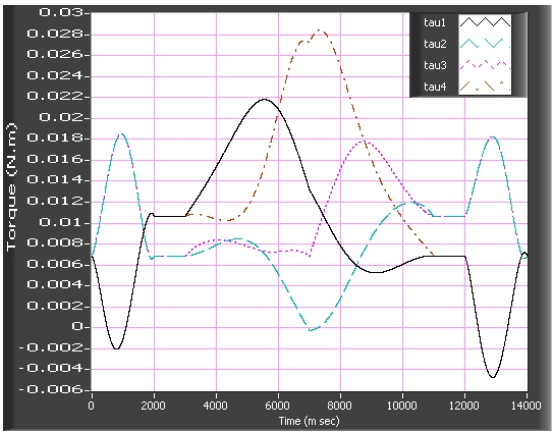

(d) Torque of actuators with $t_{min} = 1\,N$

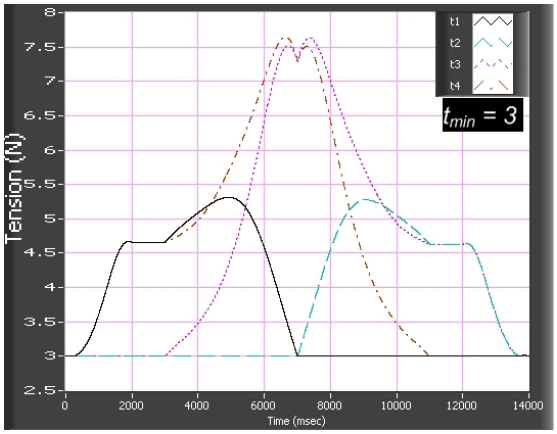

(e) Tension of cables with $t_{min} = 3\,N$

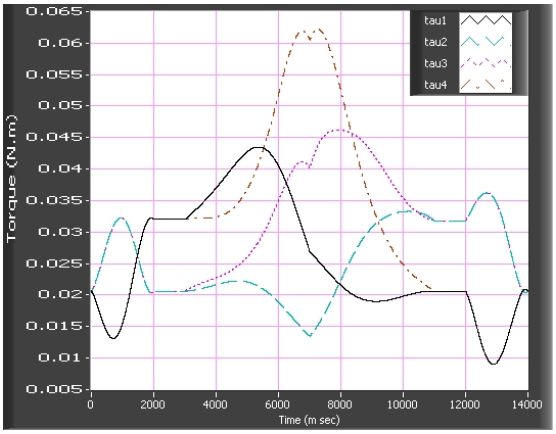

(f) Torque of actuators with $t_{min} = 3\,N$

Figure 5.6: Dynamic Simulation: Cables' tension and Actuators' torque

In order to prevent slackness of cables, it is essential to have positive actuators' torque. However, in $t_{min} = 0\,(N)$ and $t_{min} = 1\,(N)$, the actuators' torque are negative (5.6 (b),(d)). Therefore, these values for t_{min} should be avoided in order to prevent the slackness. Furthermore, it can be seen from these figures that, increasing the pre-tension, results in increasing the torques as well as the cables' tension. In other words, it shifts up the torque diagram. This effect is desirable, provided that the increased torque does not exceed the maximum allowable value, i.e. the actuators are able to support the required torque. Using $t_{min} = 3\,(N)$ results in positive actuators' torque, which are less than $\tau_{max} = 0.12\,(N\,m)$ and all of the cables' tension are also less than $t_{max} = 10\,(N)$ (5.6(e),(f)).

It is also observed that, torque profile and tension profile are not the same. The reason is, the static condition ($\tau_{static} = r\,t$) is not valid any more during the motion, since the inertia and viscous terms affect the actuators' torque (Eqn. (5.4)). Moreover, quintic trajectory planning results in torque values, which do not change drastically, while the end-effector remains within the static workspace.

5.7 Summary

The dynamic analysis of fully restrained cable-driven robots was the major study of this chapter. A complete dynamic model of a system including the end-effector dynamics and actuator dynamics has been derived. Furthermore, the dynamic equations of a planar CDR has been simulated for a semicircular path. Simulation results illustrated that, the actuator torques can be obtained as long as the tension solution exists. It was also realized that, if the trajectory profile is planned in a quintic polynomial, the resultant torques changes quite smoothly and increasing the pre-tension value, results in positive torque values that guarantees the positive tension of the cables.

Chapter 6

Prototype Development

This chapter explains the design and fabrication of a planar cable-driven robot. The main objective is to develop a prototype, which is flexible enough for investigation of different modes of *real-time* (RT) control and experimental verification of the theory. The conceptual design of this planar CDR is shown in Figure 6.1.

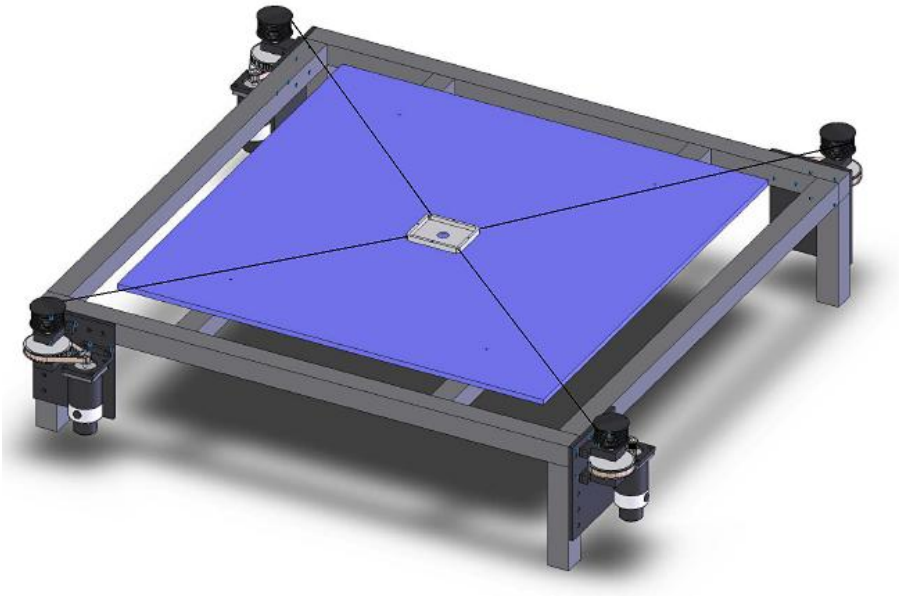

Figure 6.1: Conceptual Model of Planar Cable-Driven Robot

6.1 Design Specifications

The mechanical design process comprises of motor selection, speed reduction mechanism, cable winding mechanism, end-effector design, and frame design. The power of the motor and the desired performance of the CDR are the fundamental factors considered in the design process. It was decided at the beginning of the project that the CDR should have a maximum cable tension of 10 N during operations and approximately one square meter of workspace. In addition, real-time control of the robot requires choosing proper RT-software and RT-hardware which are compatible with input/output devices such as amplifiers and sensors. Based on the geometrical constraints and the availability of products, planar CDR has been developed, using the following components.

Motors: For this project, four Aerotech DC1017 servomotors have been used (shown in Figure 6.2). An encoder is incorporated at the end of each motor to read the angular position. The encoder provides feedback resolution of 1000 counts per revolution.

MOTOR MODEL	UNITS	1017
Stall Torque, Continuous	N-m oz-in	0.12 17
Torque Constant	N-m/Amp oz-in/Amp	0.03 4.1
Maximum Speed	rpm	6,500
Rated Power	W hp	60 0.1

Figure 6.2: AEROTECH-1017 DC Servomotor

Cable Winding Unit: The assembly of the motor, the speed reduction mechanism, and the threaded drum with the shafts and bearings is identified as the

cable winding unit (CDU), which is shown in Figure 6.3. Speed reduction has been implemented with the aim of getting the required torque and threaded drum helps to wind the cable side by side. The reason for choosing the threaded drum was that overlapping of the cables will change the winding radios continuously. This will affect the positional accuracy , consequently. The specifications of the CDU is also shown in Figure 6.3. The maximum applied torque of CDU is τ_{max}=0.48 (N.m) and it is able to wind/unwid the cable up to Δl_{max}=1.555 (m), which is enough for covering the entire workspace. Detailed drawings of mechanical parts are given in Appendix B.

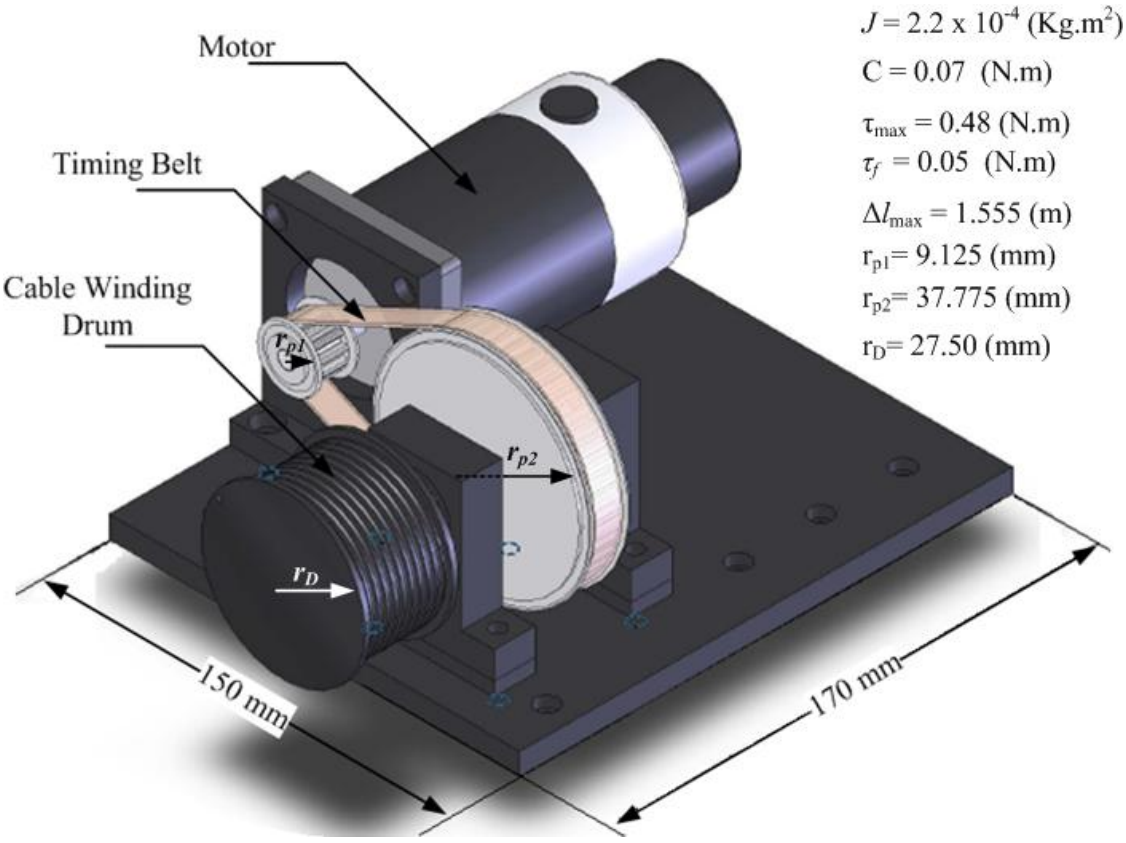

Figure 6.3: Cable Winding Unit

End-effector: In general, the end-effector is designed based on the application of the CDR. Different applications, may require different devices, to be attached to the end effector. For example, in painting CDR, a paint sprayer is attached to the

end effector. Hence, application of the CDR plays important role in determining the design of this component. The CDR was designed in a way that enable us to investigate its control performance and also to monitor its end-effector position, using a computer mouse. Therefore, the space at the center of the end effector (Figure 6.4) was purposely created for attaching a computer mouse components inside. It also gave flexibility to put additional elements inside the end effector like circuit board, pen or pencil and etc. that might be needed in later applications. Cables were attached to the corners of the end effector and four holes were considered at the center of end-effector sides for the purpose of home positioning and pre-tensioning. The shape of the end effector was chosen to be a rectangular with dimension ($100 \times 80 \times 10$) mm. Detailed drawing of end effector is located at Appendix B.

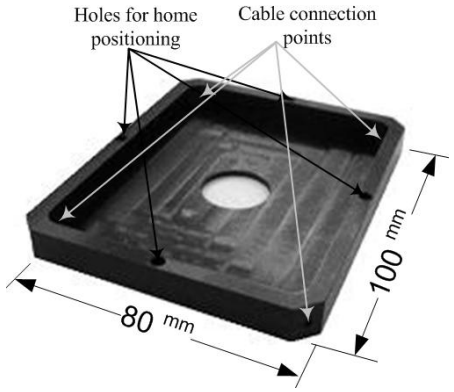

Figure 6.4: The End-effector

Table of Cable-Driven Robot: Table of the CDR is a structure where all the components are attached to it. The structure is made of aluminum profiles that were cut accordingly to the desired dimension. It supported four winding units at its four corners. At the top of it, a board made from acrylic was placed. The acrylic was covered by a white paper to support the operation of the computer mouse that would be used later in the project. The end-effector was located at the top of the

board and slide on it. Detailed dimension of the table can be seen in Appendix B.

Amplifiers: The motors require a higher voltage and current supply than the data acquisition board could supply. In order to provide necessary driving current and voltage source, amplifiers were used. The amplifiers used here are PWM (pulse width modulated) servo amplifiers from Advance motion controls (shown in Figure 6.5). The 12A8 amplifier is protected against over-voltage, over-current, over-heating and short circuits across the motor, ground and power leads. It interfaces with digital controllers or can be used as stand-alone drive. It requires only a single unregulated DC power supply. An important feature of the amplifier is that it offers current and voltage limiting. The amplifier can be set to voltage or current mode, based on the individual needs of the user. For servomotors, input current is linearly related to the output torque, thus for torque control, amplifiers are set in current mode. By commanding and controlling the current applied to the motors, the programmer can control the torque. However, for the position control loop, amplifiers are configured in voltage mode. In voltage mode, the output is proportional to input voltage.

Figure 6.5: 12A8 PWM Servo Amplifiers from AMC

Data Acquisition Card: Considering a cable-driven robot as a mechatronic system, it is essential to have a suitable connection between the microprocessor-based controller and the mechanical devices. This involves the appropriate electronic circuitry, generally referred as the interface, which makes the computer and the controlled devices compatible. A commercial plug-in National Instrument data acquisition card (NI PCI-6221 DAQ) is used to interface with the sensors and to control the actuators (Figure 6.6). It has eight analog inputs, two analog outputs with 16 bits of resolution,and two dedicated counters to read incremental encoders.

Figure 6.6: NI PCI-6221 M-Series DAQ card

Tension Sensor: The MPMC3 is a tension transducer from TMI (Tension Measurement Inc.) shown in Figure 6.7. It is basically a strain-gauged sensor with a digital indicator that provides sensor power and signal conditioning. It also provides analog output which is directly proportional to the tension applied to the sensor. The calibration procedure of the sensor is simply done by hanging known weights. The sensor output signal is linear in the full scale range of tension, which is set manually during the calibration procedure.

6.1.1 Development Software

All of the control programs are developed in LabView 7.1 from National Instruments. LabView is a graphical programming language (G-language) and it uses

Figure 6.7: The Tension Sensor

the concept of Virtual Instruments (VIs), which is distinct from other text-based programming languages and the intuitive graphical development environment combines the ease of using configuration-based tools with the flexibility of a powerful programming language. Moreover, the LabView compiler generates optimized code with execution speeds comparable to that of compiled C programs. Since the execution order is determined by the flow of data between nodes and not by sequential lines of text, it is easily possible to create block diagrams that execute multiple operations in parallel. This parallel nature of LabView makes implementing multitasking and multi-threading simple by assigning thread priorities. In addition, it can be configured with LabView R-T software, for real time implementation of the control system.

6.2 Real-Time Control Scheme

The schematic diagram of the CDR control system is shown in Figure 6.8. It consists of a host computer and a real-time target. Host computer was a Pentium IV running on Windows XP platform, which was configured with LabView 7.1 and LabView RT software and the real-time target was a Pentium IV computer runs on

the LabView Real-Time OS. Additionally, the target PC was integrated with two PCI-6221 DAQ boards to interface it with the CDR hardware. Motor amplifiers and encoders were connected to target PC throughout the PCI cards.

The control programs (VIs) were written in the host computer and downloaded to the target PC. Once the program is downloaded, target PC executes the control programs in deterministic time loops and sends back the processed data to the host computer for displaying. Host computer and target PC communicate with each other via ethernet cable.

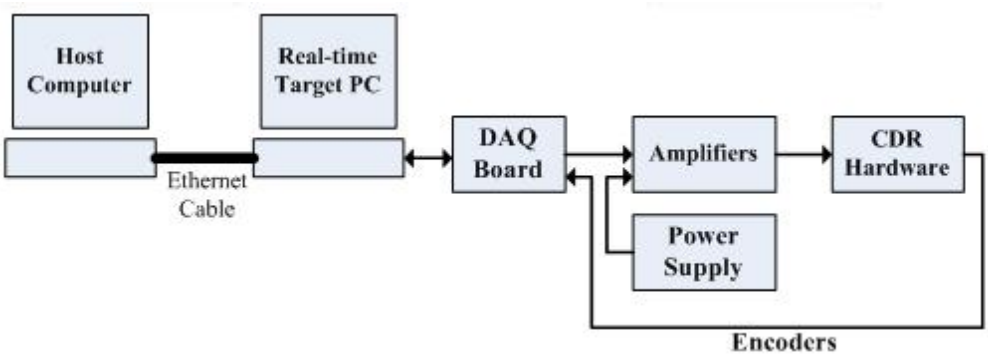

Figure 6.8: The Control System Scheme

6.3 Summary

In this chapter, the design and fabrication of a planar cable-driven robot prototype (Figure 6.9) was described. The main objective of the development of the prototype was investigating the real-time control of cable-driven robots and experimental verification of the formulations in kinematic analysis, tension analysis and dynamic analysis. The control algorithms and software architecture will be explained in next chapters.

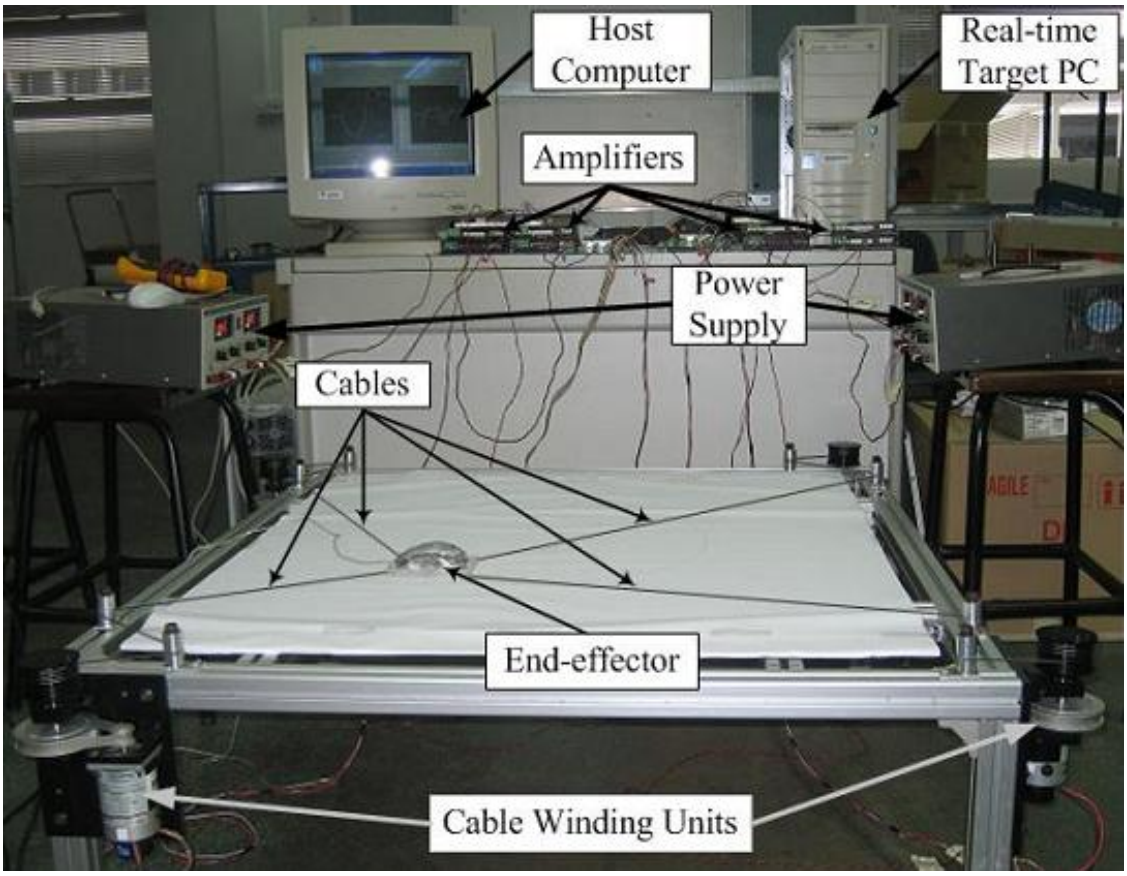

Figure 6.9: The Planar Prototype

Chapter 7

Control Architecture

This chapter presents cable-driven robot control architecture. For controlling the cable-driven robot two approaches are described. The first one is *independent joint control* (IJC) approach, which uses local independent PID control law at each joint to control the position of the end-effector. The second one is based on the control law development using *computed torque* method [71], followed by the method for resolving the actuation redundancy and maintaining positive tensions dynamically. Independent joint control and computed torque approach are implemented on the planar prototype and their experimental results are compared.

7.1 Independent Joint Control (IJC) Approach

The purpose of a IJC is to control the motors so that the end-effector traces a desired path. Although joint torque equations are highly coupled as seen in equation (5.14), a simple independent joint control approach with a PID control law will stabilize joint performance. This individual joint PID approach totally ignores dynamic equations and attempts to control the end-effector by using local, decoupled

PID controllers at each joint. The motion control system for an actuator of each local joint is shown in Figure 7.1.

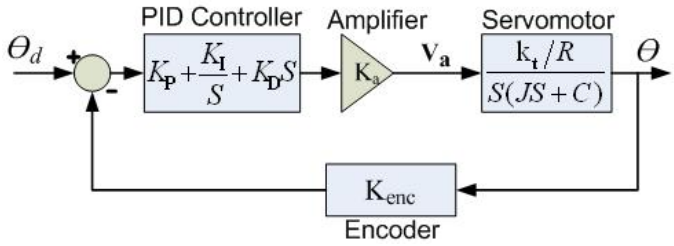

Figure 7.1: Block Diagram of an Individual PID Controller

DC servomotors have been used in this thesis as the actuators and their transfer function is [48]:

$$\frac{\theta(s)}{V_a(s)} = \frac{K_t/R}{s(Js+C)} \tag{7.1}$$

Where, V_a and R are the armature voltage and resistance, k_t is torque constant, and (J, C) are the combined inertia and viscous damping (Eqn. (5.5)).

The closed-loop transfer function of each independent joint controller is represented by equation (7.2), which is a third order system.

$$\frac{\theta(s)}{\theta_d(s)} = \frac{(K_D s^2 + K_P s + K_I)(K_a)(k_t/R)}{[s^2(Js+C) + (K_D s^2 + K_P s + K_I)(K_a)(k_t/R)(k_{enc})]} \tag{7.2}$$

The proportional (K_P), integral (K_I), and derivative (K_I) gains of the controller can be determined by locating the dominant closed-loop poles, near the poles of a system with the desired natural frequency and damping ratio [48]. Besides, damping ratio and natural frequency could be computed by substituting the desired maximum overshoot M_p and settling time t_s into equation (7.3).

$$\begin{aligned} \zeta &= \frac{-\ln M_P}{\sqrt{\pi^2+(\ln M_P)^2}} \\ \omega_n &= \frac{4}{\zeta \times t_s} \end{aligned} \tag{7.3}$$

$$\begin{aligned} &(s+A_1)(s^2+2\zeta\omega_n s+\omega_n^2) = \\ &[s^2(Js+C)+(K_D s^2+K_P s+K_I)(K_a)(k_t/R)(K_{enc})] \end{aligned} \tag{7.4}$$

In equation 7.4, an additional pole (A_1) is added to make the order of the desired system similar to the controller system. Additional pole (A_1) has to be big enough to make its effect insignificant compared to other poles of the system [48]. Equating coefficients of Eqn. (7.4) will result in:

$$\begin{aligned} K_P &= (2A_1\zeta\omega_n+\omega_n^2)\frac{RJ}{K_a k_t K_{enc}} \\ K_I &= (A_1\omega_n^2)\frac{RJ}{K_a k_t K_{enc}} \\ K_D &= (A_1+2\zeta\omega_n-\frac{C}{J})\frac{RJ}{K_a k_t K_{enc}} \end{aligned} \tag{7.5}$$

The PID gains of IJC controllers for $M_P = 5\%$ and $t_s = 0.5$ sec. are obtained and shown in Table 7.1, by substituting the Aerotech-1017 DC servomotor parameters in equation 7.5. The same PID gains are used for all of the joint controllers.

M_P	t_s	ζ	ω_n	K_P	K_I	K_D
5 %	0.5 sec	0.69	11.59	13.73	95.32	1.00

Table 7.1: PID gains of IJC controller

Having the desired trajectory, cables' length can be calculated, using inverse kinematics. Then, the change in the length of each cable gives the desired angular position of related actuator using equation (5.7). This angular position should be followed by each actuator independently. Figure 7.2 shows the IJC control architecture for CDRs which is used to move the end-effector from the current posture to the desired posture.

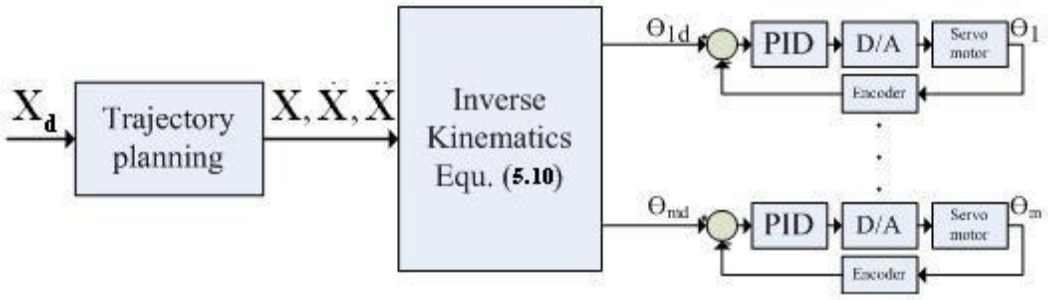

Figure 7.2: Independent Joint Controller Architecture

Even though the dynamics is not taken into account in this control laws, it is necessary to ensure that the resultant torques do not exceed the maximum torque of the actuators as the end-effector tracks the desired trajectories.

7.2 Computed Torque Control

Although IJC control approach results in acceptable positional accuracies, it does not control the tension of the cables, which is an important issue in cable-driven robots. Therefore, it is necessary to use a control method that consider the cables' tension as well as the end-effector positional accuracy. This section presents the computed torque control method including the controller architecture and control law development for planar CDRs based on the overall dynamic equations the system (5.16). The input to the system is the vector of positive torques $\boldsymbol{\tau}$, that is produced by motors to keep the cables in tension. The position of the end-effector is obtained from the change of length of the cables due to the rotation of motors. In order to obtain $\boldsymbol{\tau}$ vector, a virtual generalized wrench input $\mathbf{W}_v$ is introduced:

$$\mathbf{W}_v = \mathbf{S}.\boldsymbol{\tau} \tag{7.6}$$

Since the dimension of Jacobian matrix $\mathbf{S}$ is $(n \times m)$, the virtual generalized

wrench input has the dimension of the Cartesian space n (e.g. for a planar CDR n=3 and m=4). A control law should be developed for the virtual wrench input to find a real control positive torque input vector $\boldsymbol{\tau}$, that satisfies (7.6). For control law development, the following dynamic equation is considered:

$$\mathbf{M}_{eq}(\mathbf{X})\ddot{\mathbf{X}} + \mathbf{N}(\mathbf{X}, \dot{\mathbf{X}}) = \mathbf{W}_v \tag{7.7}$$

By using the well-known *computed torque* technique [71], the effects of the nonlinear dynamics terms $\mathbf{N}(\mathbf{X}, \dot{\mathbf{X}})$ canceled and inertial terms are counted. Implementation of a PD controller reduces the tracking error $\mathbf{e} = \mathbf{X}_d - \mathbf{X}$, where $\mathbf{X}_d$ is the commanded (reference) Cartesian pose. Following that, the computed-torque control law for the virtual wrench input $\mathbf{W}_v$ becomes:

$$\mathbf{W}_v = \mathbf{M}_{eq}(\mathbf{X}) \left(\ddot{\mathbf{X}}_d + \mathbf{K}_P \mathbf{e} + \mathbf{K}_D \dot{\mathbf{e}} \right) + \mathbf{N}(\mathbf{X}, \dot{\mathbf{X}}) \tag{7.8}$$

where $\dot{\mathbf{e}} = \dot{\mathbf{X}}_d - \dot{\mathbf{X}}$. Finally, equating the left side of equation (7.7) and the right side of equation (7.8) yields:

$$\ddot{\mathbf{e}} + \mathbf{K_D}\dot{\mathbf{e}} + \mathbf{K_P}\mathbf{e} = 0 \tag{7.9}$$

Equation (7.9) shows the effectiveness of the computed torque method, since all of the nonlinear terms have been canceled and the obtained equation is a second order linear system. The PD controller gains can be chosen to obtain desired close loop natural frequency ($K_P = {\omega_n}^2$) and damping ratio(i.e. $K_D = 2\zeta\sqrt{K_P}$). It is important to note that, since the matrix gains are chosen diagonal ($\mathbf{K_P} = diag(K_P)$ and $\mathbf{K_D} = diag(K_I)$), the servo control is accomplished independently for each of the Cartesian pose motion, even though the dynamics model is highly coupled.

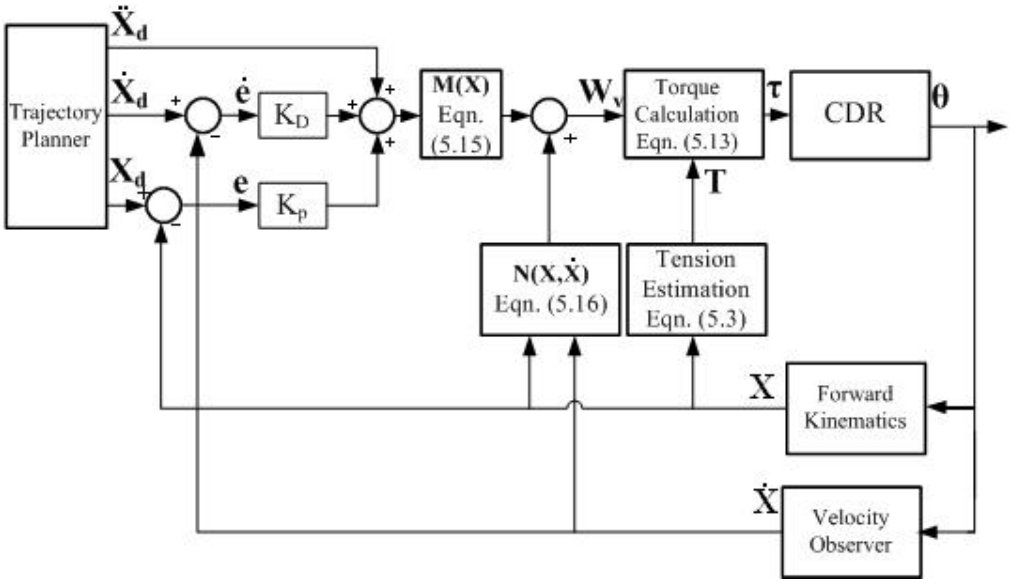

Figure 7.3: Computed Torque Controller Architecture block diagram

Figure 7.3 shows the computed torque control architecture for CDRs. It consists of five major sub-tasks: the PD controller, forward kinematics solver, velocity observer, tension estimator, and torque calculator.

The position feedback ($\mathbf{X}$) is calculated based on the encoder reading of motors ($\boldsymbol{\theta}$) using forward kinematics (Eqn. (3.4)). Velocity feedback, can be obtained either by velocity sensors (direct measurement) or estimations of the velocity from the encoder readings (velocity observer). The tension estimation has to deal with the problem of inverting non-square matrix $\mathbf{S(X)}$ and obtaining positive tension results using equation (4.4), in each control loop cycle. The resulted tension values are then used for computing the positive actuator torques to ensure positive cables' tension at all times (Eqn. (5.6)). The inertial term $\mathbf{M}_{eq}(\mathbf{X})$ is composed of the overall pose-dependent inertia matrix and the reference acceleration components (Eqn. (5.15)), and nonlinear terms are $\mathbf{N}(\mathbf{X}, \dot{\mathbf{X}})$, given in equation (5.16).

The implementation of the computed control approach on the planar prototype and the functionality of each block is presented in section 7.5.

7.3 One-DOF Experiments

At the beginning of the project, a one-DOF CDR has been built to investigate the fundamental concepts of cable-driven systems. It consists of two DC motors, incremental encoders, amplifiers, cable winding pulleys and the end-effector as shown in Figure 7.4. The functionality and specifications of its component was described in Chapter 6.

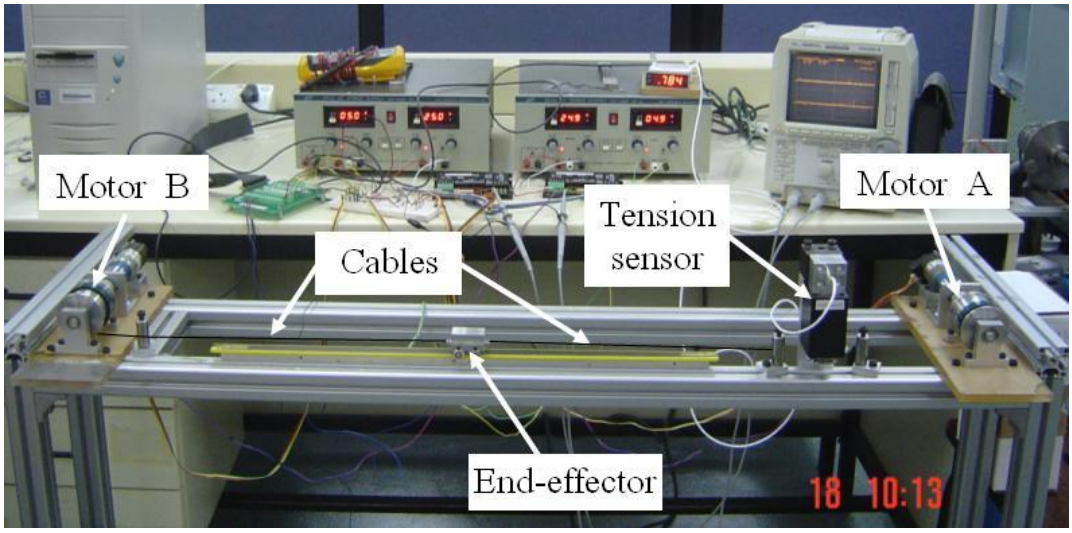

Figure 7.4: 1-DOF experimental setup

Different sets of experiments were carried out on 1-DOF prototype by implementing the IJC controllers. The main objective was to study the effect of pre-tension (t_0) on the performance of IJC controllers in CDRs by measuring the cables' tension. In these experiment the end-effector was commanded to move 10^{cm} to the right direction i.e. from motor B to motor A shown in Fig. 7.4. This motion was accomplished in two seconds. Before starting the movement, certain amount of pre-tension was applied to the cables. The pre-tensioning was done by small rotation of motors in a direction that reduce the cables' length. After obtaining the desired pre-tension, which was read by the tension sensor, the motion was started. Since only one tension sensor was available, tension in cables A and B were mea-

sured separately i.e. the motion was conducted twice; once the sensor was mounted on side A to measure t_A and once on side B to measure t_B. The values of t_A and t_B are compared with different pre-tensions in Figures 7.5 and 7.6, respectively.

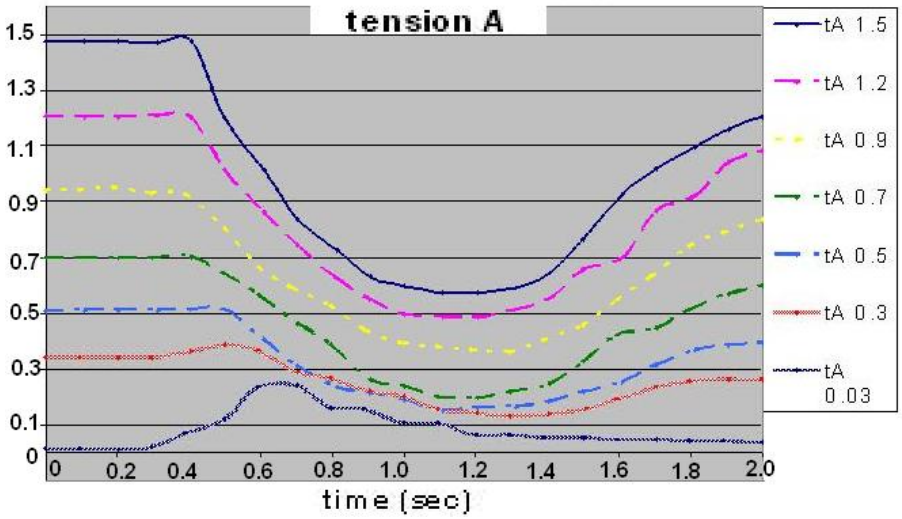

Figure 7.5: t_A with different pretension

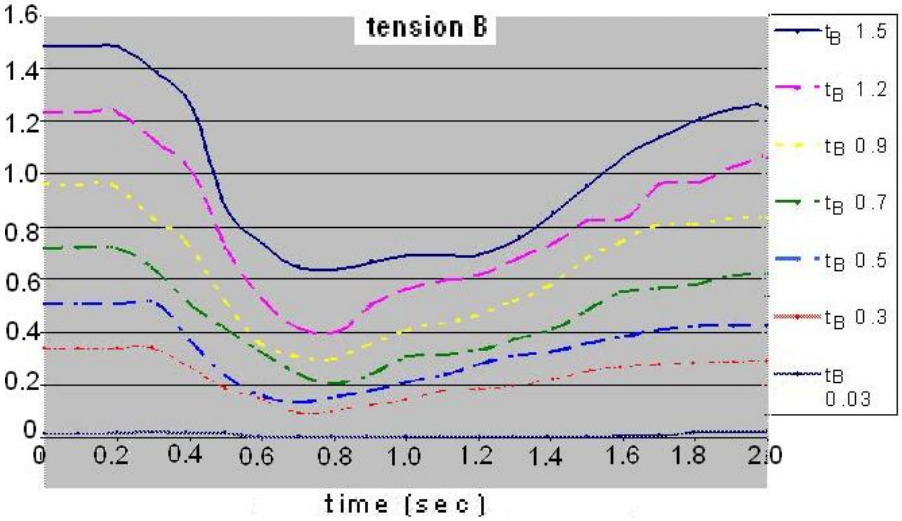

Figure 7.6: t_B with different pretension

Although it is desirable for cable-driven robots to keep a certain amount of tension (t_0) in the cables (in order to satisfy the stiffness requirements), but is observed that the cables' tension drops after the motion is started (Figure 7.5 and 7.6). This is explainable due to the lack of control on the tension of the cables in

IJC controllers, as they only control the angular position of actuators to change the cables' length. With small pre-tension values, the cable may lose its tension totally and get slack (e.g. when $t_0 = 0.05(N)$). It is also observed that, with pre-tension values greater than $t_0 = 0.5(N)$, both t_A and t_B first decrease and then increases nearly to the t_0. During the first half of motion t_B decreases more than t_A, since the difference of t_A and t_B ($F_x = t_A - t_A$) must accelerate the end-effector to the right, while during the second half of motion t_B starts to increase and try to decelerate the end-effector. At the end of motion, t_A and t_B must be equal and their value should be close to the initial pre-tension. However, a difference between the final value of tensions and the pre-tension values is observed, which is mostly due to the friction of the system.

One-DOF experimental tension measurement show that, although the positional accuracy of the end-effector is good, but the performance of the system in terms of maintaining the cables' tension is not satisfactory. Therefore, using the computed torque method that control the cables' tension seems to be useful. Moreover, increasing the pre-tension value improves the performance of the system, as with small pre-tension cables may loose their tension in motion specially when the motors unwind the cables.

Some other issues that have been faced in One-DOF experiment were cable selection and winding drum design. In our experiments, nylon coated steel wires, which was suggested by Pham [54], with different diameters were tested. It was observed that, a cable with a greater diameter, has higher stiffness and hence less elongation under the operation. On the other hand, it has more tendency to unwind from the drum due to its stiffness and more tension is required for winding the cables. A simple method of estimating the required pre-tension value for winding the cables, is using the torsion spring model for a wound cable, which is shown in Figure 7.7 [60]. Using the angular form of Hook's law, results in:

$$\begin{aligned} \tau_s &= k_\theta . \theta_w \\ k_\theta &= \frac{\pi G \, {d_w}^4}{32 l_w} \end{aligned} \tag{7.10}$$

where, k_θ is the torsional stiffness of spring, G is the shear modulus of rigidity of the wire, d_w and l_w are the diameter and the length of the wire, and r_D is the radius of winding drum. Knowing that $\tau_s = r_D \, t$ and $l_w = r_D \, \theta_w$, the required tension for winding the cable becomes:

$$t = \frac{\pi G {d_w}^4}{32 r_D^2} \tag{7.11}$$

Equation (7.11) states that required tension for winding the cables is highly dependant on the diameter of the cables. From our experiments, a nylon coated steel wire with diameter of $d = 0.5$ mm was finally selected. During the experiments, its elongation was small and the required tension for winding it around a drum with $r_D = 2.5$ cm was $t = 1.96(N)$. Note that this tension should be provided by the actuators when the end-effector is stopped, otherwise cables unwind from the drum. Another problem that was faced in One-DOF experiments was the slipping of the cable on the winding drum, which causes inaccuracies. In order to solve this problem threaded drums have been designed and used in the planar prototype.

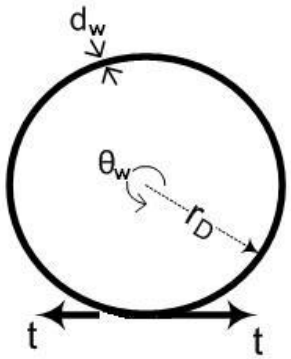

Figure 7.7: wound cable around the drum

In addition, dynamic simulations show that, increasing the pre-tension value will improve the performance of the CDR and helps to prevent cables' slackness. But generating and maintaining pre-tension values in the cables by using IJC controllers is a difficult task. One possible solution is to rotate the actuators in a direction that reduce the cables' length, while the end-effector is fixed. However, the amount of pre-tension is not under control in this method. Based on the experiences of One-DOF system, a planar prototype was designed and fabricated to study the main issues of CDRs in a general case.

7.4 Implementation of IJC on planar CDR

Independent joint control approach is also implemented on the planar CDR prototype based on the real-time control scheme of Figure 6.8. For this purpose, the amplifiers were set in the voltage mode to regulate the voltage of the motors. Different sets of experiments were carried out and PID gains of controllers were tuned for the best performance of the end-effector in terms of trajectory following. The improved PID gains for each joint is shown in Table 7.2.

	Theoretical Values	motor 1	motor 2	motor 3	motor 4
K_P	13.73	14	15	14	15
K_I	95.32	83.33	116.6	83.33	116.6
K_D	1.00	1.02	1.25	1.02	1.25

Table 7.2: Tuned PID gains of IJC controller

7.4.1 Experimental Results:

The same circular trajectory, which was simulated for dynamic analysis, was chosen for the end-effector to follow (Figure 5.4). In this experiment the end-effector was first placed to its starting point at the center of the base plate and a pre-tension of $t_{min} = 3$ (N) was applied. Then, it was commanded to trace a line followed by a half-circle of $r_c = 0.2$ m radius, centered at the origin, and return back to the origin. The end-effector was also commanded to maintain $\varphi = 0$ during the motion. The followed trajectory of the end-effector in X-Y plane is shown in Figure 7.8. Tracking error of the actuators in radian, which is the difference between desired angular position and encoder reading, is also shown in Figure 7.9(a). Moreover, Figure 7.9(b) presents the X-Y errors of the end-effector, which is the difference between the desired path and X-Y position obtained form forward kinematics. Experimental results shows that the tracking errors of the actuators are less than 0.05 rad, which

is explicable in terms of the overshoot of the system, while the steady state error is less than 0.005 rad. The maximum errors occur when the end-effector change its direction suddenly. The X-Y tracking error of the end-effector is also observed to be less than 5 mm through out the motion, which is acceptable compared to the workspace of the Robot. The steady state positional error of the end-effector at the end of the motion is 0.4 mm in the X direction and 0.6 mm in the Y direction. One possible source of error is the Coulomb friction between the end-effector and the base plate, which could be minimized by reducing the contact area of the end-effector and base plate. Another problem that affects the positional accuracy is caused by cables' slackness during the unwinding process, which is because IJC controllers do not take the tension of the cables into consideration.

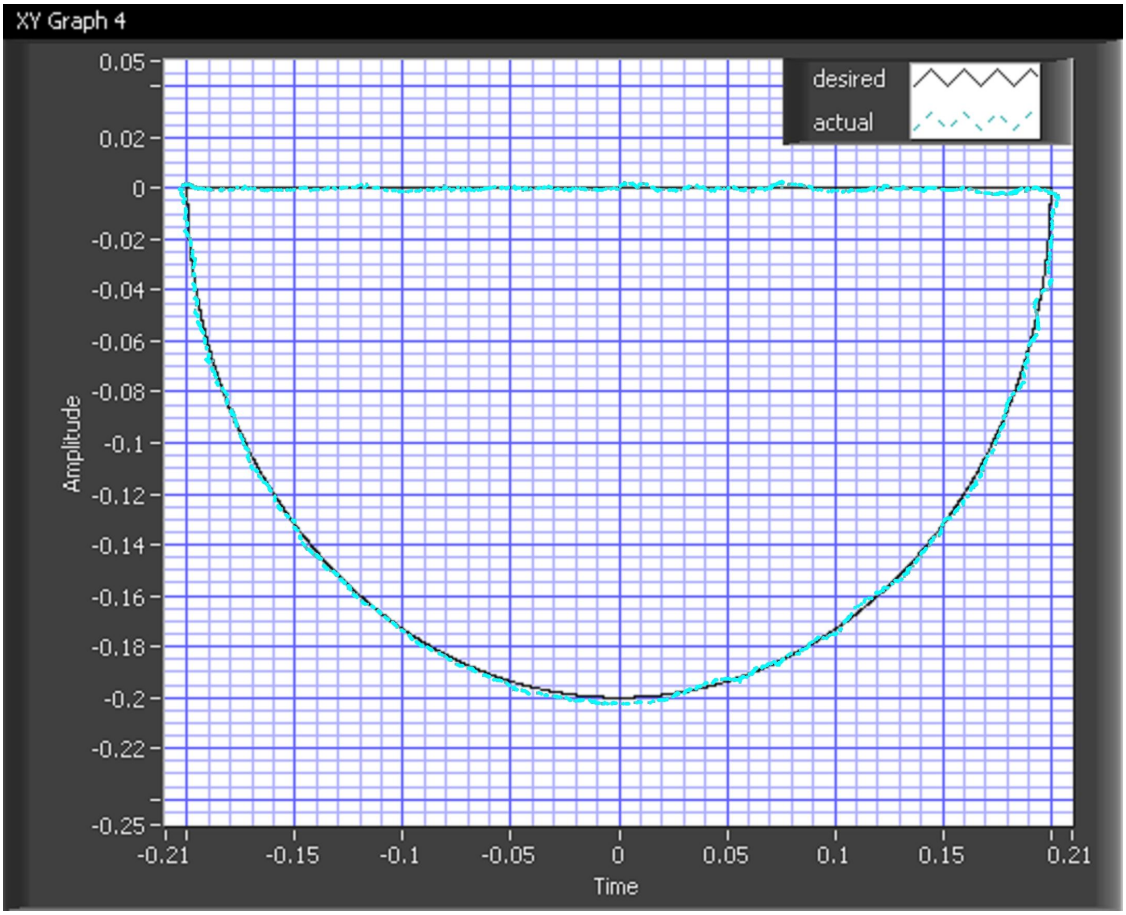

Figure 7.8: X-Y Graph of the end-effector with IJC controller

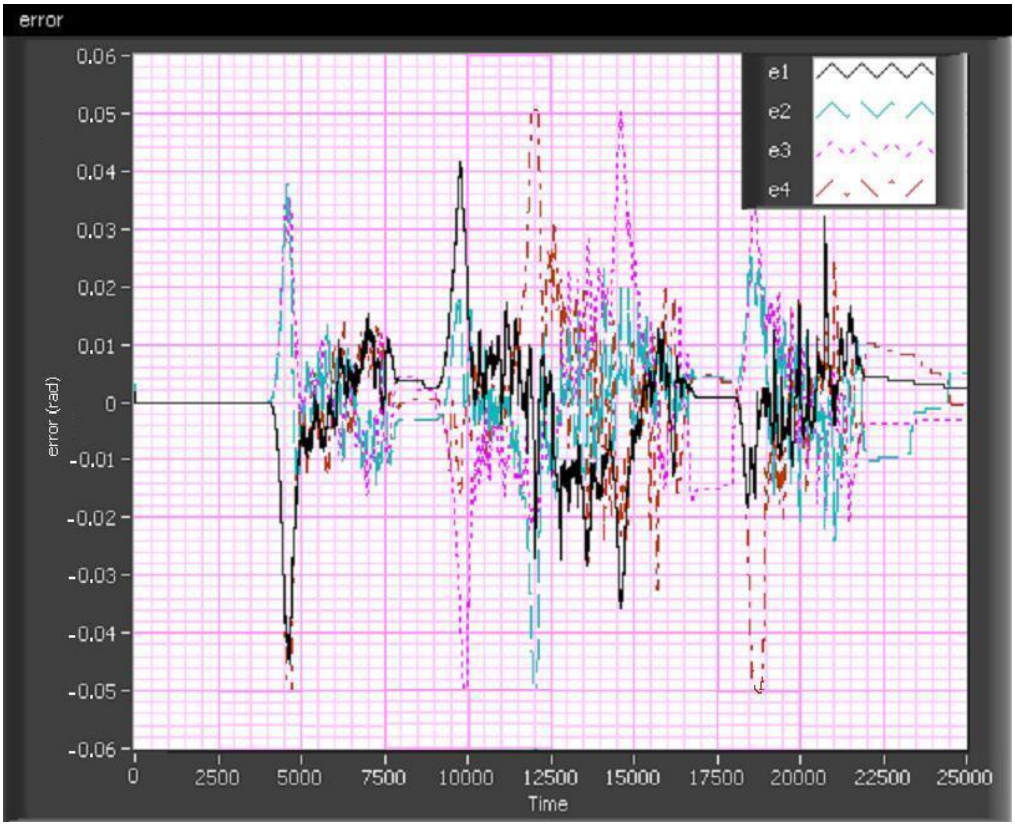

(a) Angular Position Error of Actuators

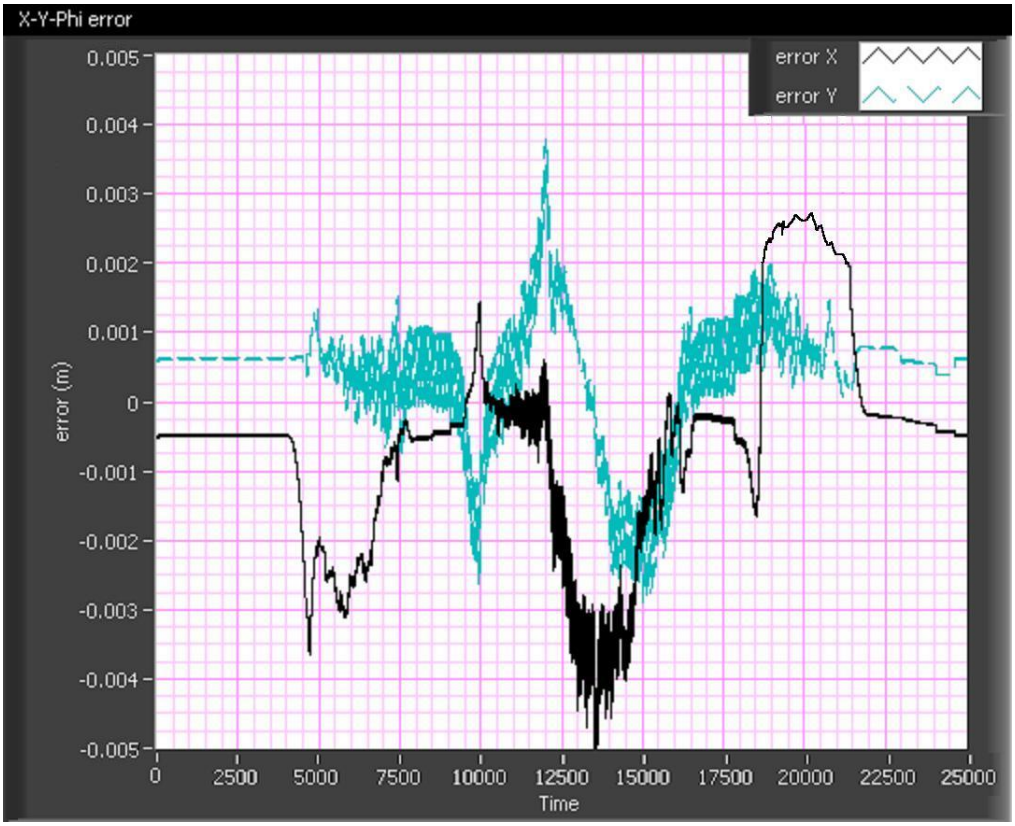

(b) X-Y Tracking Error

Figure 7.9: Errors in Circular Movement; Independent Joint Control

7.5 Implementation of Computed Torque Control on planar CDR

Implementation of computed torque approach (Figure 7.3) requires velocity feedback for canceling the effect of nonlinear terms. However, in our case we faced some limitations in using the velocity feedback. Since tachometers were not available for direct reading of the joint velocities. Moreover, the encoder noise problem makes digitally differentiating of the position quite hard. Therefore, the desired velocity terms ($\dot{\mathbf{X}}_\mathbf{d}$) were used instead of the actual velocity feedback ($\dot{\mathbf{X}}$). The effect of this simplification on the computed torque controller on the planar CDR can be obtained by substituting $\mathbf{N}(\mathbf{X}, \dot{\mathbf{X}}_\mathbf{d})$ in equation (7.7) as follows:

$$\mathbf{W}_v = \mathbf{M}(\mathbf{X}) \left(\ddot{\mathbf{X}}_d + \mathbf{K}_P \mathbf{e} + \mathbf{K}_D \dot{\mathbf{e}} \right) + \mathbf{N}(\mathbf{X}, \dot{\mathbf{X}}_d) \tag{7.12}$$

Equating (7.7) and (7.12) and substituting (5.16) in the result with the assumption of small angular velocity of the end-effector yields:

$$\begin{aligned} \mathbf{M}(\mathbf{X})(\ddot{\mathbf{e}} + \mathbf{K}_D \dot{\mathbf{e}} + \mathbf{K}_P \mathbf{e}) &= \mathbf{N}(\mathbf{X}, \dot{\mathbf{X}}) - \mathbf{N}(\mathbf{X}, \dot{\mathbf{X}}_d) \\ &= \mathbf{S}\left[\mathbf{J} \tfrac{d}{dt}\left(\tfrac{\partial \boldsymbol{\theta}}{\partial \mathbf{X}}\right) + \mathbf{C}\left(\tfrac{\partial \boldsymbol{\theta}}{\partial \mathbf{X}}\right)\right](\underbrace{\dot{\mathbf{X}} - \dot{\mathbf{X}}_d}_{-\dot{\mathbf{e}}}) \end{aligned} \tag{7.13}$$

It is observed that, the nonlinear terms are not canceled completely without velocity feedback. The schematic diagram of the implemented computed torque method on the planar CDR is shown in Figure 7.10, and its performance has been tested experimentally.

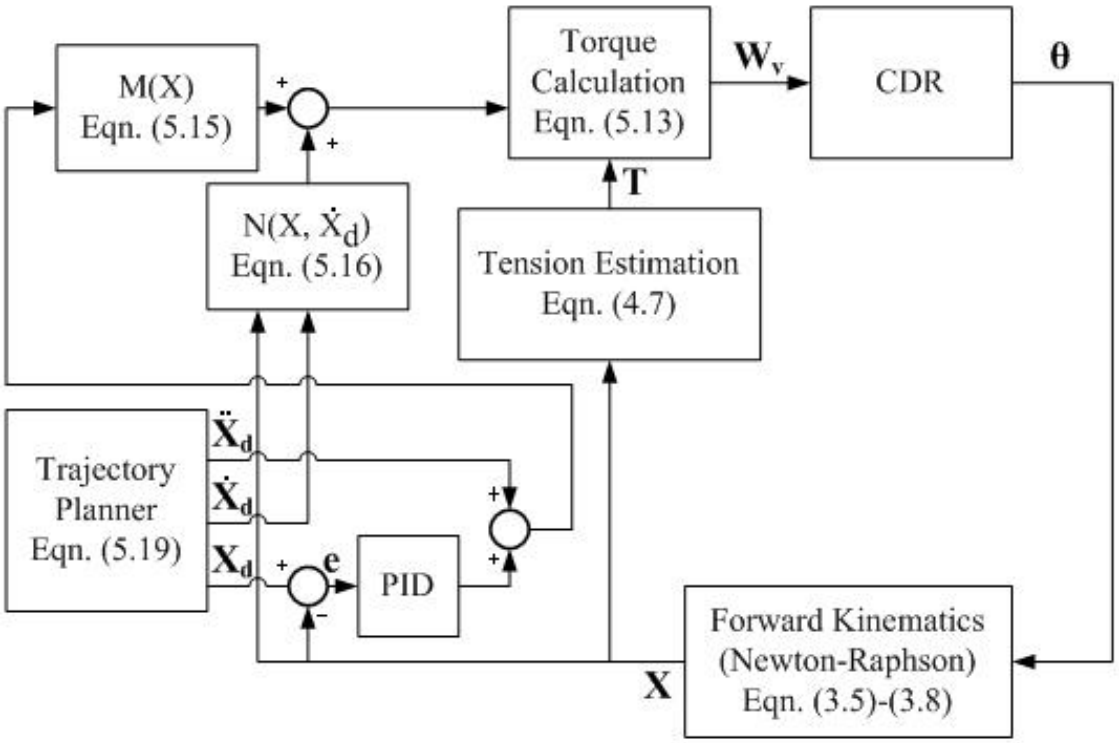

Figure 7.10: Computed Torque Scheme Implemented on Planar CDR

7.5.1 Description of Computed Torque Control Architecture for Planar CDR

The computed torque controller, which is implemented on the planar CDR prototype, contains the following parts:

Tension Estimation: The cables' tension **T** is calculated for the given dynamic wrenches **W**, using the following equation:

$$T = \begin{Bmatrix} t_{p_1} \\ t_{p_1} \\ t_{p_1} \\ t_{p_1} \end{Bmatrix} + \lambda \begin{Bmatrix} n_1 \\ n_2 \\ n_3 \\ n_4 \end{Bmatrix} \geq t_{\min} \begin{Bmatrix} 1 \\ 1 \\ 1 \\ 1 \end{Bmatrix} \tag{7.14}$$

The goal of tension estimation is finding an optimal tension solution, by minimizing the Euclidean norm of $\mathbf{T}$. Moreover, each component of $\mathbf{T}$ must be greater than or equal to a specified minimum tension $t_{\min}$, in order to prevent cables' slackness. For this purpose, λ is calculated at each control cycle to ensure that the minimum positive tension is satisfied for all cables. For each particular tension component, $\lambda_i = \frac{(t_{\min} - t_{p_i})}{n_i}$ is calculated; then the largest magnitude of these λ_i's is selected to be the λ at each control cycle ($\lambda = max\{\lambda_1, ..., \lambda_4\}$). This single λ value has to be then used for all components in equation (7.14).

Actuator Torques Calculation: After estimating the tension values, the positive actuator torque components are calculated using equation (5.13). Then, the computed torque values are converted into current and send to the amplifiers to drive the motors.

Controller Feedback Driving the motors with current amplifiers, results is angular motion (θ_i), which is obtained from encoders reading. Having θ_i and hence l_i, the pose of the end-effector is computed by Newton-Raphson iterative method (Eqn. 3.4). The pose value is compared with the reference value and the error goes to PID controller, which tries to minimize the tracking errors.

7.5.2 Experimental Results

The first experiment aims at generating a linear profiles: move the end-effector from the origin (center of the plate) to (-0.10,-0.10) in six seconds and return to the origin. Second experiment represents a circular profile: trace a line from origin to (-0.2,0.0) and starts a half-circle of 0.20 meter radius to (0.2,0.0), and finally return back to the origin (0,0). The control programs were written in LabView based on the controller architecture of Figure 7.3 and quintic polynomials were used for

trajectory generation. For reducing the tracking errors of the CDR, PID controller was used instead of PD controllers. The proportional (K_P), integral (K_I), and derivative (K_D) gains of the PID controller were determined by specifying desired settling time $t_s = 0.5$ sec. and maximum overshoot $M_p = 5\%$ for a unit step input. For this purpose, the closed-loop poles of the system were located at ($s_{1,2} = -8.0 \pm 8.39i$, $s_3 = -40$), which results in $\mathbf{K}_P = diag(774.1)$, $\mathbf{K}_I = diag(5373.1)$ and $\mathbf{K}_D = diag(56.0)$ shown in Table 7.3.

M_P	t_s	ζ	ω_n	Closed-loop Poles	K_P	K_I	K_D
5 %	0.5 sec	0.69	11.59	$S_{1,2} = -8.0 \pm 8.39i$ $S_3 = -40.0$	774.1	5373.1	56.0

Table 7.3: PID gains of Computed Torque controller

Linear Trajectory: In this example, the pre-tensioning process was done first. For pre-tensioning process, the end-effector was first fixed at the center of the base plate, with the aid of some set screws. Then, the program runs and makes the motors apply enough torque for generating desired pre-tension value ($t_{\min}$=3 N in this example). After that, the screws are removed and the motion starts. This experiment is a linear motion, from (0,0) to (-0.1,-0.1). After reaching the destination end-effector wait for a while and then returns back to the origin. During the motion the end-effector attempts to maintain the zero orientation ($\varphi = 0$). The experimental results are shown in Figures 7.11-7.13.

Figure 7.11 shows the X-Y graph of the end-effector motion and Figure 7.12(a) indicates the desired and actual length of the cables in meter. For the first part of this movement ($1 \rightarrow 2$), L_2 and L_3 were required to release the cables but keep a minimum tension to avoid slackness; however, cable L_4 were required to pull the cables and hence the end-effector. Therefore, an increase in the length of cables L_2 and L_3, and a decrease in L_4 is observed. The length of cable L_1 is first decreased and then increased accordingly. The change of the cable lengths in return motion

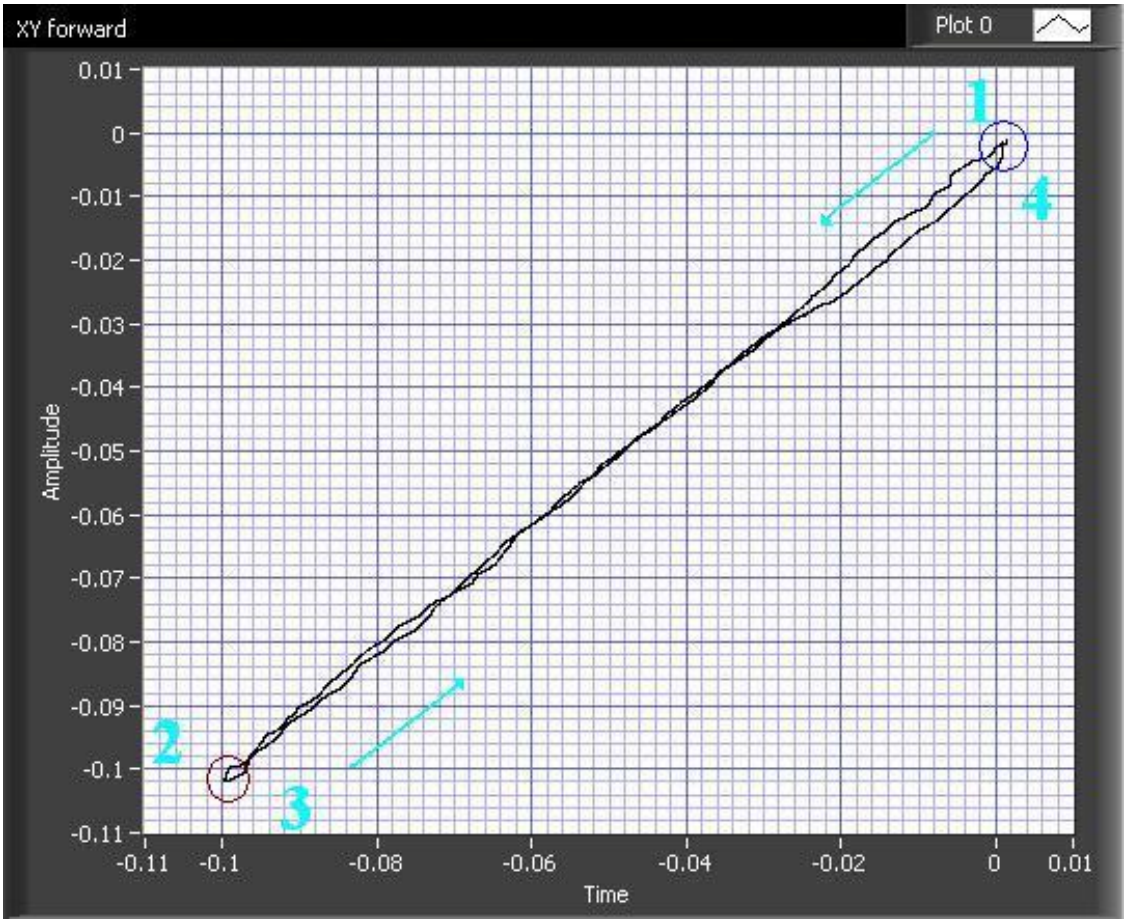

Figure 7.11: X-Y Graph of Linear Trajectory

(3 $\rightarrow$ 4) from (-0.1,-0.1) to (0,0) is vice versa. The tracking error of actuators in the linear movement is also shown in Figure 7.12(b). It is observed that, the maximum tracking error occurs at the beginning of the motion (1) and decreases gradually. There exists another peak of error at point (3), while the end-effector starts its return motion from rest. The steady-state error of the actuators at the end of motion (point 4) is less that 0.05 rad.

Figure 7.13 shows the end-effector tracking errors in the linear motion. The desired and actual X and Y positions of the end-effector are shown in Figure 7.13(a), and the corresponding Cartesian error is represented in Figure 7.13(b). Note that, due to the symmetry of the robot and the trajectory, the desired X and Y positions (X_d and Y_d) are the same. It is observed that, the maximum error is approximately

7 mm in the X-direction, and 5 mm in the Y-direction, that occurs when the end-effector starts its motion from rest (point 1 for X and point 3 for Y), and reduce gradually during the motion. Moreover, an error of approximately 1 mm is observed in both X and Y coordinates at the beginning of motion (at point 1 of Figure 7.11), which is due to pre-tensioning process. An error of 2 mm is also observed at point 2, which can be explained in terms of the overshoot of the actuators.

Circular Trajectory: The first step in this experiment is also the pre-tensioning process. After that, the end-effector starts its movement from (0,0) to (-0.2,0) and wait for a while to settle in the position. Then starts its circular motion (trace a half-circle of $r_c = 0.2$ m radius and centered at the origin), while attempting to maintain $\varphi = 0$ for all motion. After reaching (0.2,0), it returns back to the origin (Figure 7.14). The experimental results are shown in Figure 7.15 - 7.16.

The desired and actual cables' length are shown in Figure 7.15(a). It is observed that, the rate of the cables' length change is greater, in comparison with the linear motion; that is because, rotating direction of the motors changes frequently in circular motion. Figure 7.15(b) is also shown the tracking error of actuators, through out the motion.

Figure 7.16 shows the tracking errors of the end-effector in the half-circular motion. The desired and actual X-Y position of the end-effector are shown in Figure 7.16(a), and the corresponding Cartesian errors are presented in 7.16(b). In addition, the desired and actual followed trajectory by the end-effector is shown in Figure 7.14. Besides that, the computed torque of actuators is also shown in Figure 7.17.

It is observed from experimental results that, the maximum error in X-direction is approximately 20 mm (at point 3), while it is 15 mm in the Y-direction. An error of 1 mm is also observed in both X and Y coordinates at the beginning,

which is mostly because of the pre-tensioning process (Figure 7.16). Moreover, at the end of the motion, the steady-state error is found to be less than 1 mm. Besides the above experiments, in order to verify the actuators dynamic modeling and generated tensions, the tension of the cables are measured through out the half-circular motion, once for "independent joint control" approach and once for "computed torque" approach. The obtaining results are shown and compared in Figures 7.18 and 7.19.

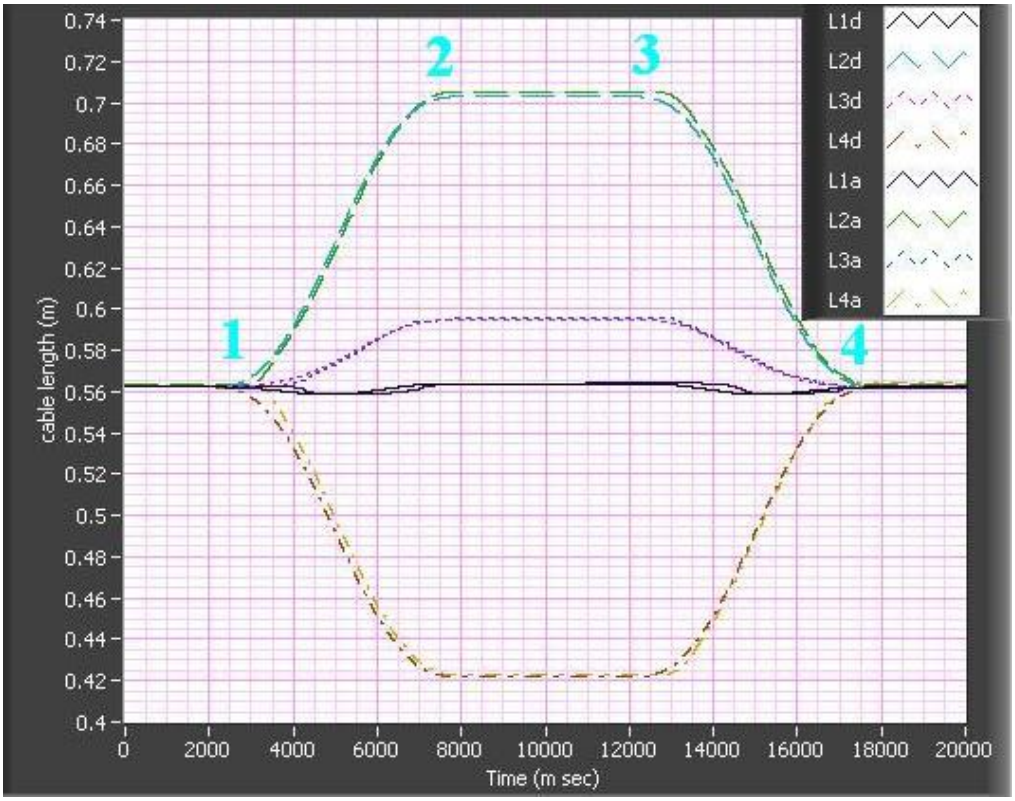

(a) Length Control for the Linear Trajectory

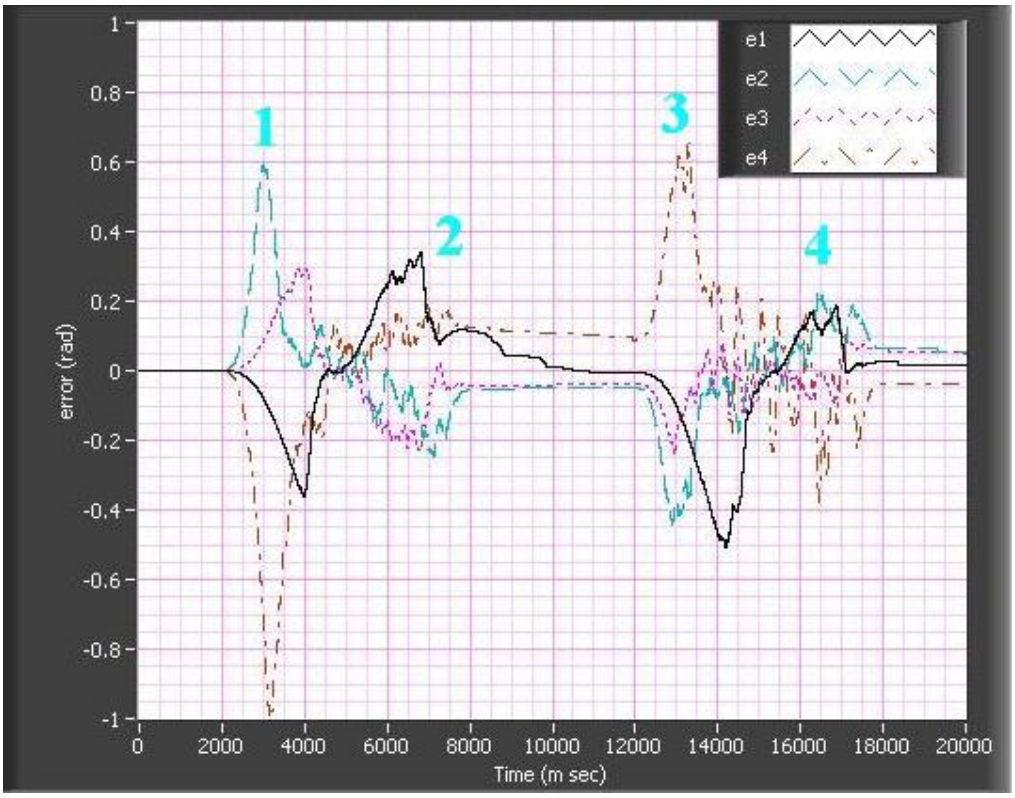

(b) Angular Position Error of Actuators

Figure 7.12: Length Control of the Cables in Linear Trajectory

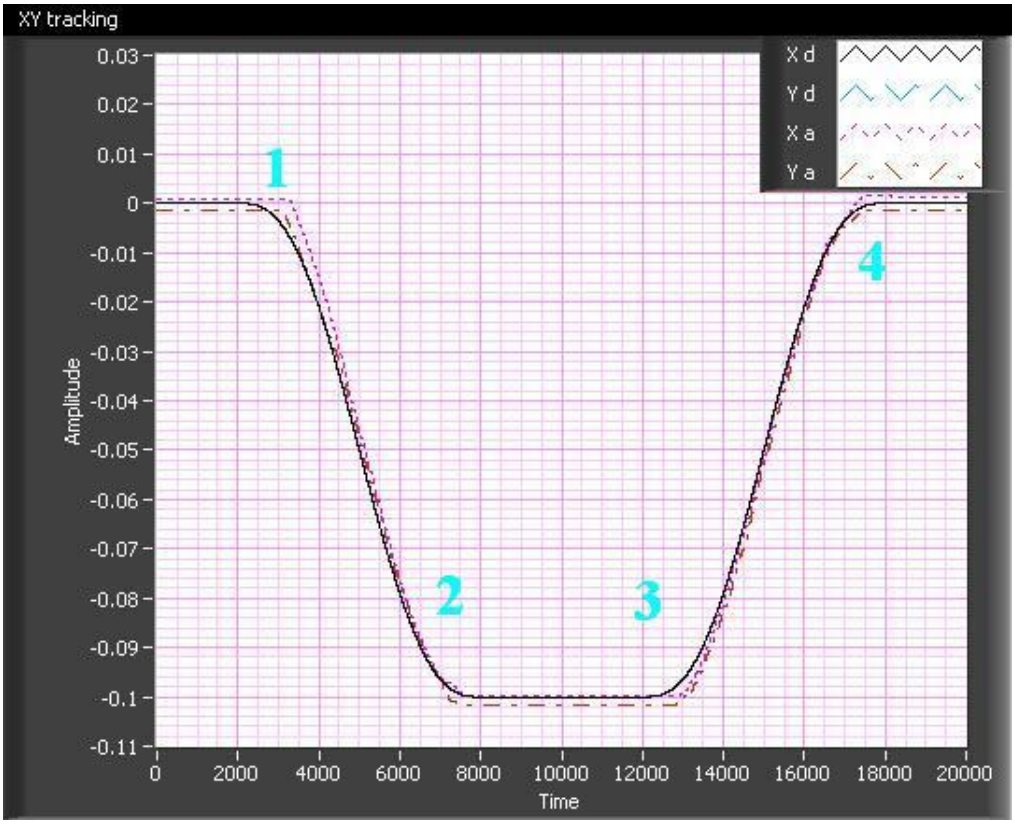

(a) X-Y tracking of End-effector

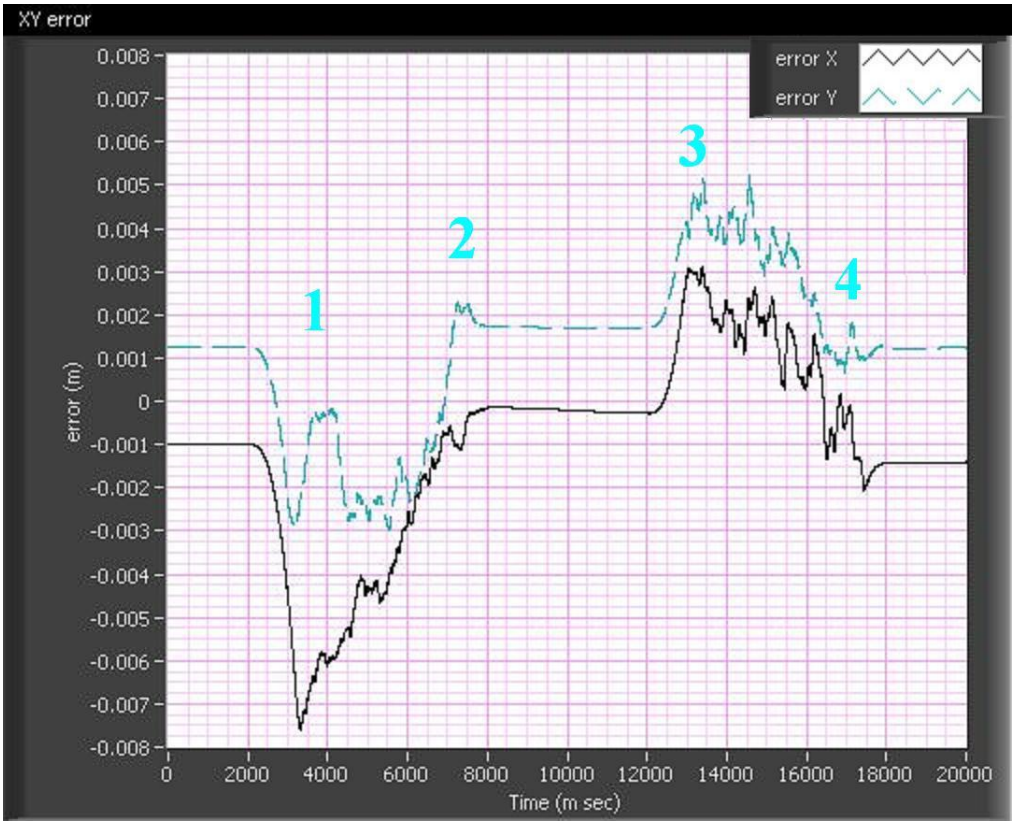

(b) X-Y end-effector Error

Figure 7.13: Errors in Linear Trajectory from (0,0) to (-0.1,-0.1)

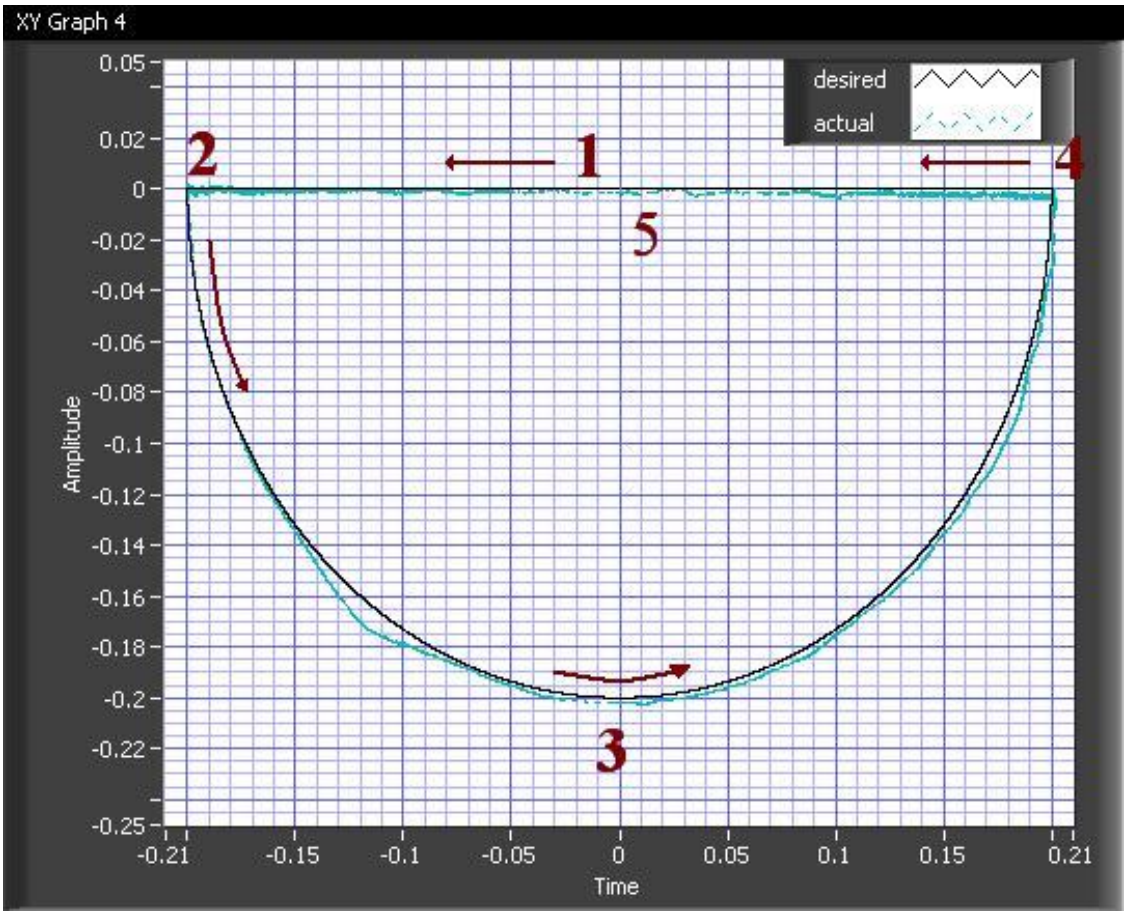

Figure 7.14: X-Y Graph of Circular Trajectory

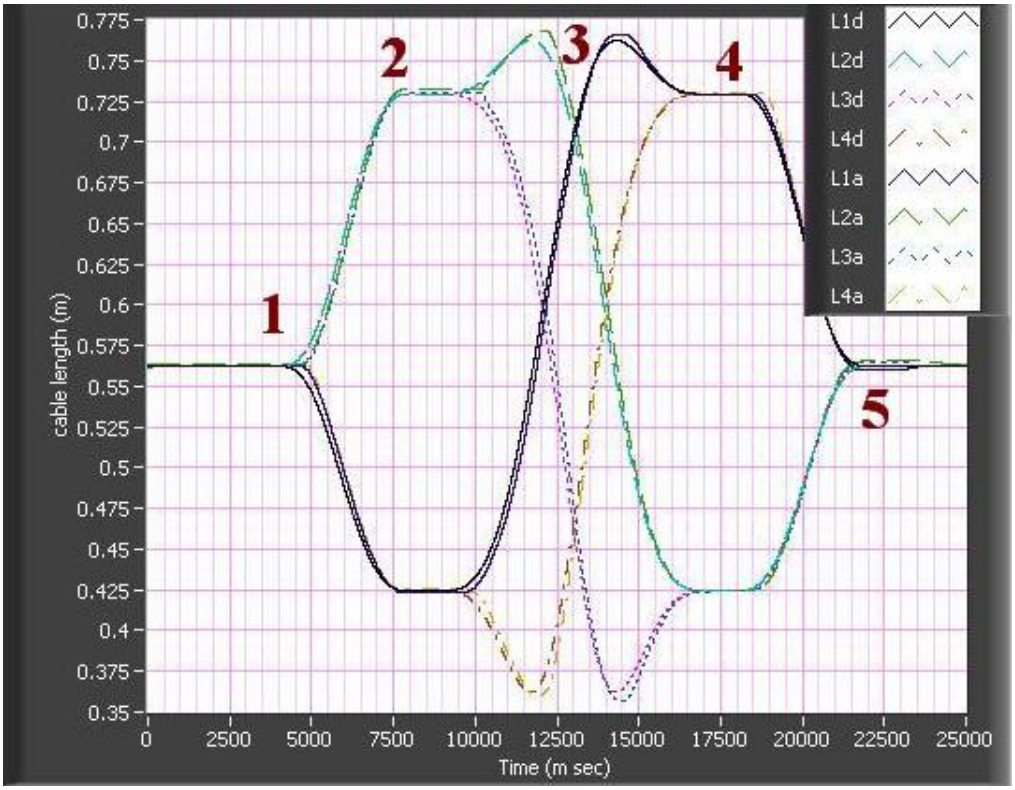

(a) Length Control for the Linear Trajectory

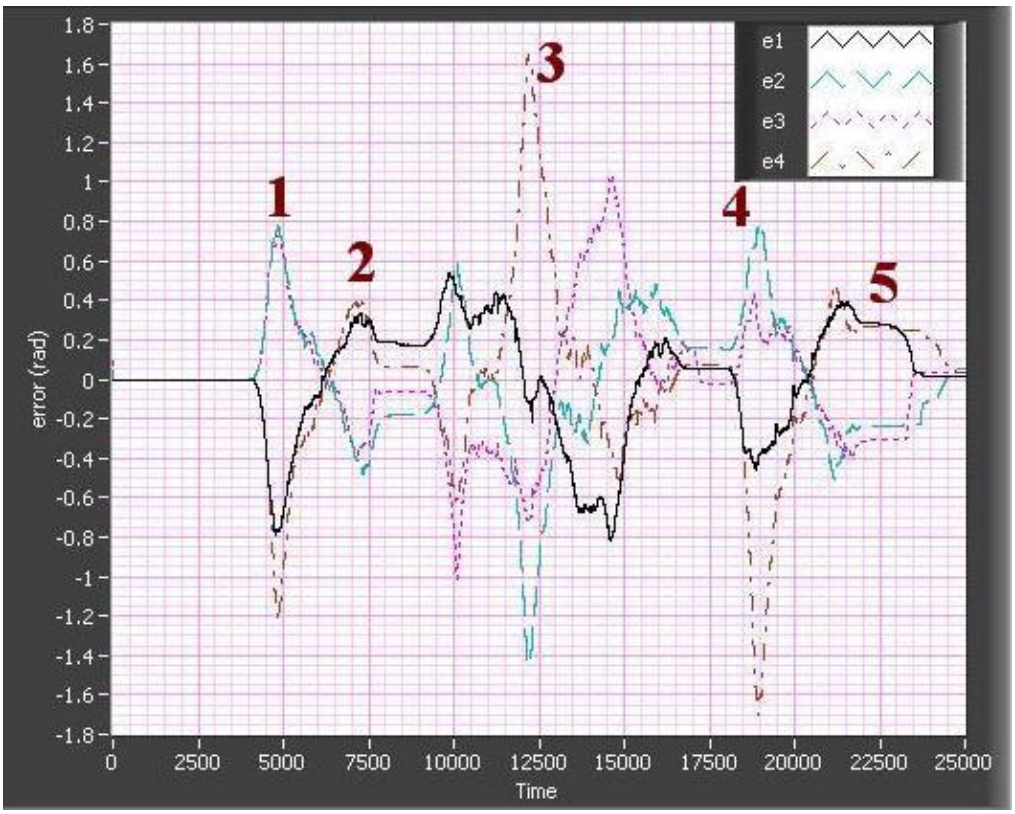

(b) Angular Position Error of Actuators

Figure 7.15: Length Control of the Cables in Half-circular Trajectory

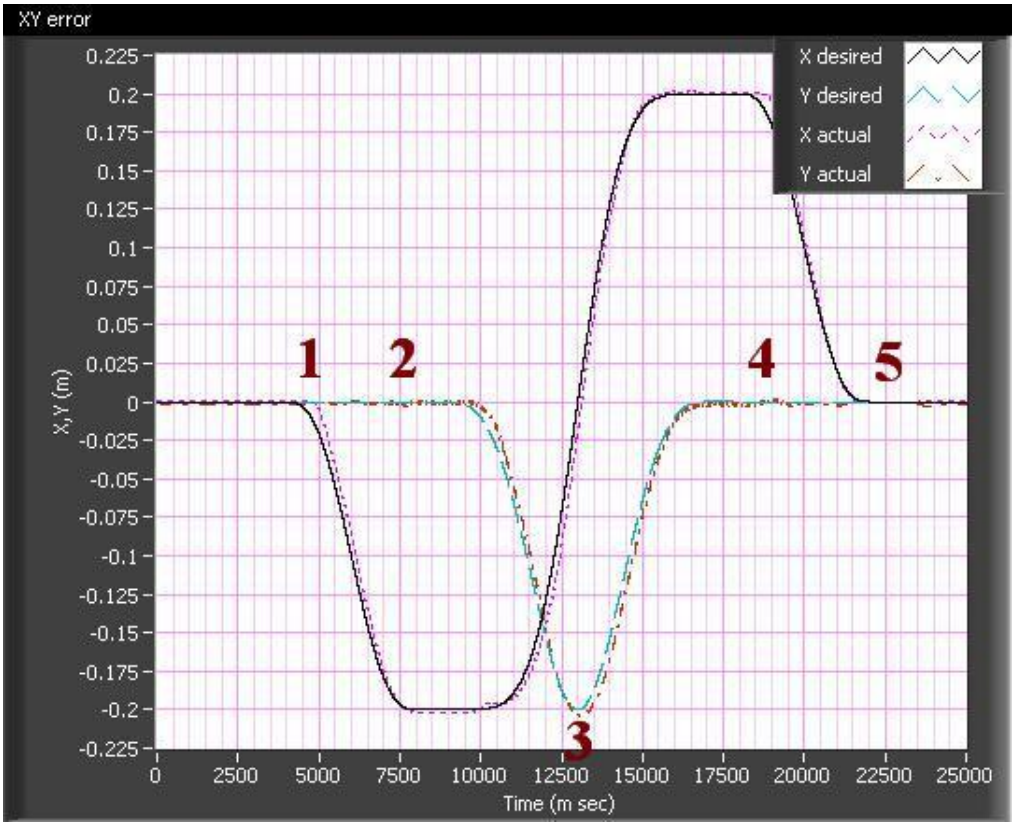

(a) X-Y tracking of End-effector

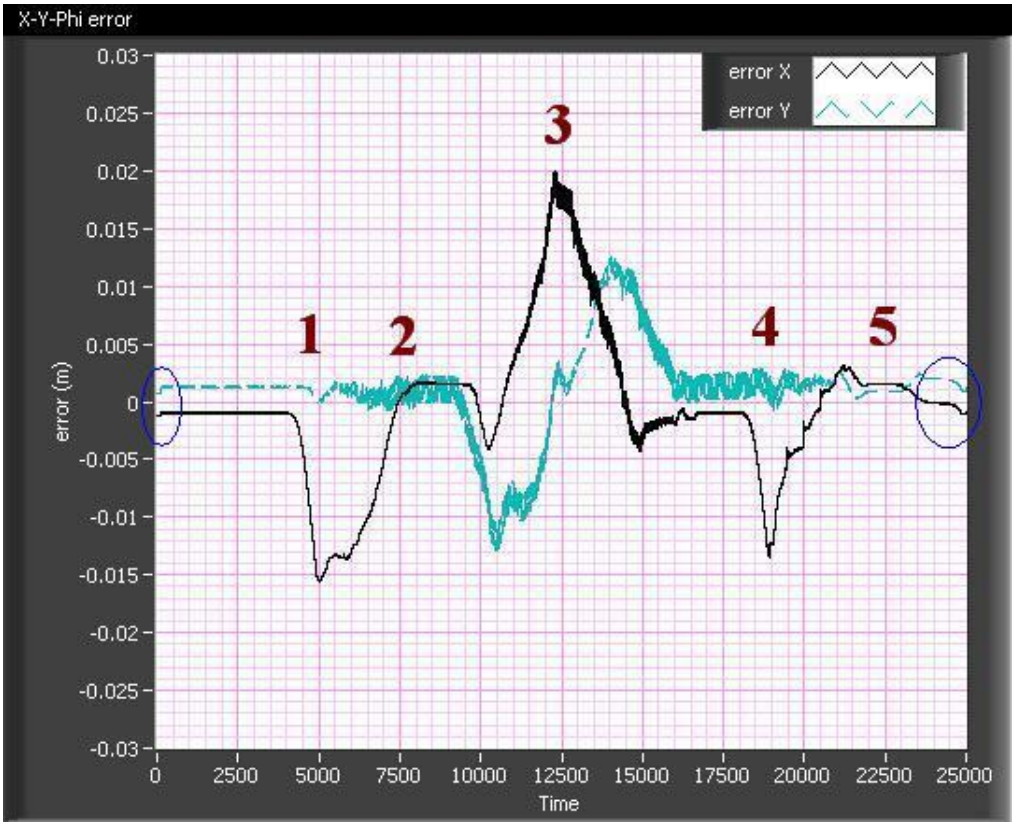

(b) X-Y Error Control

Figure 7.16: Errors in Half-Circular Trajectory

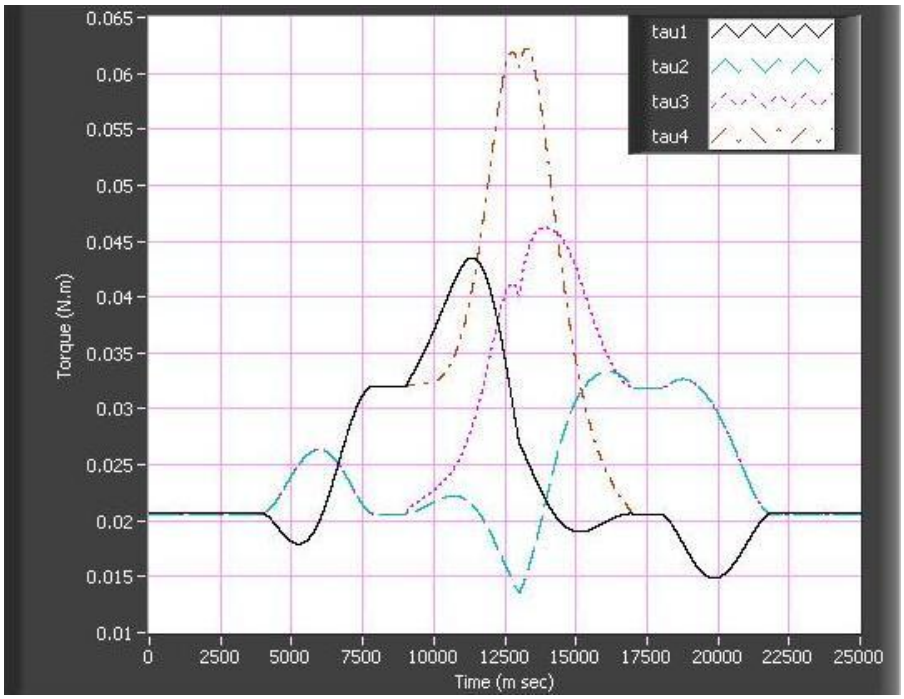

Figure 7.17: Actuator Torques for Half-circular Trajectory ($t_{\min} = 3N$)

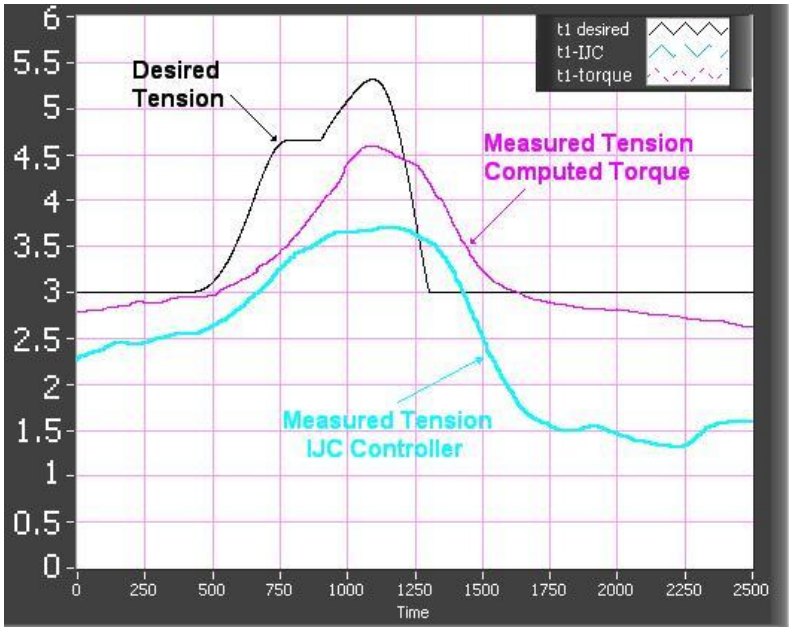

(a) t_1

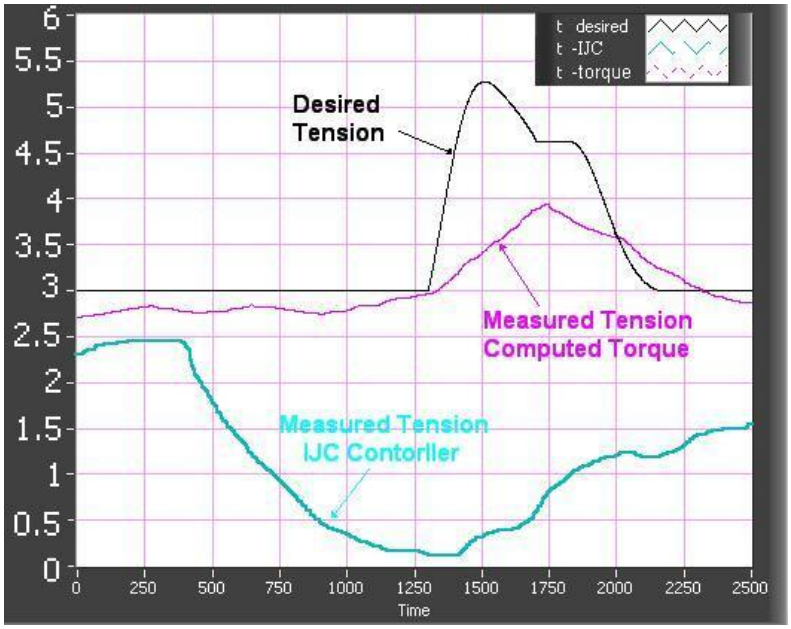

(b) t_2

Figure 7.18: Comparison of t_1 and t_2 in IJC and Computed Torque Controller

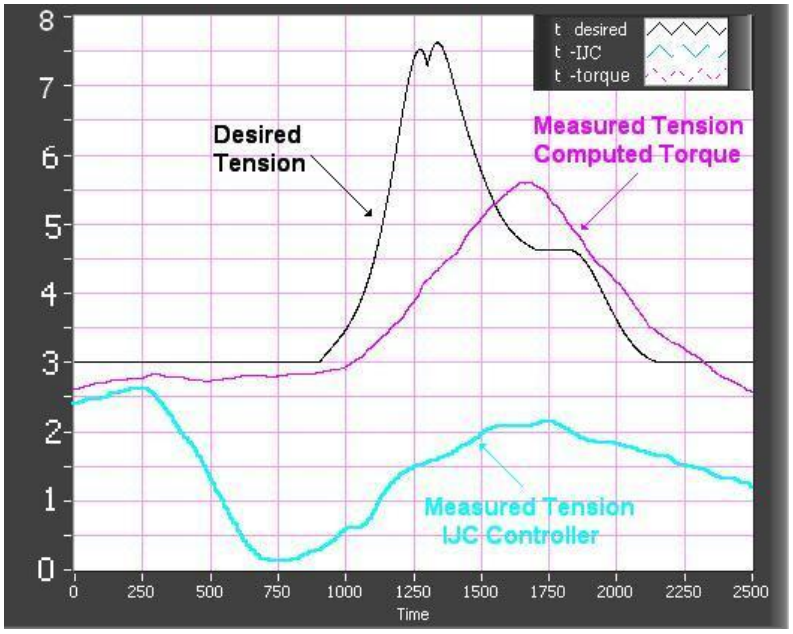

(a) t_3

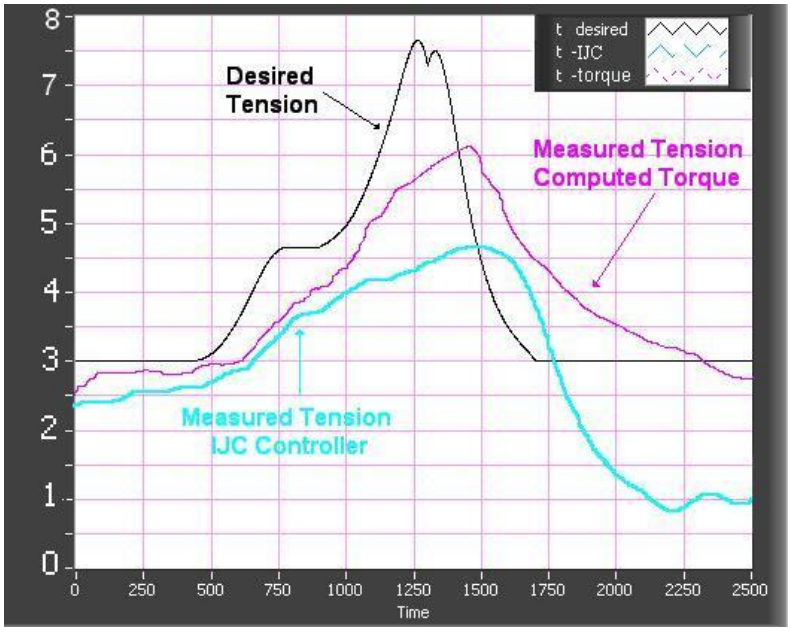

(b) t_4

Figure 7.19: Comparison of t_3 and t_4 in IJC and Computed Torque Controller

It is observed that, using the IJC approach, the cables' tension drop after motion starts, specially for those motors which release the cable (t_2 and t_3). The reason is the lack of control on the tension of the cables, as only the change of the length of cables is taken into consideration by the PID joint controllers. However, using the computed torque method, which tries to control the torque of the motors, shows a better performance in terms of maintaining cables' tension. As it can be seen from the experimental results, in this method, the minimum tension of the cables are kept during the whole motion and also the tension tracking is more satisfactory than IJC method.

On the other hand, comparing Figures 7.9(b) and 7.16(b), one can conclude that the positional accuracy of computed torque method is not as good as IJC controller, which is due to the inherent properties of computed torque controller, i.e. it does not control the position directly but tries to compensate the error by controlling the torque of the actuators using the dynamics of the robot. Therefore, the dynamic parameters of the system (e.g. inertia of the motors and end-effector) affects the performance of the controller. Moreover, in the proposed computed torque method velocity feedback was not used, and the nonlinear terms were calculated based on the desired velocity profile of the motion. As a result, the uncertainties due to dynamic parameters estimation and excluding the velocity feedback terms affect the performance of the controller and probably increase the tracking error. Velocity observers should be designed and implemented on the computed torque control to improve the dynamic performance of CDRs, which requires further studies.

It is also concluded that IJC method provides better positional accuracy. While, computed torque method results in better tension tracking and hence provides higher stiffness. Therefore, it is preferred to use IJC method wherever higher positional accuracy is needed and use the computed torque method when higher stiffness and tension accuracy is needed, i.e. computed torque method can be used

for point to point movement and IJC approach may be implemented for trajectory following.

Last but not the least, it seems that a combination of position control and torque control running together (*hybrid control*) is highly desired for cable-driven robots. In this hybrid system, torque control maintains the cables' tension and hance the robot stiffness, during the movement, while position control may be used at the endpoints where higher positional accuracy is needed. Hybrid control can be implemented by using two sets of amplifiers at the same time, one runs in voltage mode for position control and the other one runs in current mode for torque control. High frequency switches, must be used to switch between position control and torque control, whenever it is necessary. However, implementation of hybrid controllers are very difficult in practice. For example, in our prototype eight sets of amplifiers were used, four in current mode for computed torque control and four in voltage mode for IJC control. The mode of the amplifiers was set manually throughout DSP switches. Besides that, each amplifier has two wires as power line and two wires to output the signal to the motor. Therefor, each amplifier needs four high frequency switches, which their synchronization is not an easy task and requires further studies.

7.6 Summary

In this chapter, two approaches for the control of cable-driven robots was pointed out mainly. The first one was an independent joint control (IJC) approach, which uses local independent PID controllers at each joint to control its angular position, while the second approach was based on the control law development using computed torque method. Both of the control approaches were implemented on the planar prototype and compared with experimental results. It was concluded

that IJC controller results in better positional accuracy in terms of tracking error and steady state error, but suffers from loosing the tension during the motion (especially when actuators release the cables). On the other hand, computed torque controller was found to be useful in maintaining the positive tension during the motion and providing pretension in the cables.

Chapter 8

Cable-Driven Robot Application as a Hand Rehabilitation Device

A rehabilitation application of our planar cable-driven robot is demonstrated in this chapter, in order to show the efficiency and capability of our prototype. Cable-driven robots are proper choices for rehabilitation applications, since their workspace is large and multiple-DOF motion can be achieved with relatively low powered actuators compared with the mechanisms that use conventional rigid links. In addition, CDRs are light and flexible, which makes them human-friendly systems for rehabilitation processes. Our eventual goal is a rehabilitation system that carries out 3-DOF motions of hand.

8.1 Rehabilitation

Rehabilitation is a therapy which has the purpose to recover partially or totally the motion abilities of a patient. In the last years, there was an increasing demand of rehabilitation therapist, due to many factors such as the increasing of the average

age of the population, the advancement in the treatment of pathologies that in the past were incurable and the increasing of activities with high risk of incidents or traumas [45].

Hand Rehabilitation: General hand rehabilitation goals are to restore motion and strength for optimal function while protecting injured and repaired structures. The trend in rehabilitation has been toward early mobility with less immobilization [33]. The greatest challenge facing therapists is determining the balance between mobility and stability. Often, attention is given to mobility and strength at the expense of stability and comfort. Range of motion (ROM) is initiated as early as possible within safe parameters to prevent the development of stiffness. The following guideline outlines appropriate treatment to restore joint motion and function after fractures, while avoiding damage to repaired and injured structures [83]. Generally, the hand rehabilitation process consists of three stages:

- **Postoperative Phase I: Inflammation/Protection** (Weeks 0 to 2): In this phase, therapy focuses on protection of repaired or injured structures. No significant motion can be done in this phase.
- **Postoperative Phase II: Fibroblastic/Fracture Stability** (Weeks 2 to 8): In the early part of this phase, the protective splint is removed frequently for exercises and light, functional activities. Controlled stress to the healing tissue is most effective during the Fibroblastic phase. Early joint stiffness is treated with serial static or static progressive mobilization. Applied force is steady and prolonged to gain tissue length. Passive stretching is applied to the point of discomfort.
- **Postoperative Treatment Phase III: Scar Maturation and Fracture Consolidation** (Week 8 to Month 6): The primary goal in this phase is to achieve maximum ROM, increase strength and endurance, and resume

normal activity. There are no longer precautions that limit motion. If stiffness persists, capsular stretching, soft tissue mobilization, joint mobilization, and low load prolonged stretch via static progressive splints are used [83].

8.1.1 Concept of Hand Rehabilitator CDR

Our planar cable-driven prototype is well suited for rehabilitation purpose, due to its inherent potentials such as large workspace, high load capacity, and low cost due to the simplicity of components. The end-effector design should be modified to be adapted for hand rehabilitation. It means that the end-effector should be designed in the way that the patient can hold it easily. A simple joy-stick type end-effector seems to be useful, since the patient can easily grip the handle and apply the force. It is also practical for both left and right hand with different sizes. Moreover, the patient can start or stop the program by pressing the switches which are implemented on the joy-stick handle.

As mentioned earlier, the rehabilitation phase II includes active-assisted, gentle passive exercises over several repetitions and contract/relax exercises. Planar CDR is a very useful rehabilitation device in this phase, since it can apply certain amount of force in any desired direction in the X-Y plane by generating required tension in cables. According to static analysis of a CDR, the required tensions in the cables are calculated to resist the desired external force. This external force should be applied by the patient. The objective for the patient is to maintain the end-effector of the CDR in a pre-defined position by applying required force. Failing to do so, the end-effector starts to move in the X-Y plane. This method is quite useful as we can gradually increase the force in any desired direction to improve the patient strength. Moreover, the planar CDR highly meets the requirements for the rehabilitation phase III. In this phase we focus on the quality of the motion. The objective for the patient is to follow a pre-defined path with some required force.

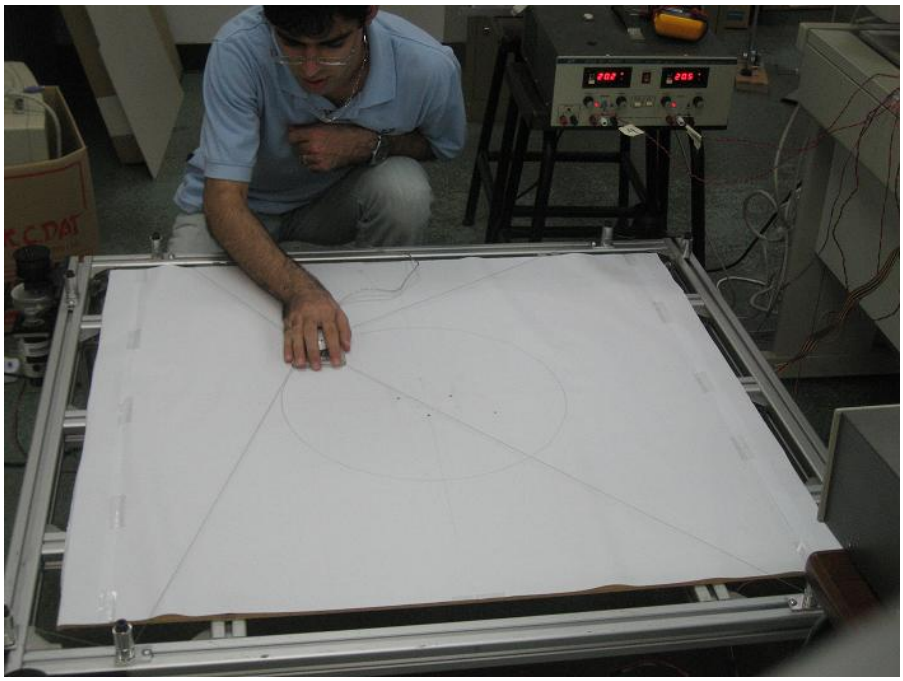

Figure 8.1: Cable-Driven Robot Application as a Hand Rehabilitation Device

For this purpose, we programmed the CDR end-effector to follow a trajectory as the patient applies the force continuously (8.1). Besides that, the motion of the end-effector can be monitored.

In order to show the capabilities of our prototype, two experiments are demonstrated and the results are shown in Figures 8.2 and 8.3, respectively. In the first example, the patient tries to follow a pre-defined semi-circular path while attempting to apply a force of t=3 N in the X direction. In the second example, patient moves his/her hand arbitrarily and CDR tries to balance the tension of the cables in order to maintain a net force of three Newton in the X direction. Figures 8.2(a) and 8.3(a) show the angular position of the actuators, whereas Figures 8.2(b) and 8.3(b) represent the actuator torques during the semi-circular and arbitrary paths, respectively. Moreover, the trajectory following of the end-effector is shown in Figures 8.2(c) and 8.3(c).

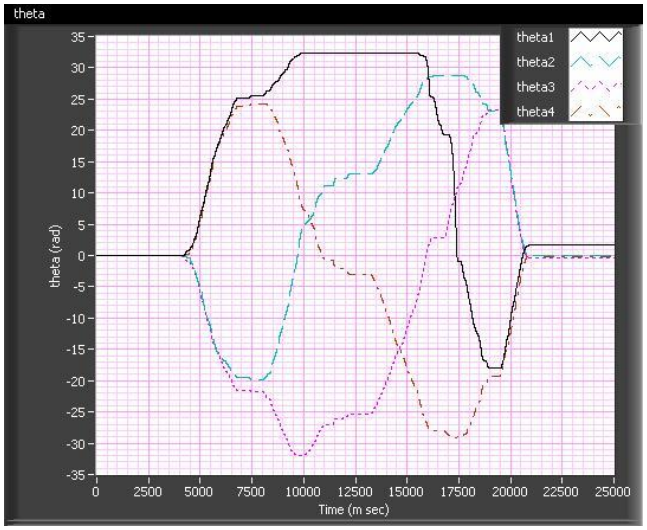

(a) Angular Position of Actuators

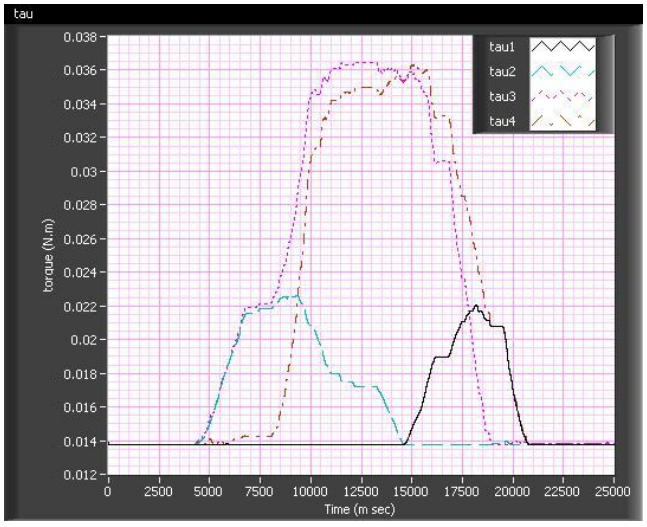

(b) Actuator Torques

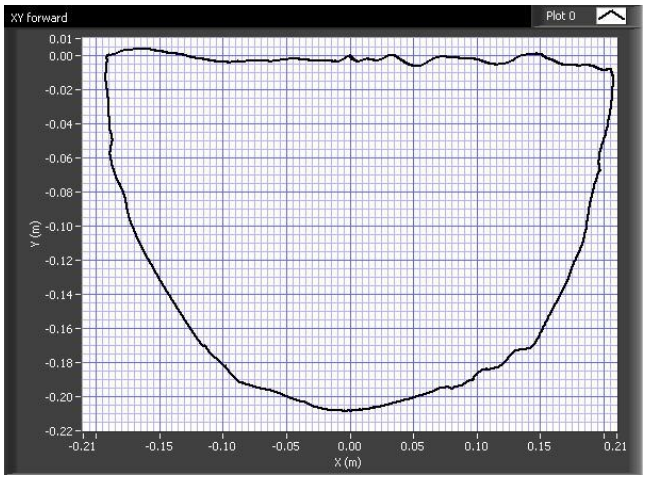

(c) X-Y tracking of End-effector

Figure 8.2: Rehabilitation Application: Circular Trajectory

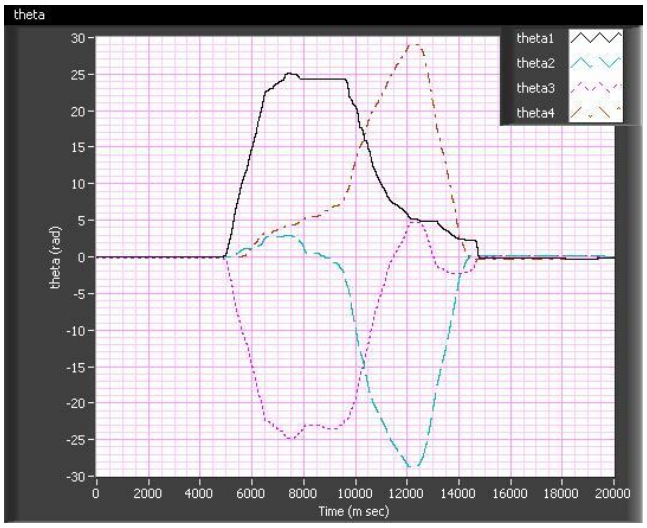

(a) Angular Position of Actuators

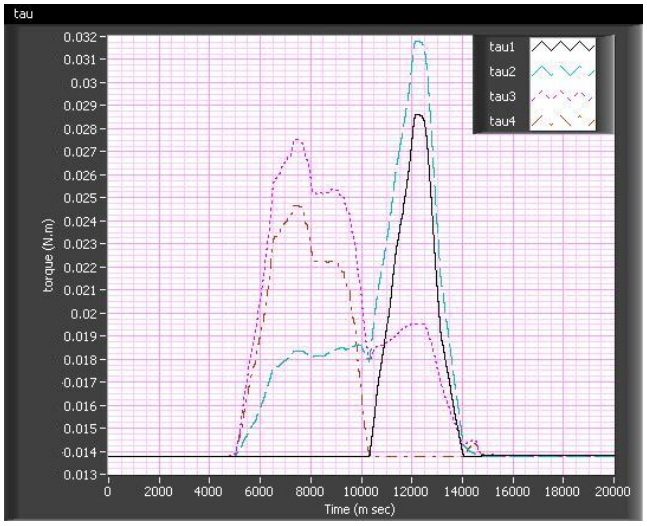

(b) Actuator Torques

(c) X-Y tracking of End-effector

Figure 8.3: Rehabilitation Application: Arbitrary Path

The force of a whole hand of a well-trained person is known to be 268 N [52]. Our prototype is able to apply a force up to 30 N in X-Y plane, which is high enough for the phase II of rehabilitation process. By using larger actuators, the load capacity of the robot would be increased, subsequently. Moreover, for improvement of the performance of the rehabilitator, some limiting switches and in-line tension sensors can be used to shut down the system, whenever the end-effector reaches the boundary of the workspace or the cables looses their tensions. Another feature that can be added to the device, is the remote monitoring of the patient, which is empowered by LabView. This feature of the LabView programs let the patient connect the device to the internet and transfer the data to a therapist, who is able to see the screen. The therapist is also able to increase or decrease the applied force of the device or change the motion, based on the performance of the patient, which is monitored online. It should be noted that, this feature does not affect the real-time control of the robot, since all of the communication is done by the host computer.

8.1.2 Position Monitoring of End-effector with a Computer Mouse

In order to monitor the translational motion of the end-effector in X and Y coordinates, an optical computer mouse was used. The mouse was attached to the end effector as shown in Figure 8.4, and communicate with the host computer (Windows based PC) through a USB transmitter. A program was built in LabView 7.1 to get the position of the pointer in pixels and convert it to millimeters.

Since the mouse reading program consisted of ¡User32.dll¿ functions of Windows, it can not be executed in LabView RT. Hence, for monitoring the position of end-effector the RT target computer should execute the control programs in

Figure 8.4: End-effector and the attached mouse

real-time and at the same time, the mouse reading program should run on host computer. To observe the performance of the USB optical mouse, different trajectories were tested. As an example a diagonal linear a semicircle trajectory monitoring are shown in Figures 8.5 and 8.6, respectively.

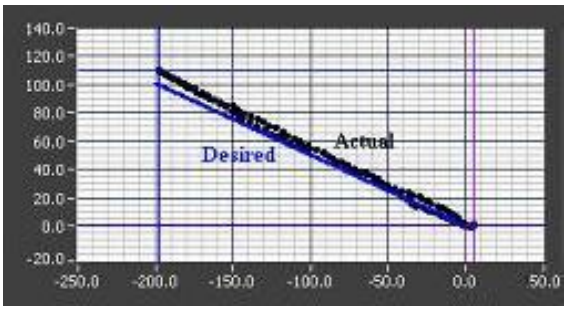

Figure 8.5: Mouse Reading for Diagonal Trajectory from (0, 0) to (-200,100)

Mouse reading from the host computer is not fast and accurate enough to be used as the position feedback of the encoder. It should be noted that the optical mouse can detect X and Y positions correctly if the end-effector does not rotate. Although the accuracy of mouse reading is not high enough that can be used as a position feedback, but it seems to be useful for monitoring the patient exercise. Furthermore, in order to use the mouse data as a position feedback, it is necessary to process its signal in advance, before sending it to the real-time target.

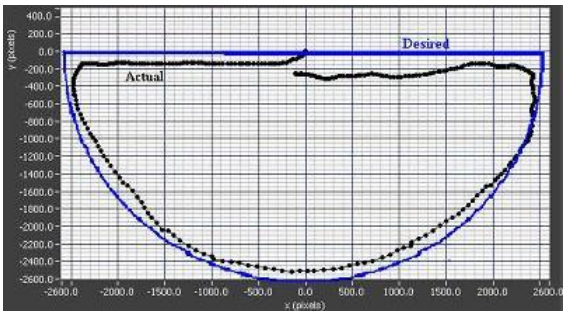

Figure 8.6: Mouse Reading for Semicircle Trajectory

8.2 Summary

In this chapter an application of the planar prototype in rehabilitation was presented. At first the hand rehabilitation process and its phases were introduced. Then, the concept of hand rehabilitator cable-driven robot was explained and some experiments were carried out to investigate the performance of the hand rehabilitator CDR. It was observed that, the planar CDR performance was satisfactory and its capabilities as a hand-rehabilitator device were proved.

Chapter 9

Conclusion and Future Work

The fundamental research issues of cable-driven robots (CDRs) including kinematic analysis, tension analysis, workspace analysis, dynamic analysis, and control strategies have been studied, in this thesis. This chapter, provides the main contributions and the possible future research directions, of our work.

9.1 Contributions

- **Kinematic Analysis:** Due to the kinematic redundancy in CDRs, the analytical displacement solution for a general CDR is hardly obtainable. In this thesis, the forward displacement solution was approached by the numerical Newton-Raphson method, which is as effective method due to its property of quadratic convergence. Some computational examples were given to shown the effectiveness of this method. Following that, the expressions of the velocity and acceleration analysis for a planar cable-driven robot were derived.

- **Tension analysis:** The tension solution for the class of completely restrained CDRs was discussed in details, with the use of Null space approach. Based

on the existence of the positive solution, the static workspace of the planar CDR was obtained and it was concluded that, the workspace of the planar CDRs is limited in term of orientation angle of the end-effector.

- **Stiffness Modeling:** A complete stiffness model, including passive stiffness and active stiffness of CDRs was introduced. In addition, the stiffness matrix of a planar CDR was derived in details. By introducing the concept of stabilizability, the stiffness workspace of planar CDR was obtained as the set of the poses with positive definite stiffness matrix. It was observed that the stiffness workspace is a sub-set of a static workspace and the torsional stiffness of CDRs is much lower than their translational stiffness.

- **Dynamic Modeling:** A complete dynamic model of CDRs including the end-effector dynamic model and actuator dynamic model was derived. This dynamic model was used to find torque values which are necessary for control and actuator selection. Moreover, the dynamic equations of a planar CDR were simulated for a semicircular trajectory. Simulation results illustrated that the actuator torques can be obtained as long as the tension solution exists and the resultant torque changes quite smoothly through out the trajectory. This derived dynamic model, is reliable to be applied to any CDR, together with a general formulation of kinematics, due to its general formulation.

- **Control of CDRs:** Two approaches for the control of cable-driven robots were pointed out mainly. The first one was an independent joint control (IJC) approach, which used local independent PID controllers at each joint, while the second approach was based on the control law development using computed torque method. Both of the control approaches were implemented on the planar prototype. Experimental results showed that, IJC controller has better positional accuracy, but suffers from cables' slackness during the motion. On the other hand, computed torque controller was found to be use-

ful in maintaining the positive tension dynamically and providing pretension in the cables.

- **Application:** Finally, a rehabilitation application of planar prototype was presented. Experimental results proved the capabilities and effectiveness of CDRs for rehabilitation purposes.

9.2 Future Work

This thesis opens up some interesting directions for further investigation, that are described in below.

In the computed torque method, which is implemented on CDRs, the velocity feedback is not considered and hence the overall system is not linearized yet. Although the controller performance in terms of maintaining the cables' tension seems to be good, but inserting velocity observers in the controller will improve the control system and hence reduce the end-effector tracking error. However, the velocity signal, which is obtained by differentiating the position feedback, is usually noisy and requires additional signal processing that increase the computational cost of the program. Velocity observers should be designed and implemented in real-time for improving the control of CDRs.

The positional accuracy and the tension of the cables are equivalently important for the cable-driven robots. Therefore, a hybrid control approach seems to be very useful for controlling CDRs. However, implementation of hybrid controller is very difficult in practice. Since high frequency electronic switches are needed for changing the control modes of the motors from current-mode (torque-control) to voltage-mode (position-control) and vice versa, in real time. Hybrid control method, still requires further theoretical and experimental studies.

Tension control of the cables plays an important role in cable-driven robots. Even though the computed torque method attempts to keep the tension of the cables, it is not using the tensions feedback directly. This method works based on the applied torque of the actuator, which is used to obtain the tension. However, these estimated tension values may differ from the real ones in the cables. Therefore, Using a tension sensor could be very useful; however, this sensor should be fast enough for real time applications and small in size for inline attachment to the cables. Currently, most of the commercialized tension sensors are slow, due to their strain-gauge structures. The output signal of strain-gauges is very noisy, hence, signal processing and filtering are essential that makes the time response of the sensor slower. Therefore, designing and fabricating a dynamic tension sensor seems to be essential for improving the tension control of cable-driven robots. Having used the tension feedbacks, more advanced control techniques should be implemented on the cable-driven robots.

Bibliography

[1] J. Albus, R. Bostelman, and N. Dagalakis, "The NIST robocrane", Journal of Robotic Systems, vol. 10, No. 5, pp. 709–724, 1993.

[2] A.B. Alp, and S.K. Agrawal, "Cable suspended robots: Design, planning and control", in Proceedings of IEEE Conference on Robotics and Automation, Washington, DC., USA, vol.4, pp. 4275–4280, 2002.

[3] A.B. Alp, and S.K. Agrawal, "Cable Suspended Robots: Feedback Controllers with Positive Inputs", Proceedings of the American Control Conference, Anchorage, AK, vol.1 , pp. 815–820, 2002.

[4] K.R. Atia, M.P. Cartmell, "SEPA-ROBOT: a serial-parallel manipulator with singularity-based design", Proceedings of IEEE International Conference on Industrial Technology, Goa, India, vol. 1, pp. 49–54, 2000.

[5] G. Barette, and C.M. Gosselin, "Kinematic analysis and design of planar parallel mechanisms actuated with cables", in Proceedings of the ASME 2000 Design Engineering Technical Conferences and Computers and Information in Engineering Conference, Baltimore, Maryland, USA, pp. 123–128, 2000.

[6] S. Behzadipour, A. Khajepour, "Stiffness of Cable-based Parallel Manipulators With Application to Stability Analysis", Journal of Mechanical Design - ASME, vol. 128, Issue 1, pp. 303–310, 2006.

[7] I.A. Bonev, D. Zlatanov, C.M. Gosselin,"Singularity analysis of 3-DOF planar parallel mechanisms via screw theory", Transactions of the ASME Journal of Mechanical Design, vol. 125, No. 3, pp. 573–81, 2003.

[8] R.V. Bostelman, J.S. Albus, N.G. Dagalakis, A. Jacoff, J. Gross, "Applications of the NIST RoboCrane", Proceedings of the 5th International Symposium on Robotics and Manufacturing, Maui, HI, pp. 14-18, 1994.

[9] P. Bosscher, and I. Ebert - Uphoff, "A stability measure for underconstrained cable-driven robots", in Proceedings of IEEE Conference on Robotics and Automation, New Orleans, LA, USA, vol. 5, pp. 4943-4949, 2004.

[10] R. Bostelman, R., J. Albus, N. Dagalakis, A. Jacoff, and J. Gross, "Applications of the NIST ROBOCRANE", Proceedings of the 5th International Symposium on Robotics and Manufacturing, Maui, HI, Vol. 5, pp. 403–407, 1994.

[11] E.K.J. Chadwick, and A.C. Nicol, "Elbow and Wrist Joint Contact Forces During Occupational Pick and Place Activities", Journal of Biomechanics, vol. 33, No. 5, pp. 591–600, 2000.

[12] W. Choe, H. Kino, K. Katsuta, and S. Kawamura, "A Design of Parallel Wire Driven Robots for Ultrahigh Speed Motion Based On Stiffness Analysis", Proceedings of The JAPAN-USA Symposium on Flexible Automation - ASME, BOSTON, USA, vol.1, pp.159–166, 1996.

[13] C.L. Collins, G.L. Long, "The singularity analysis of an In-Parallel Hand Controller for Force-Reflected Teleoperation", IEEE Transactions on Robotics and Automation, vol. 11, No. 5, pp. 661–669, 1995.

[14] J.J. Craig, "Introduction to Robotics - Mechanics and Control", Addison-Wesley Publishing Company, 1986.

[15] A.S. Deif, "Advanced Matrix Theory for Scientists and Engineers", Abacus Press, 1991.

[16] E.J. Dougherty, D.E. Lee, and P.D. Shively, "Automated All-weather Cargo Transfer System (AACTS)", Society of Naval Architects and Marine Engineers, STAR Symposium, pp. S2-3-1, S2-3-6, 1989.

[17] A. Fattah, S.K. Agrawal, "Design of cable-suspended planar parallel robots for an optimal workspace", in Proceedings of the Workshop on Fundamental Issues and Future Research Directions for Parallel Mechanisms and Manipulators, Quebec City, Canada, pp. 195–202, 2002.

[18] I. Ebert-Uphoff, and P.A. Voglewede, "On the connections between cable-driven robots, parallel robots and grasping", in IEEE international Conference on Robotics and Automation, Atlanta, GA, USA, vol. 5, pp. 4521–4526, 2004.

[19] P. Gallina, G. Rosati, and A. Rossi, "3-d.o.f. Wire Driven Planar Haptic Interface", Journal of Intelligent and Robotic Systems, vol. 32, No. 1, pp. 23–36, 2001.

[20] J.J. Gorman, K.W. Jablokow, and D.J. Cannon, "The cable array robot: Theory and experiment", in Proceedings of the IEEE International Conference on Robotics and Automation, Seoul, Korea, vol. 3, pp. 2804–2810, 2001.

[21] C.M. Gosselin, "Parallel computational algorithm for the kinematics and dynamics of planar and spacial parallel manipulators", ASME journal of dynamics systems, measurment, and control, vol. 118, No.1, pp. 22–28, 1996.

[22] C. Gosselin, and J. Angeles, "Singularity Analysis of Closed-Loop Kinematic Chains", IEEE Transaction on Robotics and Automation, vol. 6, No. 3, pp. 281–290, 1990.

[23] M. Gouttefarde, and C.M. Gosselin, "On the properties and the determination of the wrench-closure workspace of planar parallel cable-driven mechanisms", in Proceedings of the ASME 2004 Design Engineering Technical Conferences and Computers and Information in Engineering Conference, Salt Lake City, UT, pp. 1–10, 2004.

[24] F. Hao, and J.M. McCarthy, "Conditions for line based Singularities in Spatial Platform Manipulators", Journal of Robotic Systems, vol. 15, No.1, pp. 43–55, 1998.

[25] C. Hee-Byoung, K. Atsushi, "Closed-Form Solutions for the Forward Kinematics of a 4-DOFs Parallel Robot", IEEE International Conference on Intelligent Robots and Systems, Uchiyama, Masaru, vol. 4, pp. 3312–3317, 2003.

[26] K. Homma, O. Fukuda, Y. Yoshihiko, "Study of a wire-driven leg rehabilitation system", Proceedings of the IEEE International Conference on Intelligent Robots and Systems, Lausanne, Switzerland, vol. 2, pp. 1451–1456, 2002.

[27] M. Kalyan, S.R. Oh, S.K. Agrawal, "A Dual-Stage Planar Cable Robot: Dynamic Modeling and Design of A Robust Controller with Positive Inputs", Transactions of the ASME Journal of Mechanical Design, vol. 127 , Issue 4, pp. 612-620, JULY 2005.

[28] S. Kawamura, W. Choe, S. Tanaka, S. and Pandian, "Development of an ultrahigh speed robot FALCON using wire drive system", Proceedings of the IEEE/ICRA International Conference on Robotics and Automation, Nagoya, Japan, vol. 1, pp. 215–220, 1995.

[29] S. Kawamura, M. Ida, T. Wada, and J.L. Wu, "Development of Virtual Sports Machine Using a Wire Drive System- A Trial of Virtual Tennis", Proceeding of IEEE/RSJ International Conference on Intelligent Robots and Systems, Washington, DC, USA, vol. 1, pp. 111–116, 1995.

[30] H. Kino, "Principle of orthogonalization for completely restrained parallel wire driven robot", in Proceedings of the IEEE/ASME International Conference on Advanced Intelligent Mechatronics (AIM 2003), Como, Italy, vol. 1, pp. 509–514, 2003.

[31] H.I. Krebs, N. Hogan, M.L. Aisen, and B.T. Volpe, "Robot-Aided Neurorehabilitation", IEEE Transactions on Rehabilitation Engineering, vol. 6, No. 1, pp. 75–87, 1998.6

[32] D.M. Ku, "Forward Kinematics Analysis of a 6-3 type Stewart Platform Machanism", Proceedings of the Institution of Mechanical Engineers, Part K: Journal of Multi-body Dynamics, vol. 214, No. 4, pp. 233-241, 2000.

[33] G. Kurillo, N. Goljar, T. Bajd, "Force tracking systems for training of hand function in stroke patients", IEEE 2nd international conference on Neural engineering, Washington D.C., USA, vol. 1, pp. 438–441, 2005.

[34] P. Levi, M. Muscholl, Th. Braunl, "Cooperative Mobile Robots Stuttgart: Architecture and Tasks", Proceedings of the 4th International Conference on Intelligent Autonomous Systems, Karlsruhe, Germany, vol. 1, pp. 310-317, 1995.

[35] F.L. Lewis, C.T. Abdullah, and D.M. Dawson, "Control of Robot Manipulators", MacMillan, New York, 1993.

[36] P.S. Lum, C.G. Burgar, H.F.M. Van der Loos, "The Use of a Robotic Device for Post-Stroke Movement Therapy", Proceedings of the International Conference on Rehabilitation Robotics, Beirut, Lebanon, pp. 107–110, 1997.

[37] K. Maeda, S. Tadokoro, T. Takamori, M. Hiller, and R. Verhoeven, "On design of a redundant wire-driven parallel robot WARP manipulator", in Proceedings of the IEEE International Conference on Robotics and Automation, Detroit, Michigan, USA, pp. 895–900, 1999.

[38] T. Maier, and C. Woernle, "Flatness-based control of underconstrained cable suspension manipulators", in Proceedings of DETC'99 ASME Design Engineering Technical Conferences, Las Vegas, Neveda, USA, vol. 4, pp. 129 - 130, 1999.

[39] F. Majou, P. Wenger, and D. Chablat, "Design of a 3 Axis Parallel Machine Tool for High Speed Machining : The Orthoglide", 4th International Conference on Integrated Design and Manufacturing in Mechanical Engineering (IDMME), Clemont-Ferrand, France, 2002.

[40] J.P. Merlet, "Singularity Configurations of Parallel Manipulators and Grassmann Geometry", The International Journal of Robotics Researchm, vol. 8, pp. 45–56, 1989.

[41] J.P. Merlet, "Parallel Robots", vol. 74, Netherlands: Kluwer Academic Publishers, 2000.

[42] A. Ming, and T. Higuchi, "Study of Multiple Degree-Of-Freedom Positioning Mech Using Wires (Part 1) - Concept, Design and Control", International Journal of Japan Society Precision Engineering, vol. 28, No.2, pp.131–138, 1994.

[43] A. Ming, and T. Higuchi, "Study of Multiple Degree-Of-Freedom Positioning Mech Using Wires (Part 2) - Development Of Planar Completely Restrained Positioned Mechanism", International Journal of Japan Society Precision Engineering, vol. 28, No. 2, pp.235–242, 1994.

[44] T. Morizono, K. Kurahashi, and S. Kawamura, "Realization of a virtual sports training system with parallel wire mechanism", in Proceedings of the 1997 IEEE International Conference on Robotics and Automation, Albuquerque, New Mexico, vol. 3, pp. 3025–3030, 1997.

[45] M. Mulas, M. Folgheraiter, and G. Gini, "An EMG-controlled exoskeleton for hand rehabilitation", IEEE 9th International Conference on Rehabilitation Robotics, Chicago, Illinois, USA, vol. 2, pp. 371–374, 2005.

[46] Y. Nakamura, "Advanced Robotics - Redundancy and Optimization", Addison-Wesley Publishing Company, 1991.

[47] N. Nanua, K.J. Waldron, and V. Murphy, "Direct kinematic solution of a stewart platform", in IEEE Transactions on Robotics and Automation, vol. 6, No. 4, pp. 438–444, 1990.

[48] K. Ogata, "Modern Control Engineering", Prentice-Hall, 1996.

[49] S.R. Oh, S.K. Agrawal, "Nonlinear Sliding Mode Control and Feasible Workspace Analysis for a Cable Suspended Robot with Input Constraints and Disturbances", Proceeding of the American Control Conference, Boston, Massachusette, USA, vol. 5, pp. 4631–4636, 2004.

[50] S.R. Oh, S.K. Agrawal, "Cable-Suspended Planar Parallel Robots with Redundant Cables: Controllers with Positive Cable Tensions", Proceedings of the IEEE International Conference on Robotics and Automation, Taipei, Taiwan, vol. 3, pp. 3023–3028, 2003.

[51] S.R. Oh, S.K. Agrawal, "Cable Suspended Planar Robots With Redundant Cables: Controllers With Positive Tensions", IEEE Transactions on Robotics, vol. 21, No. 3, pp. 457–464, 2005.

[52] S. Olandersson, H. Lundqvist, "Finger-Force measurement device for hand rehabilitation", IEEE 9th International conference on rehabilitation robotics, Chicago, Illinois, USA, vol. 1, pp. 135–138, 2005.

[53] H. Osumi, Y. Utsugi, and M. Koshikawa, "Development of a manipulator suspended by parallel wire structure", in Proceedings of the IEEE/RSJ In-

ternational Conference on Intelligent Robots and Systems (IROS 2000), Takamatsu, Japan, vol.1, pp. 498–503, 2000.

[54] C.B. Pham, "Analysis and design of cable-driven parallel kinematic mechanisms", PhD dissertation, Nanyang Technological University, Singapore, 2005.

[55] C.B. Pham, S.H. Yeo, G. Yang, "Tension analysis of cable-driven parallel mechanisms", Proc. Of IEEE/RSJ International conference on Intelligent Robots and systems, Edmonton, Alta., Canada, pp. 257-62, 2005.

[56] T. Sakaki, S. Okada, Y. Okajima, N. Tanaka, A. Kimura, S. Uchida, M. Taki, Y. Tomita, and T. Horiuchi, "TEM: Therapeutic Exercise Machine for Hip and Knee Joints of Spastic Patients", Proceedings of the International Conference on Rehabilitation Robotics, pp. 183–186, California, USA, 1999.

[57] S. Shahin S. and L. Notash, "Kinematics, Workspace and Stiffness Analysis of Wire-Actuated Parallel Manipulators", Proceedings Of The 11th World Congress in Mechanism and Machine Scinece, Tianjin, China, pp. 87–92, 2004.

[58] Y. Shen Y., H. Osumi, and T. Arai, "Manipulability measures for multi-wire driven parallel mechanisms", in Proceedings of the IEEE International Conference on Industrial Technology, Guangzhou, China, vol.1, pp. 550–554, 1994.

[59] Y. Shen Y., H. Osumi, and T. Arai, "Set of manipulating forces in wire driven systems", in Proceedings of the IEEE/RSJ/GI International Conference on Intelligent Robots and Systems (IROS 94), vol. 3, pp. 1626–1631, 1994.

[60] J.E. Shigley, C.R. Mischke, and R. Budynas, "Mechanical Engineering Design", McGraw-Hill, 2004.

[61] ''Skycam'',AugustDesign,www.august-design.com,2006

[62] S. Slagowski, and A. Potter, "Using ADAMS to Model Cable-Driven Hyper-Redundant Flexible Manipulators", presented at International ADAMS User Conference, 2000.

[63] S.K. Song, D.S. Kwon, "Geometric Formulation Approach for Determining The Actual Solution of The Forward Kinematics of 6-DOF Parallel Manipulators", IEEE/RSJ International Conference on Intelligent Robots and System, Suwon, South Korea, vol. 2, pp. 1930–1935, 2002.

[64] T.G. Sugar, and P. Fussell, "Mouth-Operated Neurosurgical Robot", Proceedings of the ASME Design Engineering Technical Conference, Pittsburg, PA, USA, vol. 2, pp. 1113–1118, 2001.

[65] S. Tadokoro, T. Matsushima, Y. Murao, H. Kohkawa, and M. Hiller, "A Parallel Cable-Driven Motion Base for Virtual Acceleration", presented at IEEE/RSJ Intl. Conf. on Intelligent Robots and Systems, Maui, Hawaii, USA, vol. 3, pp. 1700–1705, 2001.

[66] S. Tadokoro, S. Nishioka, T. Kimura, M. Hattori, T. Takamori, and K. Maeda, "On Fundamental Design Of Wire Configurations Of Wire-Driven Parallel Manipulators With Redundancy", presented at Japan/USA Symposium on Flexible Automation, Boston, USA, pp. 151–158, 1996.

[67] S. Tadokoro, R. Verhoeven, M. Hiller, and T. Takamori, "A portable parallel manipulator for search and rescue at large-scale urban earth-quakes and an identification algorithm for the installation in unstructured environments", in Proceedings of the IEEE/RSJ International Conference on Intelligent Robots and Systems, Kyongju, South Korea, vol. 2, pp. 1222–1227, 1999.

[68] Y. Takahashi, and O. Tsubouchi, "Tension control of wire suspended mechanism and application to bathroom cleaning robot", in Proceedings of the 39th SICE Annual Conference, Iizuka, Japan, pp. 143–147, 2000.

[69] F. Thomas, E. Ottaviano, L. Ros, and M. Ceccarelli, "Uncertainty Model and Singularities of 3-2-1 Wire-Based Tracking Systems", in Advances in Robot Kinematics, pp. 107–116, Kluwer Academic Publishers, 2002.

[70] C.J. Thompson, and Jr.P.D. Campbell, "Tendon suspended platform robot", U.S. Patent No. 5,585,707, 1996.

[71] L.W. Tsai, "Robot Analysis; The Mechanics of Serial and Parallel Manipulators", USA: John-Wiley and Sons, Inc., 1999.

[72] L.W. Tsai, and S. Joshi, "Kinematic Analysis of 3-DOF Position Mechanisms for Use on Hybrid Kinematic Machines", ASME Journal of Mechanical Design, vol. 124, No. 1, pp.245–253, 2002.

[73] R. Verhoeven, M. Hiller, "Estimating the controllable workspace of tendon-based stewart platforms", in Proceedings of the ARK '00 7th Internation-al Symposium on Advances in Robot Kinematics, Protoroz, Slovenia, pp. 277–284, 2000.

[74] R. Verhoeven, M. Hiller, "Tension distribution in tendon-based stewart platforms", in Proceedings of ARK '02 8th International Symposium on Advances in Robot Kinematics, Caldes de Malavella, Spain, 2002.

[75] R. Verhoeven, M. Hiller, S. Tadokoro, "Workspace of tendon-driven stewart platforms: Basics, classification, details on the planar 2-dof class", in Proceedings of the 4th International Conference on Motion and Vibration Control, ETH-Zrich, Switzerland, vol. 3, pp. 871–876, 1998.

[76] R. Verhoeven, M. Hiller, S. Tadokoro, "Workspace, stiffness, singularities and classification of tendon-driven stewart platforms", in Proceedings of the ARK '98 6th International Symposium on Advances in Robot Kinematics, Strobl, Austria, pp. 105–114, 1998.

[77] M. Vysin, R. Knoflicek, "The hybrid mobile robot",IEEE International Conference on Industrial Technology, Maribor, Slovenia, vol. 1, pp. 262–264, 2003.

[78] L. Wei, M. Griffis, and J. Duffy, "Forward Displacement Analyses of the 4-4 Stewart Platforms", ASME journal of mechanical design, vol. 114, No. 4, pp. 444–450, 1992.

[79] R.L. Williams II, "Cable suspended haptic interface", International journal of virtual reality, vol. 3, No. 3, pp. 13–21, 1998.

[80] R.L. Williams, and P. Gallina , "Planar cable-direct-driven robots,part i: Kinematics and statics", in Proceedings of the ASME Design Technical Conferences, Pittsburgh, PA, USA, vol. 2, pp. 1233–1240, 2001.

[81] R.L. Williams II, and P. Gallina P., "Planar cable-direct-driven robots, part ii: Dynamics and control", in Proceedings of the ASME Design Technical Conferences, Pittsburgh, PA, USA, vol. 2, pp. 1241–1247, 2001.

[82] R.L. Williams II, and J. Vadia, "Planar Translational Cable-Direct-Driven Robots: Hardware Implementation", Proc. of DETC ASME Design Engineering Technical Conference, Chicago, IL., USA, vol.2, pp. 1135–1142, 2003.

[83] A. Wolff, OTR. L, "Post-surgical Rehabilitation Guidelines for the Orthopedic Clinician", Elsevier Science Health Science div, 2006.

[84] N. Yanai, M. Yamamoto, and A. Mohri, "Anti-sway control for wire-suspended mechanism based on dynamics compensation", in Proceedings of IEEE Conference on Robotics and Automation, Washington, DC, USA, vol. 4, pp. 4287- 4292, 2002.

[85] G. Yang, W. Chen, I.M. Chen, S.H. Yeo, and G. Chen, "Design and Kinematic Analysis of Modular Reconfigurable Parallel Robots", Proceedings of

the IEEE International Conference on Robotics and Automation, Detroit, MI, USA, vol. 4, pp. 2501–2506, 1999.

[86] G. Yang, W. Chen, and I.M. Chen, "A Geometrical Method for The Singularity Analysis of 3-RRR Planar Robots With Different Actuation Schemes", presented at IEEE/RSJ Intl. Conference on Intelligent Robots and Systems, EPFL, Lausanne, Switzerland, vol.3, pp. 2055–2060, 2002.

[87] G. Yang G., S.H. Yeo S.H., C.B. Pham, "Kinematic and singularity analysis of a planar cable-driven parallel manipulator", Proceeding Of IEEE/RSJ International conference on Intelligence and Robots and systems, Sendai, Japan, vol. 4, pp. 3835–3840, 2004.

[88] D. Zlatanov, S. Agrawal, and C.M. Gosselin, "Convex Cones in Screw Spaces, Journal of Mechanism and Machine Theory", vol. 40, No. 6, pp. 710–727, 2005.

Appendix A: Driving the Dynamic Equations for the Cable Winding Units

The cable winding unit including actuator, reduction gears, and cable winding drum is shown in Figure 1. The dynamic equations of the systems are:

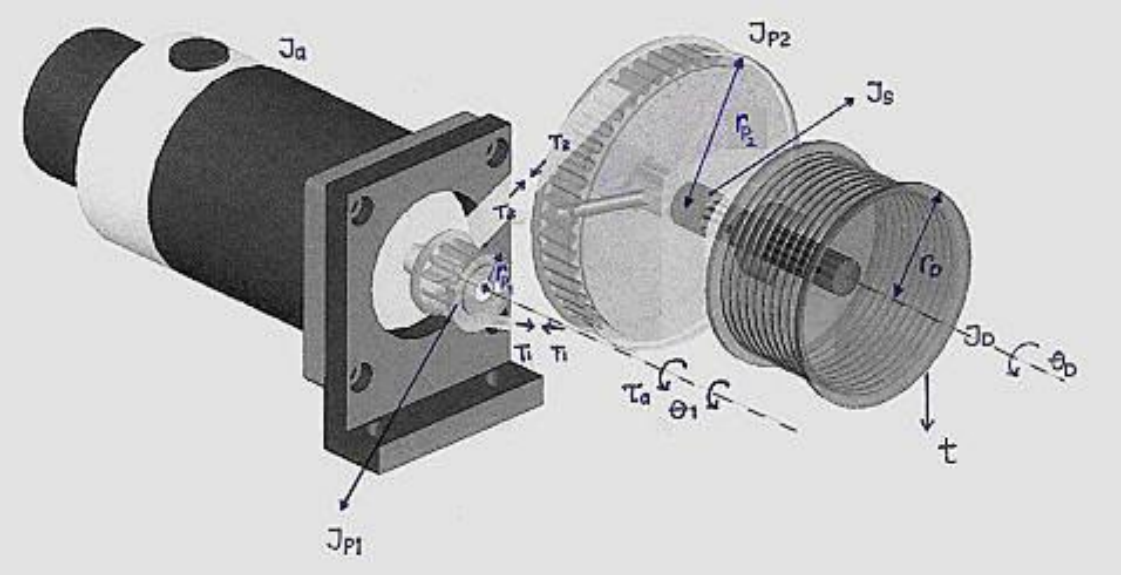

Figure 1: Free Body Diagram of Cable Winding Unit

$$r_{p_1}\theta_1 = r_{p_2}\theta_2 \tag{1}$$

$$\tau_a - (T_2 - T_1)r_{p_1} - \tau_{f_a} = (\underbrace{J_{actuator} + J_{pulley_1}}_{J_a})\ddot{\theta}_1 + (C_a)\dot{\theta}_1 \tag{2}$$

$$(T_2 - T_1)r_{p_2} - t.r_D - \tau_{f_D} = (\underbrace{J_{shaft} + J_{pulley_2} + J_{Drum}}_{J_D})\ddot{\theta}_D + (C_D)\dot{\theta}_D \tag{3}$$

The dynamic equation of cable winding unit, which is used in chapter five, will be obtained by combining equations (1), (2), and (3).

$$\tau_a - \tau_{f_1} - r_1 t = J_1\ddot{\theta}_1 + C_1\dot{\theta}_1 \tag{4}$$

Where, the equivalent inertia, referred to actuator side, is:

$$J_1 = J_a + (\tfrac{r_{p_1}}{r_{p_2}})^2 J_D \tag{5}$$

The equivalent damping, referred to actuator side, can be expressed as:

$$C_1 = C_a + (\tfrac{r_{p_1}}{r_{p_2}})^2 C_D \tag{6}$$

Moreover, the equivalent radius of the cable winding unit, referred to actuator side, is:

$$r_1 = \tfrac{r_{p_1}}{r_{p_2}} r_D \tag{7}$$

Appendix B: Dynamic equations of the planar CDR using the Lagrangian approach

End-effector Modeling

Considering the Lagrangian as $L(q,\dot{q}) = T(q,\dot{q}) - V(q)$, and the generalized coordinates of a planar CDR as $q = [x, y, \phi]^T$, the Lagrangian equation of motion can be expressed in the following forms:

$$\frac{d}{dt}\left(\frac{\partial L}{\partial \dot{q}_i}\right) - \frac{\partial L}{\partial q_i} + \frac{\partial R}{\partial \dot{q}_i} = u_i \tag{8}$$

$$\frac{d}{dt}\left(\frac{\partial T}{\partial \dot{q}_i}\right) - \frac{\partial T}{\partial q_i} + \frac{\partial V}{\partial q_i} + \frac{\partial R}{\partial \dot{q}_i} = u_i \tag{9}$$

The Kinetic Energy of the planar CDR is:

$$T(q,\dot{q}) = \tfrac{1}{2} m_e(\dot{x}^2 + \dot{y}^2) + \tfrac{1}{2} I_e \dot{\phi}^2 \tag{10}$$

and the Potential Energy includes the strain energy of the cables, that can be expressed by the following equation in pure tension condition:

$$U_{strain\ energy} = \frac{1}{2}t\delta = \frac{1}{2}(t)(\frac{t}{k}) = \frac{t^2 l}{2EA} \tag{11}$$

where,

- E: is the Young Modulus of elasticity of the cable
- A: is the cross sectional area of the cable
- l: is the active length of the cable
- σ, ε: are the tensile stress and strain, respectively
- T: is the tension force
- δ: is the elongation in the cable direction
- $k = \frac{t}{\delta} = \frac{\sigma A}{\varepsilon l} = \frac{EA}{l}$:is the elastic stiffness coefficient of the cable

Therefore, the Potential Energy of the CDR becomes:

$$V(q) = \frac{t_1^2 l_1}{2E_1 A_1} + \frac{t_2^2 l_2}{2E_2 A_2} + \frac{t_3^2 l_3}{2E_3 A_3} + \frac{t_4^2 l_4}{2E_4 A_4} \tag{12}$$

where,

$$l_i = \sqrt{(x + q_{ix}\cos\varphi - q_{iy}\sin\varphi - b_{ix})^2 + (y + q_{ix}\sin\varphi + q_{iy}\cos\varphi - b_{iy})^2} \tag{13}$$

Assuming all the cables are the same, we have:

$$E_1A_1 = E_2A_2 = E_3A_3 = E_4A_4 = EA \tag{14}$$

$$\frac{\partial V}{\partial x} = \frac{t_1^2}{2EA}\frac{\partial l_1}{\partial x} + \cdots + \frac{t_4^2}{2EA}\frac{\partial l_4}{\partial x} \tag{15}$$

$$\frac{\partial V}{\partial y} = \frac{t_1^2}{2EA}\frac{\partial l_1}{\partial y} + \cdots + \frac{t_4^2}{2EA}\frac{\partial l_4}{\partial y} \tag{16}$$

$$\frac{\partial V}{\partial \varphi} = \frac{t_1^2}{2EA}\frac{\partial l_1}{\partial \varphi} + \cdots + \frac{t_4^2}{2EA}\frac{\partial l_4}{\partial \varphi} \tag{17}$$

where,

$$\frac{\partial l_1}{\partial x} = \frac{l_{1x}}{l_1} \tag{18}$$

$$\frac{\partial l_1}{\partial y} = \frac{l_{1y}}{l_1} \tag{19}$$

$$\frac{\partial l_1}{\partial \varphi} = \frac{l_{1x}}{l_1}(-q_{1x}\sin\varphi - q_{1y}\cos\varphi) + \frac{l_{1y}}{l_1}(q_{1x}\cos\varphi - q_{1y}\sin\varphi) \tag{20}$$

$$\frac{d}{dt}\left(\frac{\partial T}{\partial \dot{x}}\right) = m_e\ddot{x} \tag{21}$$

$$\frac{d}{dt}\left(\frac{\partial T}{\partial \dot{y}}\right) = m_e\ddot{y} \tag{22}$$

$$\frac{d}{dt}\left(\frac{\partial T}{\partial \ddot{\varphi}}\right) = I_e\ddot{\varphi} \tag{23}$$

Substituting equations (10) - (26) in (9), results in the following dynamic equations of the end-effector that includes the cable tension model.

$$m_e\ddot{x} + \frac{1}{2EA}\left(t_1^2\frac{l_{1x}}{l_1} + \cdots + t_4^2\frac{l_{4x}}{l_4}\right) = t_{1x} + \cdots + t_{4x} \tag{24}$$

$$m_e\ddot{y} + \frac{1}{2EA}\left(t_1^2\frac{l_{1y}}{l_1} + \cdots + t_4^2\frac{l_{4y}}{l_4}\right) = t_{1y} + \cdots + t_{4y} \tag{25}$$

$$I_e\ddot{\varphi} + \tfrac{1}{2EA}\begin{pmatrix} t_1^2\left(\frac{l_{1x}}{l_1}(-q_{1x}\sin\varphi - q_{1y}\cos\varphi) + \frac{l_{1y}}{l_1}(q_{1x}\cos\varphi - q_{1y}\sin\varphi)\right) + \cdots \\ +t_4^2\left(\frac{l_{1x}}{l_1}(-q_{1x}\sin\varphi - q_{1y}\cos\varphi) + \frac{l_{1y}}{l_1}(q_{1x}\cos\varphi - q_{1y}\sin\varphi)\right) \end{pmatrix} =$$

$$\mathbf{q}_1 \times \mathbf{t}_1 + \cdots + \mathbf{q}_4 \times \mathbf{t}_4 \tag{26}$$

Expressing equation (27) - (29) in the matrix form results in:

$$\mathbf{S}\begin{bmatrix} t_1 + \frac{t_1^2}{2EA} \\ t_2 + \frac{t_2^2}{2EA} \\ t_3 + \frac{t_3^2}{2EA} \\ t_4 + \frac{t_4^2}{2EA} \end{bmatrix} = \mathbf{W} \tag{27}$$

where,

$$\mathbf{S} = \begin{bmatrix} u_1 & \cdots & u_4 \\ q_1 \times u_1 & \cdots & q_4 \times u_4 \end{bmatrix} \tag{28}$$

$$\mathbf{W} = \begin{Bmatrix} m_e\ddot{x} \\ m_e\ddot{y} \\ I_e\ddot{\varphi} \end{Bmatrix} \tag{29}$$

Note that the current equation of motion (equation 30) includes the higher orders of cables tension "t^2" in addition to the first order cables tensions "t" in comparison with equation equation (5.3).

Actuator Modeling

Lagrangian approach results the same dynamic equations as equation (5.4) for actuators. The kinetic energy of the actuator is $T(\theta, \dot{\theta}) = \frac{1}{2}J\dot{\theta}^2$, and the potential energy is $V(\theta) = 0$. Considering the viscous damping of the actuators as the Rayleigh dissipation function $D(\dot{\theta}) = \frac{1}{2}C\dot{\theta}^2$, the dynamic equations become:

$$\frac{d}{dt}\left(\frac{\partial L}{\partial \dot{\theta}}\right) - \frac{\partial L}{\partial \theta} + \frac{\partial D}{\partial \dot{\theta}} = u \tag{30}$$

$$J\ddot{\theta} + C\dot{\theta} = \tau_a - \tau_f - rt \tag{31}$$

Drawings

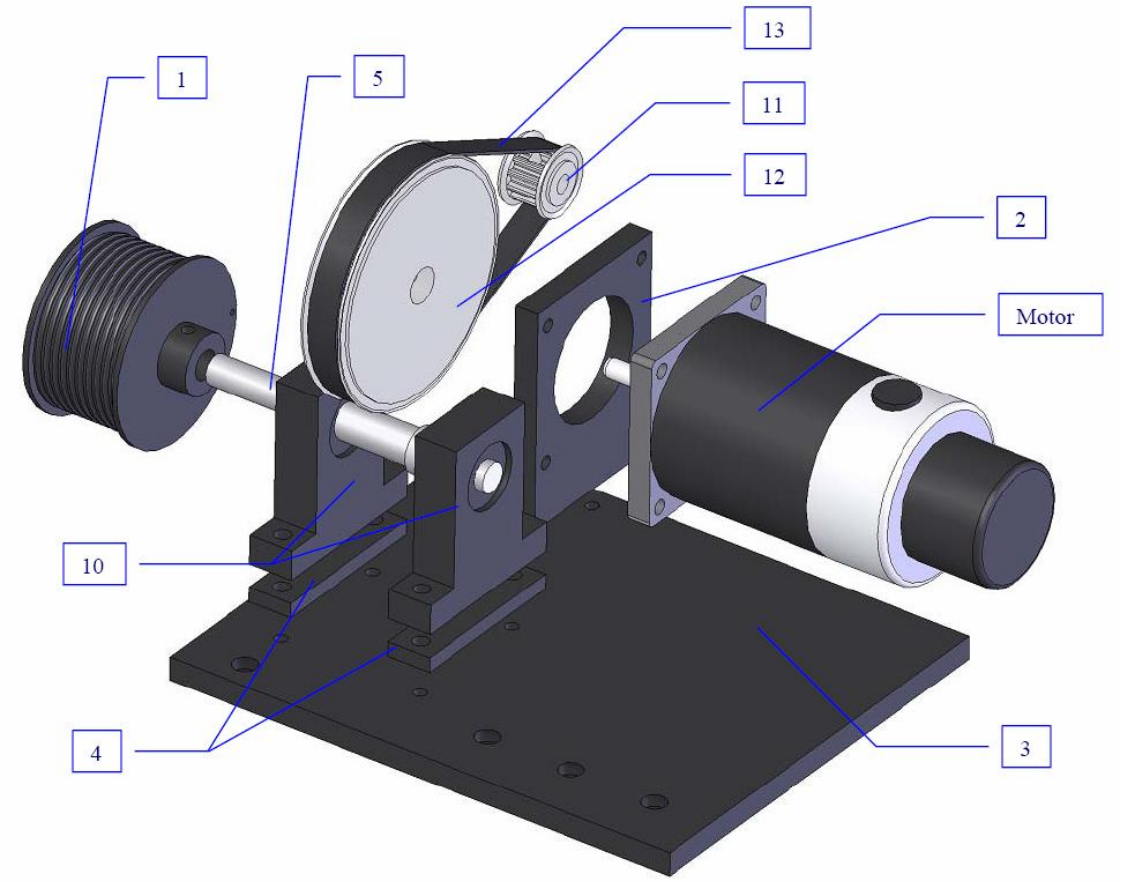

Figure 2: Exploded View of Cable Winding Unit

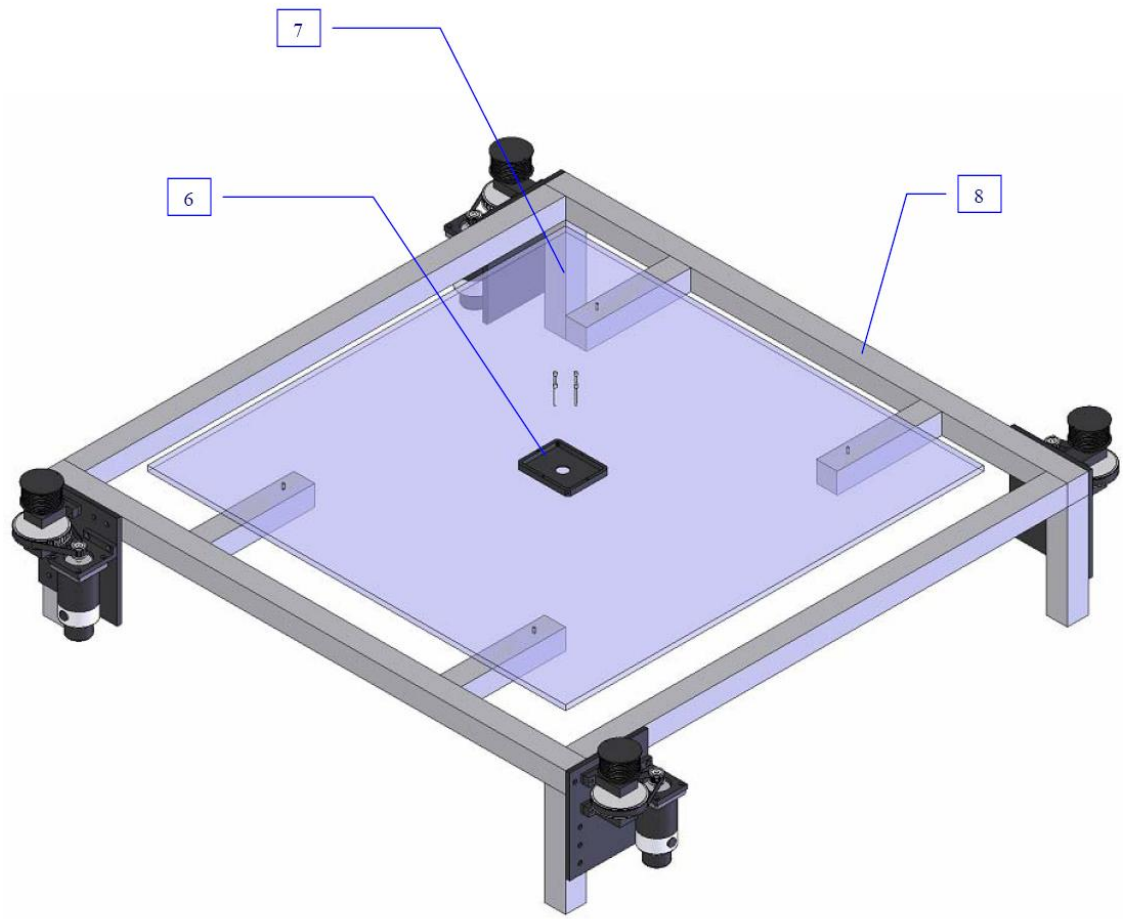

Figure 3: Final Assembly of Cable-Driven System

Part No.	Item Description	Qty	F/P[1]	Catalogue No.	Drawing No.
1.	Drum	4	F	-	B128-1
2.	Motor Bracket	4	F	-	B128-2
3.	Motor Plate	4	F	-	B128-3
4.	Bearing Stand	8	F	-	B128-4
5.	Shaft	4	F	-	B128-5
6.	End Effector	1	F	-	B128-6
7.	Workspace Board	1	F	-	B128-7
8.	Table	1	F	-	B128-8
9.	Pulley	8	F	-	B128-9
10.	Bearing	8	P	BGHKB 6000ZZ-40	-
11.	Timing Pulley1	4	P	TTPA12T5100 -A-P6.35	-
12.	Timing Pulley2	4	P	TTPA48T5100 -A-P12	-
13.	Timing Belt	4	P	TTBU300T5-100	-

Table 1: Part List

Table 1 gives the individual parts that were selected for the design of the CDR. Some of these parts were selected and purchased from mechanical standard components from Misumi. Besides that, some of the parts were fabricated[1] in workshop, for the sake of low costs. Subsequently, detailed drawings of major parts are attached.

[1]F:Fabricated, P:Purchased

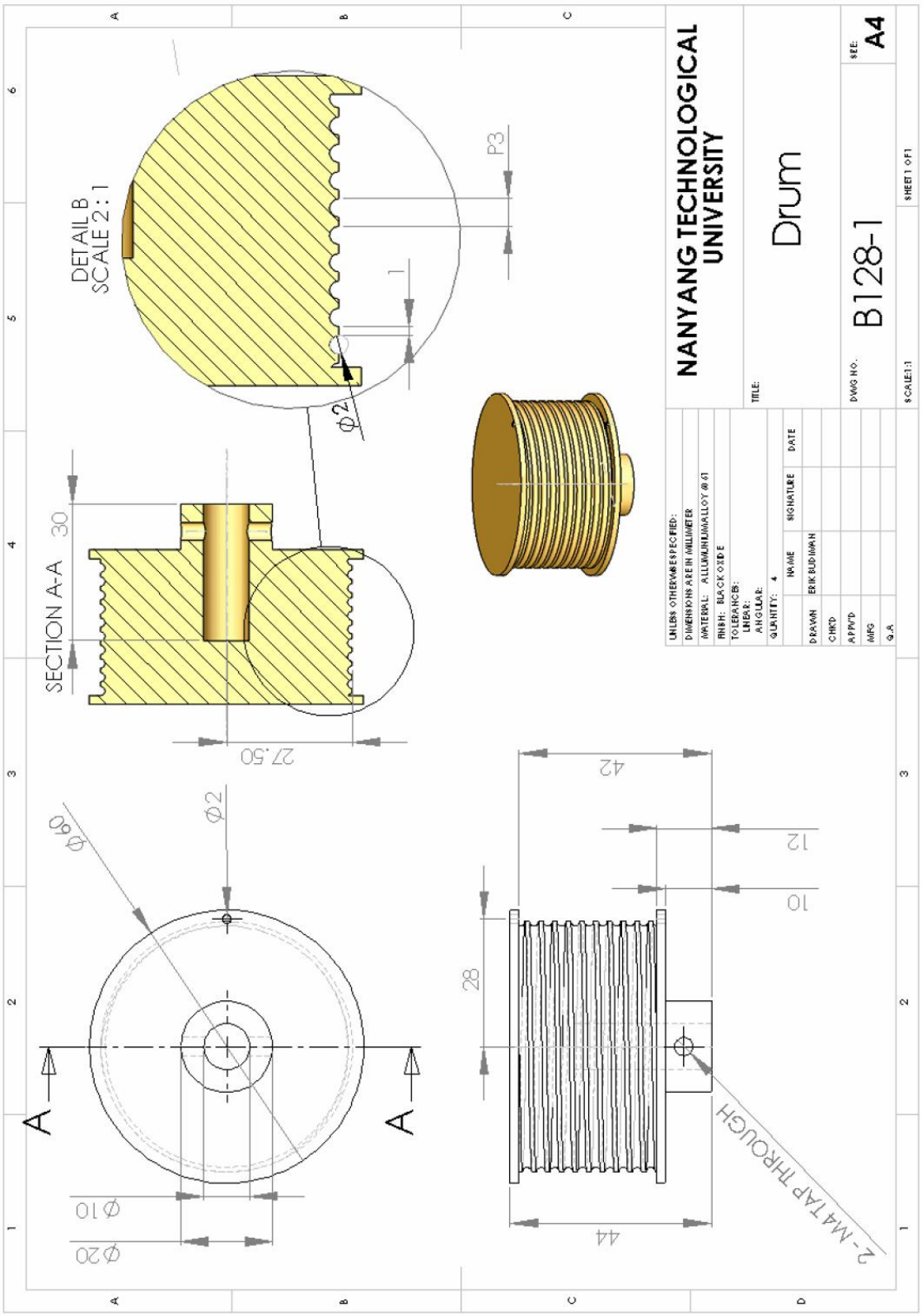

Figure 4: Cable Winding Drum Drawing

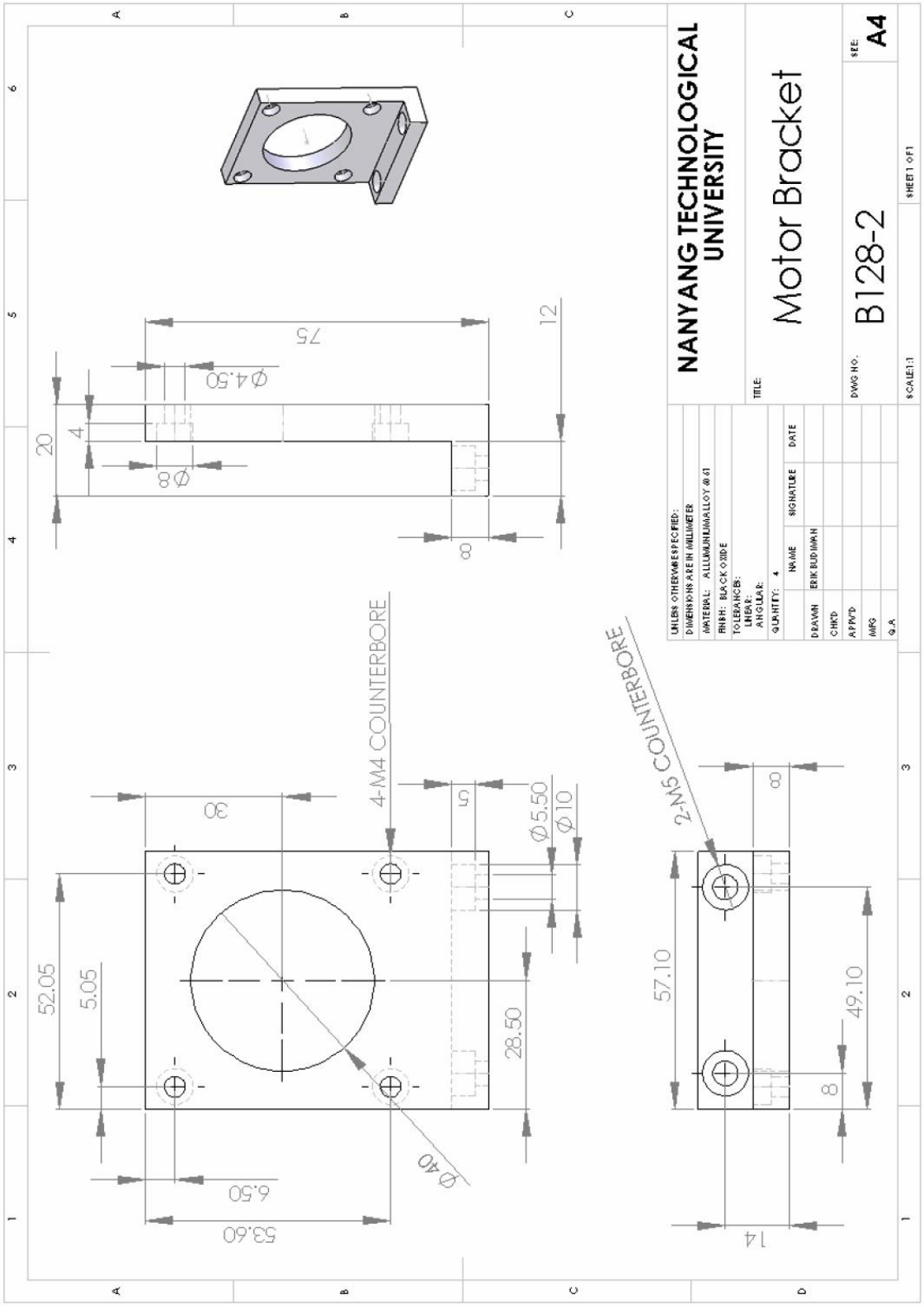

Figure 5: Motor Bracket Drawing

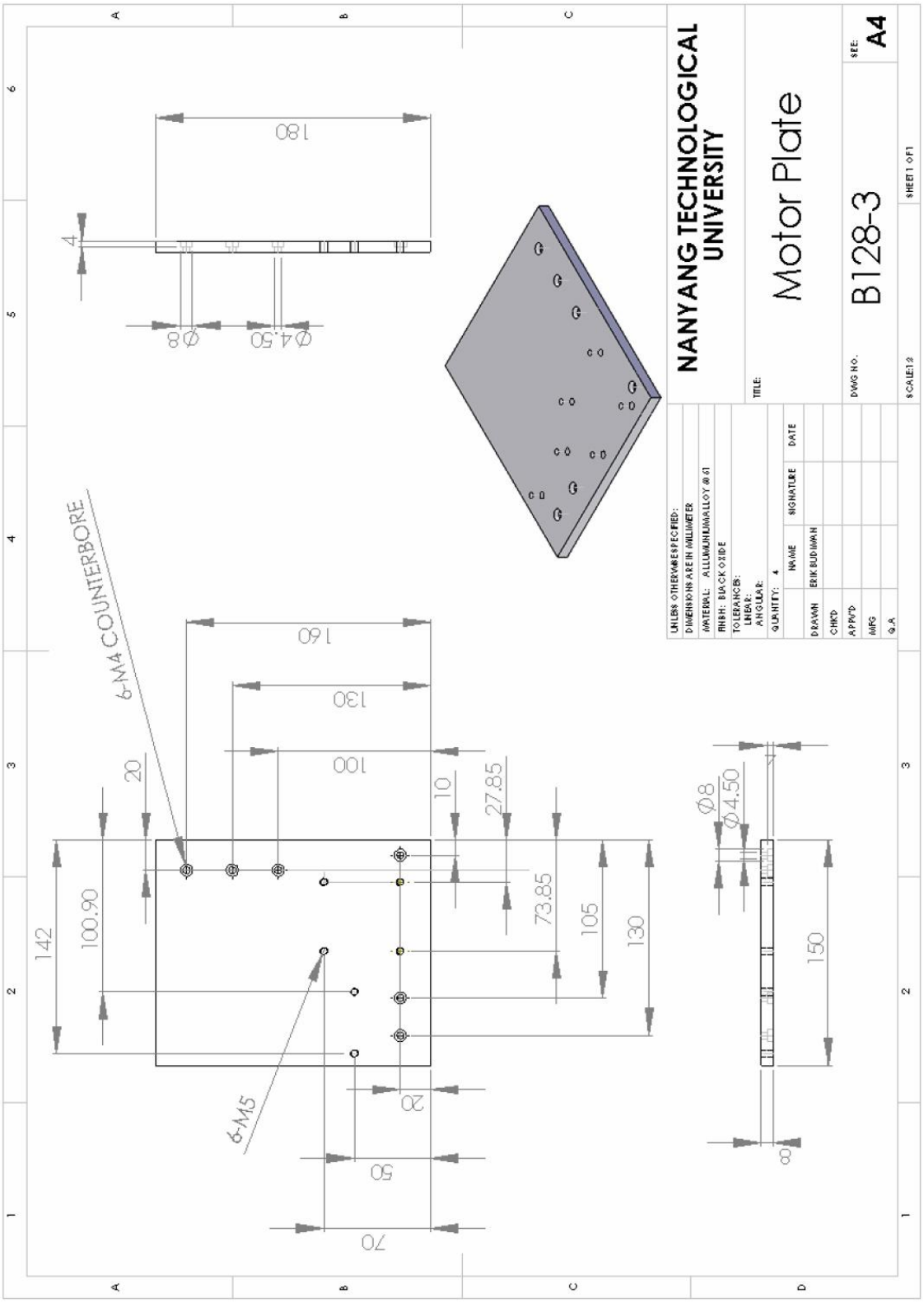

Figure 6: Motor Plate Drawing

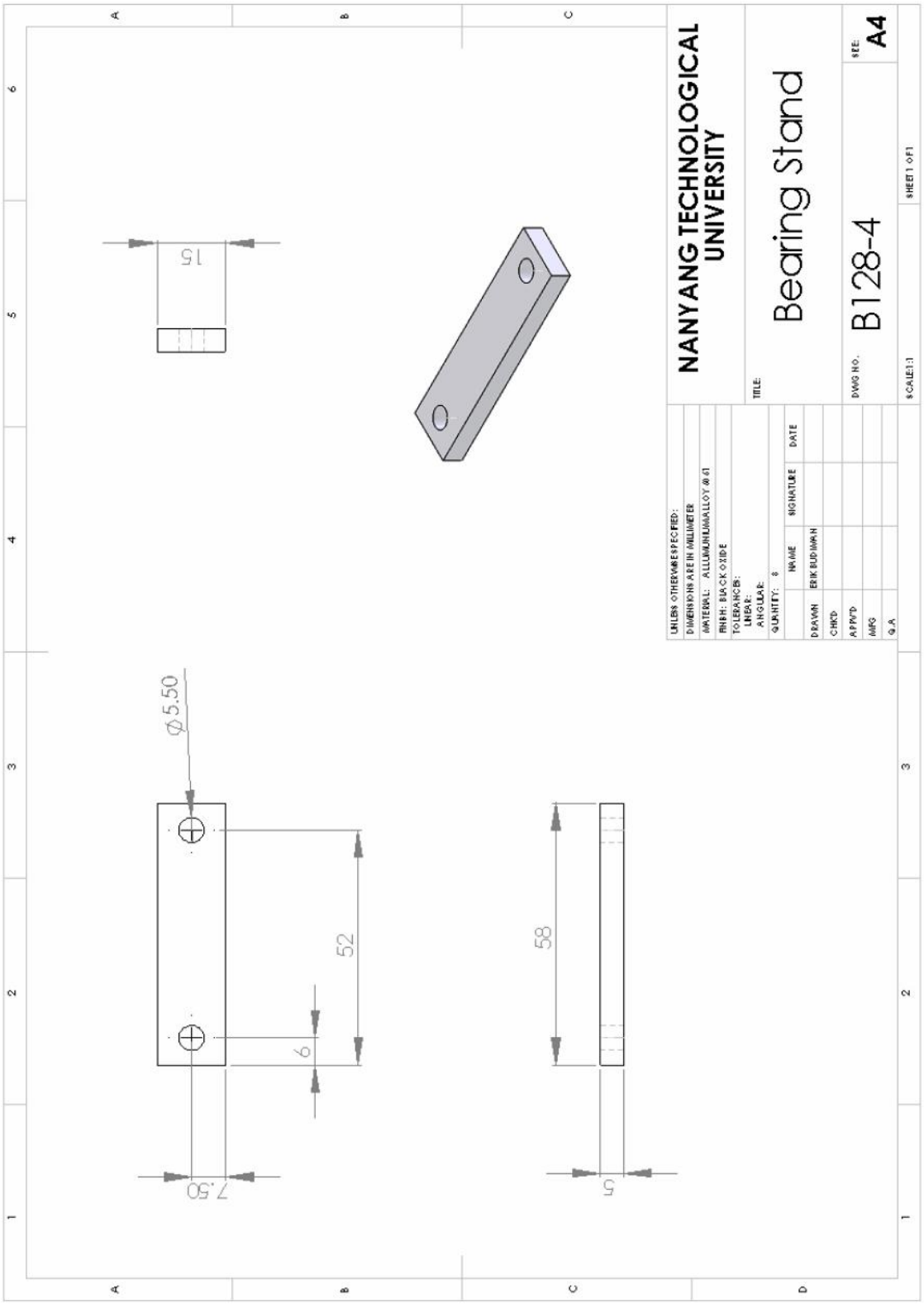

Figure 7: Bearing Stands Drawing

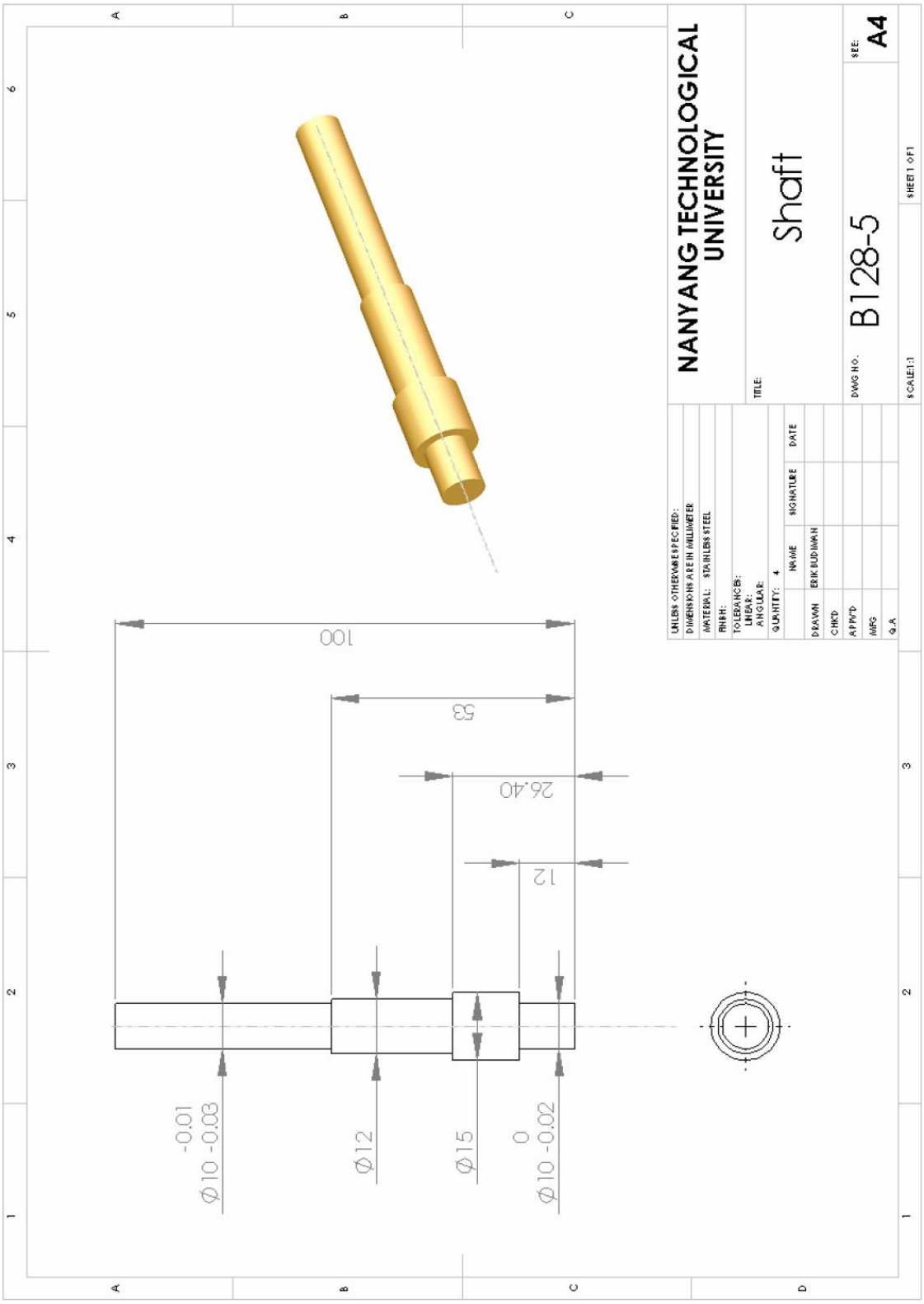

Figure 8: Shaft Drawing

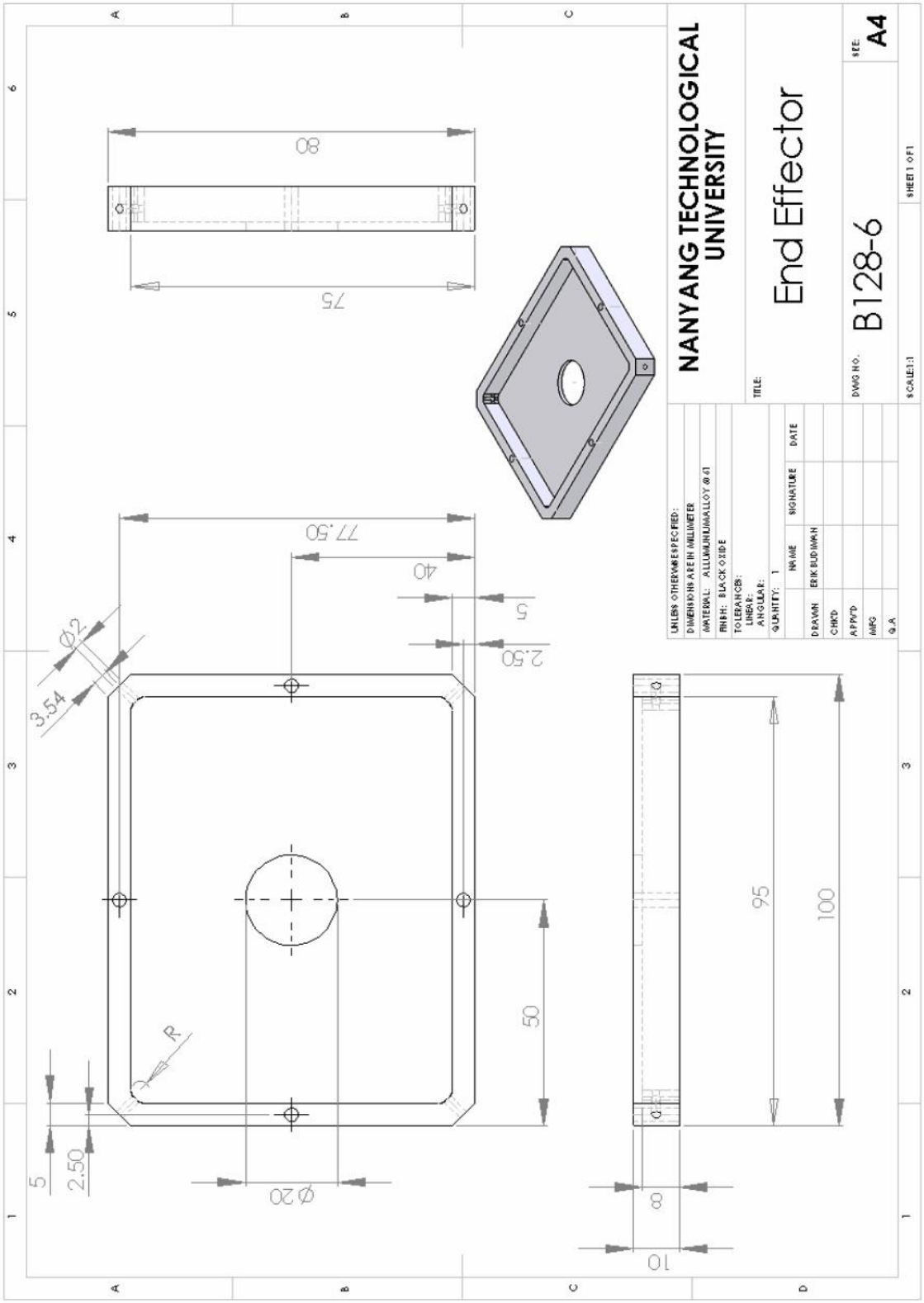

Figure 9: End-effector Drawing

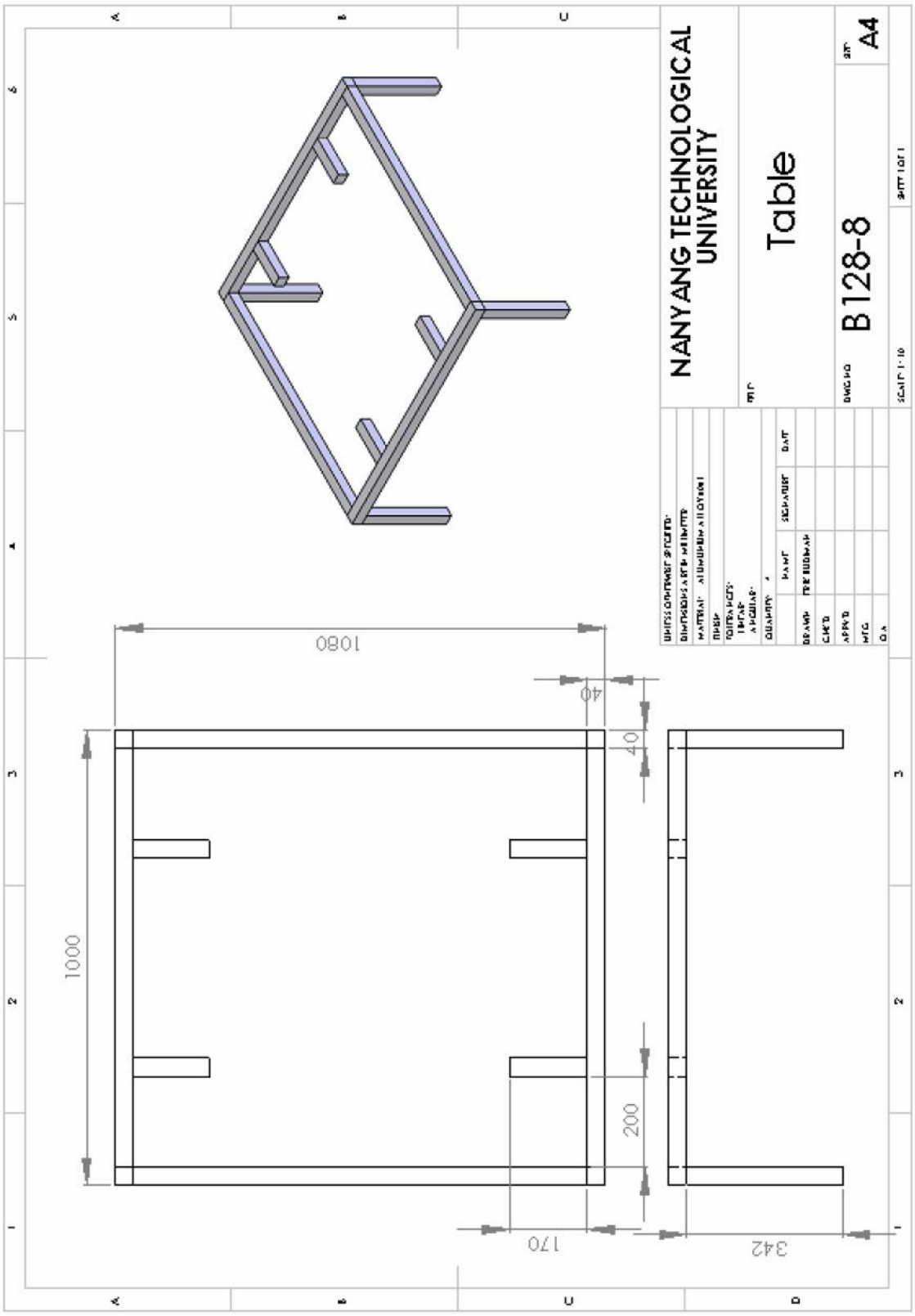

Figure 10: Table Drawing

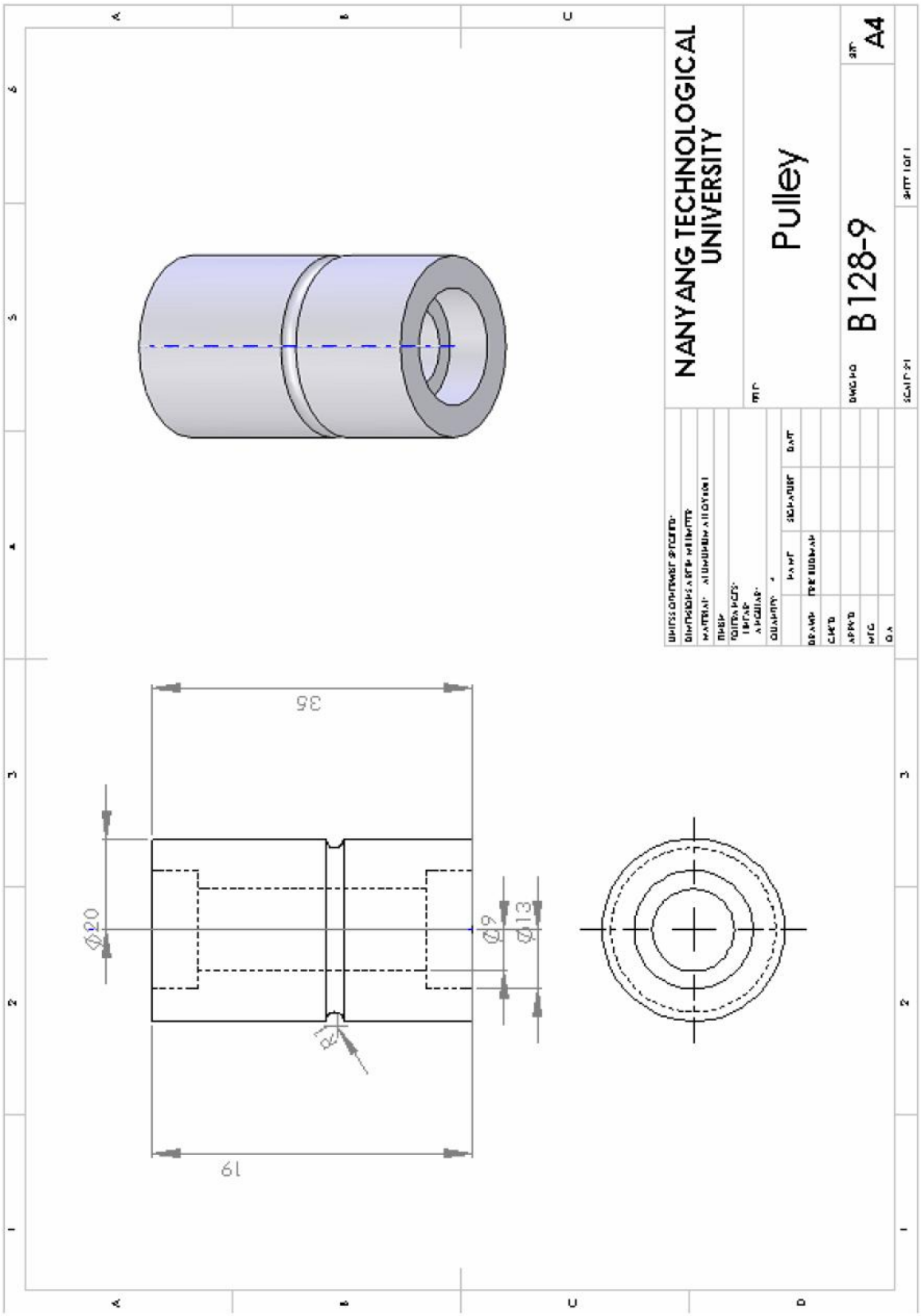

Figure 11: Pulley Drawing

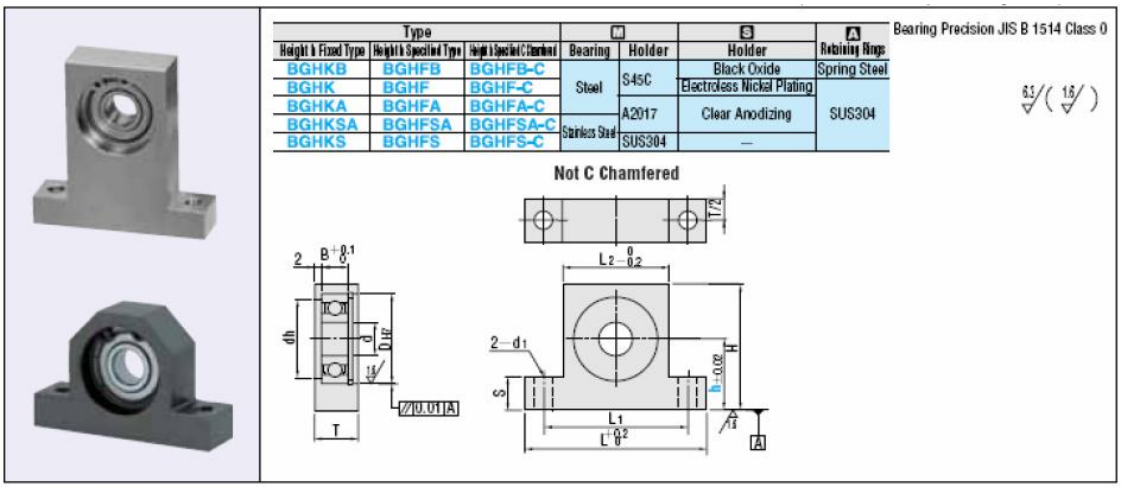

Figure 12: Bearing with Housing Drawing

Order No.	h	d	D_{H7}	Tolerance	dh	B	H	L	L1	L2	T	S	d_1
BGHKB 6000ZZ-40	40	10	26	+0.021 0	22	8	h+17	58	46	34	15	10	5.5

Table 2: Bearing with Housing Specifications

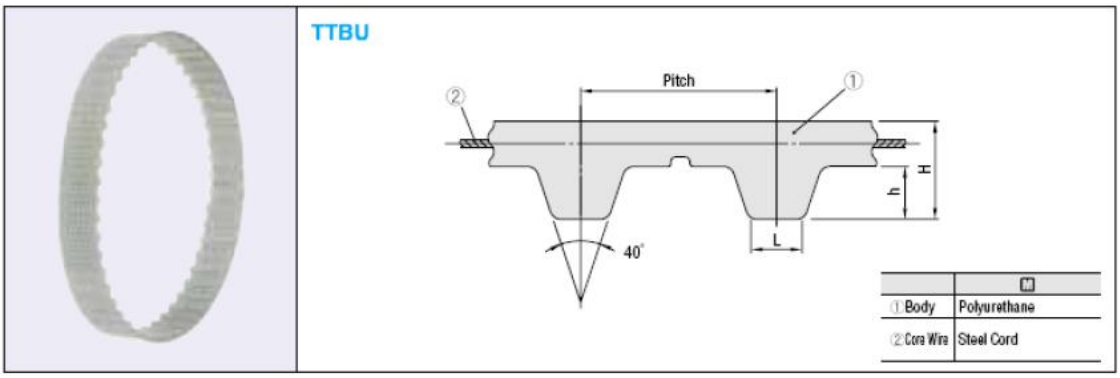

Figure 13: Timing Belt Drawing

Order No.	Width	Teeth No.	Circum. Length	Type	Pitch	H	h	L
TTBU 300T5-100	100	60	300	T5	5	2.2	1.2	1.8

Table 3: Timing Belt Specifications

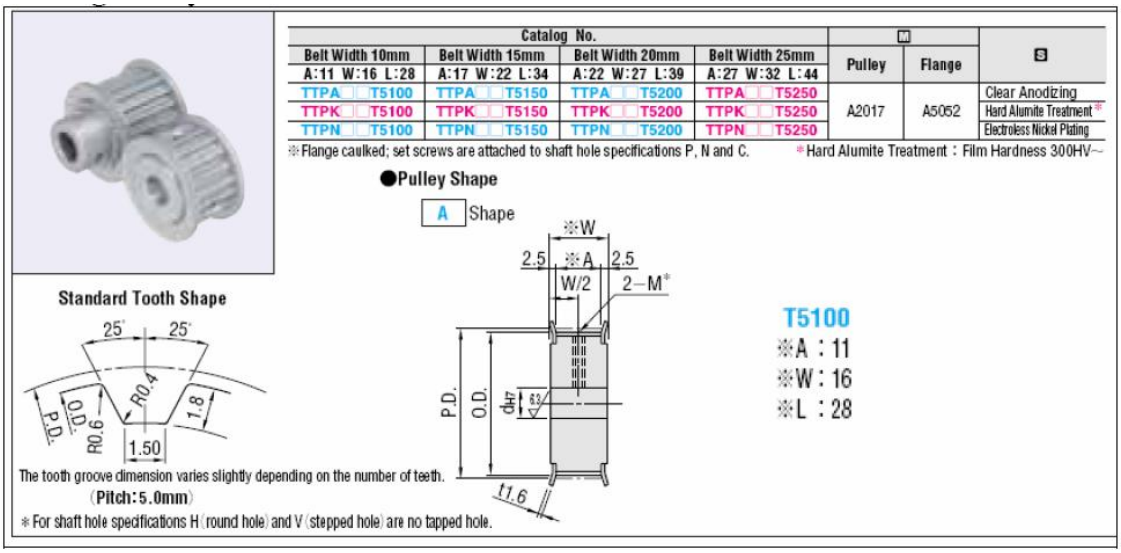

Figure 14: Timing Pulley Drawing